Distribution Agreement

In presenting this thesis or dissertation as a partial fulfillment of the requirements for an advanced degree from Emory University, I hereby grant to Emory University and its agents the non-exclusive license to archive, make accessible, and display my thesis or dissertation in whole or in part in all forms of media, now and hereafter known, including display on the world wide web. I understand that I may select some access restrictions as part of the online submission of this thesis or dissertation. I retain all ownership rights to the copyright of the thesis or dissertation. I also retain the right to use future works (such as articles or books) all or part of this thesis or dissertation.

Signature:

_____ _____

Kyuwon Cho Date

Exploring Therapeutic Strategies Targeting Cardiomyocytes for Heart Regeneration

By

Kyuwon Cho
Doctor of Philosophy

Graduate Division of Biological and Biomedical Sciences
Program in Molecular and Systems Pharmacology

_____
Young-sup Yoon, M.D., Ph.D.
Advisor

_____
Ahsan Husain, Ph.D.
Committee Member

_____
Changwon Park, Ph.D.
Committee Member

_____
John W. Calvert, Ph.D.
Committee Member

_____
Roy L. Sutliff, Ph.D.
Committee Member

Accepted:

_____
Lisa A. Tedesco, Ph.D.
Dean of the James T. Laney School of Graduate Studies

_____
Date

Exploring Therapeutic Strategies Targeting Cardiomyocytes for Heart Regeneration

By

Kyuwon Cho
M.S., Korea University, 2009

Advisor: Young-sup Yoon, M.D., Ph.D.

An abstract of
a dissertation submitted to the Faculty of the
James T. Laney School of Graduate Studies of Emory University
in partial fulfillment of the requirements for the degree of
Doctor of Philosophy
Graduate Division of Biological and Biomedical Sciences
Molecular and Systems Pharmacology
2018

Abstract

Exploring Therapeutic Strategies Targeting Cardiomyocytes for Heart Regeneration

By Kyuwon Cho

Heart failure is the leading cause of morbidity and mortality in industrialized countries and is caused by dysfunction or deficiency of cardiomyocytes (CMs). No effective treatment is available due to limited regenerative capacity of the adult heart after ischemic injury. Among therapeutic strategies to generate CMs for heart regeneration, the current study explored two promising options: transplantation of pluripotent stem cell-derived CMs (PSC-CMs) and activation of pre-existing cardiomyocyte (CM) proliferation. One of the most critical hurdles for the use of PSC-CMs is their heterogeneity that leads to ventricular arrhythmias after transplantation. Isolation of ventricular cardiomyocytes (vCMs) has been challenging due to the lack of specific surface markers. We showed that vCMs can be purified from differentiating mouse embryonic stem cells (mESCs) using molecular beacons (MBs) targeting specific intracellular mRNAs. We found that, of the cells isolated, ~98% displayed vCM-like action potentials by electrophysiological analyses. These MB-purified vCMs continuously maintained their CM characteristics as verified by spontaneous beating, $Ca2^{+}$ transient, and expression of vCM-specific proteins. Our study shows the feasibility of isolating pure vCMs via cell sorting without modifying host genes. The homogeneous and functional vCMs generated via the MB-based method can be useful for disease investigation, drug discovery, and cell-based therapies. As for the second strategy, we aimed to define regulatory mechanism how CMs lose proliferative capacity because limited proliferative capacity of adult mammalian CMs restricts heart regeneration. Polycomb

group proteins are epigenetic regulators of the cell cycle, but their role in CM proliferation is unclear. Gene expression profiling revealed that CBX7, a subunit of Polycomb Repressive Complex 1, was upregulated in the postnatal heart. To determine whether CBX7 inhibits CM proliferation, we generated double mutant mouse with haplodeficiency of CBX7 in CMs. The mutant mice exhibited perinatal lethality with cardiomegaly. Histological analyses showed increased proliferative capacity of perinatal CMs by the targeted inhibition of CBX7. Gene expression profiling revealed that mitosis-related genes were derepressed whereas cardiac maturation genes were downregulated by targeted inhibition of CBX7. Gain of function analyses using adenoviral particles showed repressed proliferative capacity and promoted multinucleation of neonatal CMs by CBX7 overexpression in vitro. These results indicate that CBX7 is a critical repressor of perinatal CM proliferation and an attractive therapeutic target for inducing CM proliferation and ultimately for heart regeneration.

Exploring Therapeutic Strategies Targeting Cardiomyocytes for Heart Regeneration

By

Kyuwon Cho
M.S., Korea University, 2009

Advisor: Young-sup Yoon, M.D., Ph.D.

A dissertation submitted to the Faculty of the
James T. Laney School of Graduate Studies of Emory University
in partial fulfillment of the requirements for the degree of
Doctor of Philosophy
Graduate Division of Biological and Biomedical Sciences
Molecular and Systems Pharmacology
2018

Table of Contents

Figures and Tables

List of frequently used abbreviations

Abbreviation	Full name
CM	Cardiomyocyte
MB	Molecular beacon
mESCs	Mouse embryonic stem cells
IRX-4	Iroquois homeobox protein 4
PcG	Polycomb group
PRC	Polycomb repressive complex
CDK	Cyclin-dependent kinase
CDKI	Cyclin-dependent kinase inhibitor
ACTN2	Actinin Alpha 2
TNNT2	Troponin T2
Myh6	Myosin heavy chain 6
pH3	Phosphorylated histone 3
WGA	Wheat germ agglutinin
ChIP	Chromatin immunoprecipitation
qRT-PCR	Quantitative real-time polymerase chain reaction
IHC	Immunohistochemistry
ICC	Immunocytochemistry

Chapter 1: General introduction

1.1 Therapeutic strategies to generate cardiomyocytes for heart regeneration

Heart failure is one of the leading causes of mortality and morbidity in the world and no effective treatment is available due to limited regenerative capacity of the adult heart after ischemic injury (1-3). For heart regeneration, several strategies have been explored such as activation of pre-existing cardiomyocyte (CM) proliferation, stimulation or transplantation of progenitor cells, in vivo reprogramming of cardiac fibroblasts into CMs, and transplantation of pluripotent stem cell-derived CMs (PSC-CMs)(4) (Figure 1-1). All these strategies have pros and cons.

As for activation of CM proliferation, it was proven that newly generated CMs are derived from pre-existing CMs via genetic lineage tracing in mice (5). CM proliferation is considered as one of critical mechanisms for heart regeneration in zebrafish, and neonatal mice (6-8). However, it is still unclear whether mature mammalian CMs can re-enter the cell cycle and undergo cytokinesis (4).

Regarding the use of cardiac stem/progenitor cells (CSCs/CPCs), they were shown to undergo clonal expansion and to have multilineage differentiation potential into CMs, ECs, and VSMCs all of which are important cell types for heart regeneration (9). Nevertheless, their contribution to heart regeneration is controversial (10; 11).

Reprogramming of cardiac fibroblasts into CMs is advantageous in terms of no immunogenicity, no requirement for embryonic tissue, and no ethical issue in comparison to the use of embryonic stem cells (ESCs) as a source for CMs (12). However, there are hurdles to overcome (4). It is difficult to selectively target cardiac fibroblasts. In addition, human cells are more epigenetically stable than mouse cells so that inducing epigenetic changes in human cardiac fibroblasts will be difficult. Furthermore, immature characteristics of reprogrammed cells is another hurdle.

Use of pluripotent stem cells (PSCs) as a source for CMs holds great therapeutic potential since large number of human CMs can be produced (4). In addition, it was shown that transplantation of PSC-CM into the myocardium improved cardiac function in small and large animals including monkeys (13; 14). Furthermore, iPSC-derived CMs enable autologous transplantation, reducing the risk of immune response. One of the most critical drawbacks, however, is induction of ventricular arrhythmias which could be due to heterogeneity of the PSC-CM population (13). Cardiac differentiation of PSC produces atrial, nodal, and ventricular CMs and transplanting mixture of these different types of cells would lead to incomplete electrical coupling to the host CMs. Thus, development of purification system for isolating pure ventricular CMs is crucial for the clinical use of PSC-CMs. Furthermore, expensive production cost and ethical concerns (when embryonic stem cells are used) are additional disadvantages (4).

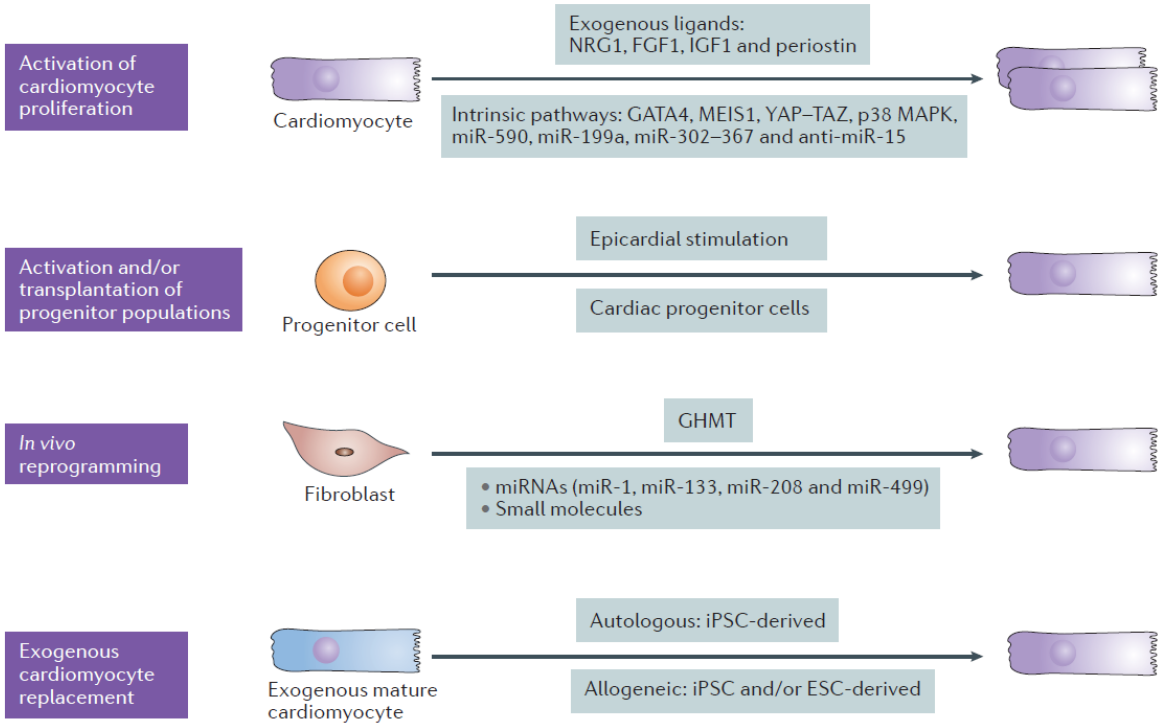

Cahill et al., Nature Reviews Drug Discovery, 2017

Figure 1-1. Therapeutic strategies for heart regeneration. To replace damaged CMs with new CMs, several strategies have been explored. First, to activate proliferation of pre-existing CMs, exogeneous ligands such as Neuregulin 1 (NRG1), Fibroblast growth factor 1 (FGF1), Insulin-like growth factor 1 (IGF1) and Periostin and modification of intrinsic pathways such as GATA binding protein 4 (GATA4), Meis homeobox 1 (MEIS1), Yes Associated Protein 1-Tafazzin (YAP-TAZ), p38 mitogen-activated protein kinase (MAPK), and microRNAs were examined. Second, activation of epicardial progenitor cells or transplantation of cardiac progenitor cells have been tested but their therapeutic effects and mechanisms are unclear. Third, cardiac fibroblasts can be converted into cardiomyocytes via introduction of transcription factors, microRNAs and small molecules. Finally, transplantation of PSC-derived CMs can replace damaged CMs.

1.2 Pluripotent stem cells (PSCs) as a source for CMs and clinical hurdles

Due to their self-renewal and multi-lineage differentiation capacity, embryonic stem cells (ESCs) and induced pluripotent stem cells (iPSCs), collectively called pluripotent stem cells (PSCs), have emerged as a highly promising and renewable source for generating CMs (15-18). Studies have shown that cell cultures directed toward differentiation into CMs include three types of CMs, nodal, atrial, and ventricular CMs, in varying ratios as well as other lineage cells (19-22). Each type of cardiac-chamber-specific CM has unique functional, structural, and electrophysiological characteristics (23). Thus, transplantation of cardiomyogenically differentiated cells, which include heterogeneous CMs and other lineage cells, into injured myocardium might induce dysrhythmia, asynchronous cardiac contraction, or aberrant tissue formation (24). Since ventricular CMs are the most extensively affected cell type in MI and the major source for generating cardiac contractile forces, there has been great interest in producing ventricular CMs from stem cells for treatment of MI (25; 26). It would therefore be ideal to generate a pure population of ventricular CMs from PSCs for cardiac-cell based therapies.

Despite the unmet medical need, to date, no studies have demonstrated the feasibility of isolating ventricular CMs without permanently altering their genome. Prior studies used genetic modification for isolating ventricular CMs by inserting a fluorescent reporter gene driven by the myosin light chain 2 (MYL2) promoter into mouse ESCs and embryonic carcinoma cell lines (25; 26). Such genetic modification precludes clinical use of the isolated cells due to concerns of tumorigenicity or adverse reactions. These ventricular CMs would not be appropriate for drug development or disease modeling due to the random and permanent changes in the genome or the use of viral vectors. Further, there are no known surface markers specific for ventricular CMs,

disallowing antibody-based cell sorting with flow cytometry, which is the most common method for isolating targeted cells from differentiating PSCs.

1.3 Molecular regulation of cardiomyocyte proliferation

Attempts have been made towards inducing cardiomyocyte (CM) proliferation since it is considered as one of the essential processes for heart regeneration. This notion has been supported by a series of studies using genetic model organisms including zebrafish and neonatal mouse in which robust division of pre-existing CMs accompanied the regenerative response (6-8). Similarly, pre-existing CMs were the primary source of newly generated CMs in the adult mammalian heart during ageing and after injury (5), but the CM renewal rate is low (1~3%) and it declines beginning at perinatal stage (27; 28). Despite extensive investigations, it is still largely unknown why and how the mammalian CMs lose proliferative capacity after birth.

So far, multiple regulators of CM proliferation have been identified (Figure 1-1). The cell cycle exit of postnatal CMs is accompanied by coherent downregulation of cell cycle activators such as cyclins and cyclin-dependent kinases (CDKs) and upregulation of cyclin-dependent kinase inhibitors (CDKIs) such as p21 and retinoblastoma (Rb) (29). Molecular mechanisms regulating cell cycle progression are shown in Figure 1-2. Ectopic introduction of cell cycle activators such as cyclin D2 and cyclin A2 and proto-oncogenes such as large T antigen promoted proliferation of postmitotic CMs (30-32). Furthermore, modulation of signaling pathways including Neuregulin1 (33), fibroblast growth factor 1 (FGF1) (34), Insulin-like growth factor 1 (IGF-1) (35) and Hippo/Wnt (36) was shown to induce CM proliferation. In addition, microRNAs regulate CM proliferation. MiR-15 family genes were upregulated in the postnatal heart and overexpression of miR-195, a member of miR-15 family genes, caused decreased CM proliferation. Despite such efforts, little is known about what occurs at the level of chromatin structure for CM cell cycle exit and what epigenetic modifiers and histone codes are involved in the process.

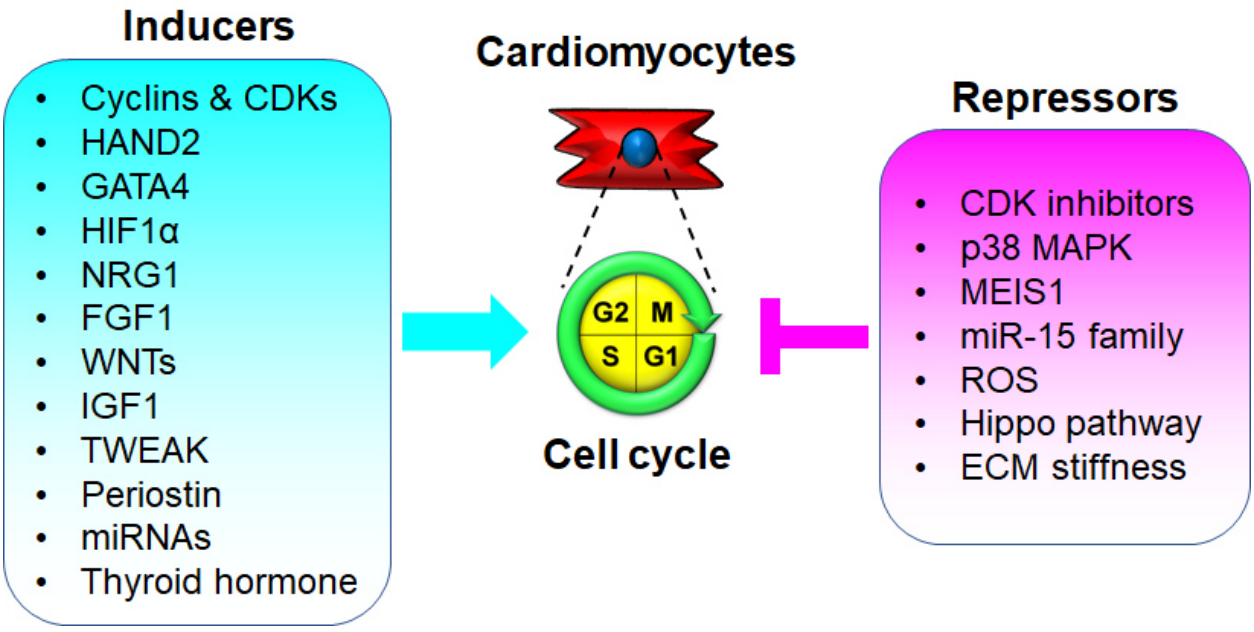

Figure 1-2. Regulators of cardiomyocyte proliferative capacity. Cell cycle activators such as Cyclins and Cyclin-dependent kinases (CDKs) are known to promote CM cell cycle activity. Transcription factors such as Heart and neural crest derivatives expressed 2 (HAND2), GATA binding protein 4 (GATA4), and Hypoxia inducible factor 1 subunit α (C) also induce CM proliferation. Growth factors and cytokines such as Neuregulin 1 (NRG1), Fibroblast growth factor (FGF1), WNTs, Insulin-like growth factor (IGF1), TNF-related weak inducer of apoptosis (TWEAK), Periostin, and Thyroid hormone play a role in stimulating CM proliferation. MicroRNAs including hsa-miR-590 and hsa-miR-199a were shown to induce CM proliferation and cardiac regeneration. On the other hand, CDK inhibitors, p38 MAPK, Meis homeobox 1 (MEIS1), miR-15 family, reactive oxygen species (ROS), Hippo/Yes-associated protein (Yap) pathway, and extracellular matrix (ECM) stiffness are known to repress CM proliferation.

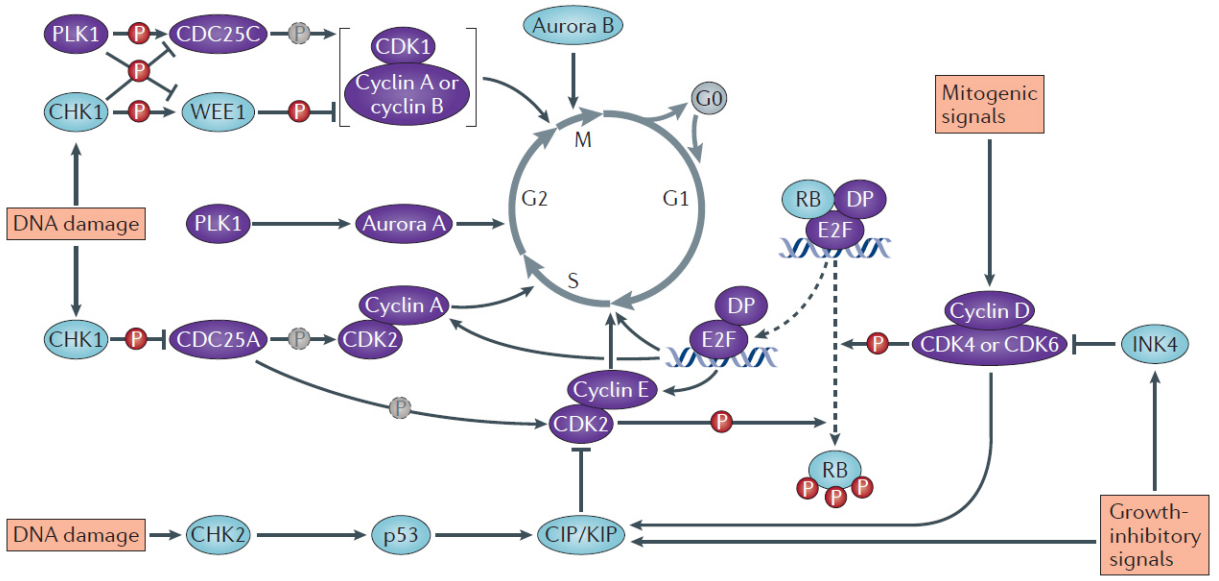

Otto et al., Nature Reviews Cancer, 2017

Figure 1-3. Major regulators of cell cycle progression. In G1/G0 phase, Retinoblastoma (RB) protein inactivates E2F/DP complex. Upon mitogenic signals, Cyclin D/CDK4 or 6 complex phosphorylates Rb, leading to its dissociation from E2F/DP complex which now work on G1/S transition together with Cyclin E/CDK2 complex. E2F/DP complex also upregulates expression of Cyclin E and Cyclin A. Cyclin A/CDK2 complex facilitates progression of S phase whereas Aurora A promotes progression of G2 phase. Transition from G2 to M phase is mediated by CDK1/Cyclin A or Cyclin B complex. CIP/KIP family proteins are inhibitors of cyclin-dependent kinases and are activated by growth inhibitory signals such as deprivation of nutrient and DNA damages. Activation of checkpoint kinase 1 (CHK1) by DNA damage results in cell cycle arrest at S and G2/M checkpoints. E2F, E2F Transcription Factor 1; DP, Differentiation regulated transcription factor proteins; CIP, CDK interacting protein; KIP, Kinase inhibitory protein.

1.4 Epigenetic regulation of cardiac development

Developmental and pathological processes in the heart are associated with coordinated epigenetic changes (37-44). As shown in Figure 1-4, chromatin remodeling proteins including JMJ, EZH2, BAF60C, and BRG1 regulate cardiac gene expression program by interacting with cardiac transcription factors such as GATA4, TBX5, NKX2-5, and TBX20. In addition, dynamic changes in DNA methylation are linked to postnatal growth of CMs (45). As shown in Figure 1-5, cardiac genes are gradually demethylated since embryonic stages. Adult CM-specific genes such as Tnnt2, Myh6, and Atp2a2 are further demethylated until adult stages and marked with active transcriptional marks such as H3K27ac. Temporarily expressed genes (fetal cardiac genes) such as Isl1 and Six1 undergo repressive chromatin modification such as H3K27me3 by EZH2 methyltransferase. Demethylated genes at neonatal stages can be repressed again by de novo methylation afterwards by DNMT3A/B. These results suggest that proliferative (fetal/neonatal) CMs have distinct epigenetic landscapes from those of post-mitotic (adult) CMs (45; 46).

Since profound chromatin changes accompany cell cycle progression (47-49), it is highly likely that postnatal cell cycle exit of CMs is mediated by global chromatin remodeling. However, critical questions remain to be answered: 1) What chromatin modifying enzymes are involved in the postnatal cell cycle exit of CMs? 2) Which genes are affected by those chromatin modifying enzymes? 3) What kind of chromatin modifications occur in target genes?

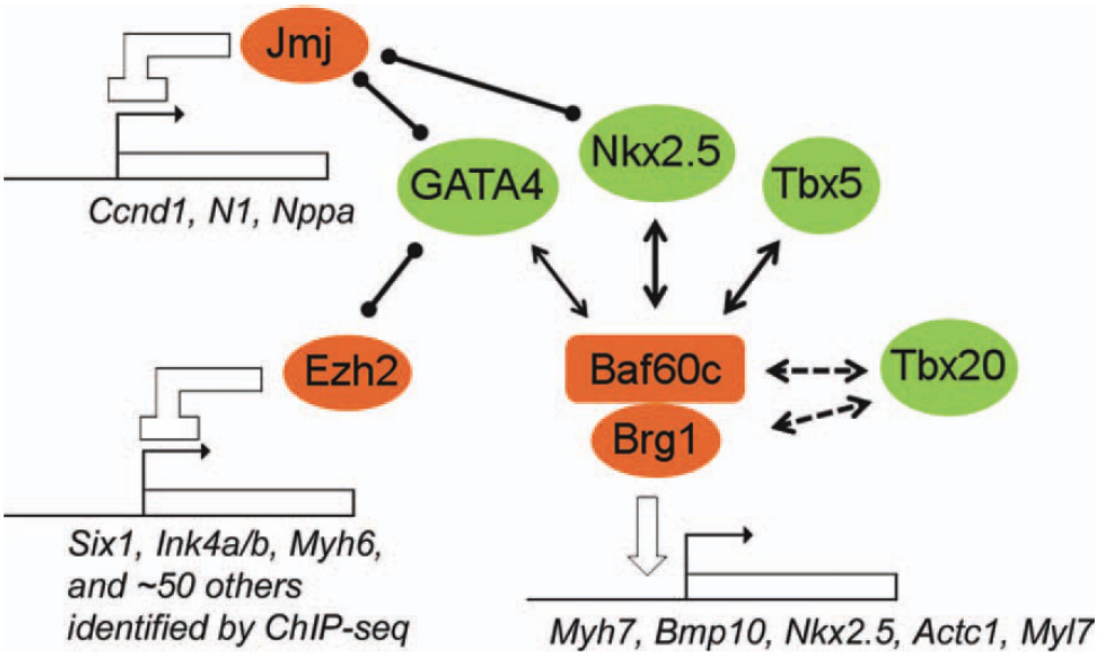

Wang et al., Developmental Dynamics, 2012

Figure 1-4. Interactions between epigenetic regulators and cardiac transcription factors. During development, cardiac gene program is controlled by epigenetic mechanisms. JMJ interacts with GATA4 and NKX2-5 whereas EZH2 binds to GATA4 to repress multiple cardiac genes. On the other hand, BAF60C interacts with GATA4, NKX2-5, and TBX5 to activate other cardiac genes. TBX20 is known to genetically interact with BAF60C and BRG1, but their physical interaction is unclear. JMJ, Jumonji-like protein; GATA4, GATA binding protein 4; NKX2-5, NK2 Homeobox 5; EZH2, Enhancer of zeste 2; BAF60C, BRG1-Associated Factor 60C; TBX5, T-Box 5; TBX20, T-Box 20; BRG1, Brahma-related gene-1.

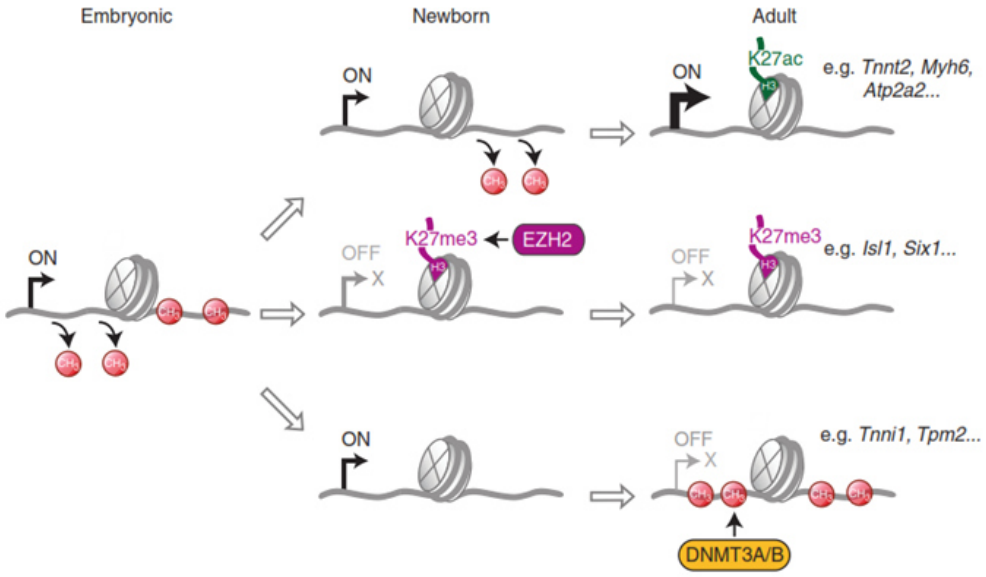

Gilsbach et al., Nature Communications, 2014

Figure 1-5. Dynamic changes in DNA methylation and histone modification during cardiac development. Overall, DNA methylation in cardiac genes are gradually decreased from embryonic stages to neonatal and adult stages. As for genes that are highly expressed in the adult heart such as cardiac troponin T and alpha myosin heavy chain, active chromatin modifications such as histone acetylation increases during adulthood. On the other hand, as for genes that are downregulated in the adult heart such as Isl1 and Six1, histone trimethylation increases since neonatal period. Finally, fetal cardiac genes such as skeletal troponin I and beta-tropomyosin are demethylated during fetal and neonatal period, but they undergo de novo methylation by DNA methyl transferease 3 (or DNMT3 in short) during adulthood. Isl1, Islet-1 (ISL LIM Homeobox 1), Six1, SIX Homeobox 1.

1.5 Polycomb group proteins and their roles in cardiac development

Polycomb group proteins are a family of proteins first discovered in fruit flies. They play a key role in epigenetic silencing of genes by remodeling chromatin structures. They regulate proliferation, differentiation, pluripotency, and senescence. Figure 1-6 shows cell cycle-related proteins controlled by Polycomb group proteins.

PcG proteins remodel chromatin structures via coordinated actions of two major types of Polycomb repressive complex (PRC) (50) (Figure 1-7). PRC2 initiates the repressing process by tri-methylation of Histone 3 tail (H3K27me3) (44). PRC1 is then recruited and stabilizes this silencing process via mono-ubiquitination of H2A tail (H2Aub) (51). Finally, H2Aub serves as a binding site for PRC2 which further propagates the H3K27me3 repressive histone mark on H2Aub nucleosomes, generating a positive feedback loop (52).

Several PcG proteins were reported to be involved in cardiac development. Deletion of EZH2 in cardiac progenitors resulted in myocardial hypoplasia, excessive trabeculation, septal defects, and RV dilation (He et al., 2012). The mechanism was that expression of cyclin-dependent kinase inhibitors such as Ink4a/b was repressed by EZH2 in the fetal CMs. Genetic ablation of EZH2 under secondary heart field driver resulted in hypertrophy and fibrosis in RV during adulthood (Delgado-Olguin et al., 2012) where EZH2 repressed fetal gene program in cardiac progenitor cells thereby maintaining postnatal cardiac homeostasis. Epithelial escape and dissemination 1 (EED1) was also reported to be essential for normal cardiac development but its exact role has not been elucidated (53; 54). Loss-of-function of JMJ resulted in excessive trabeculation, double outlet right ventricle (DORV), and ventricular septal defect (VSD). Polyhomeotic-like protein 1 (Phc1) knockout mice also exhibited cardiac defects including looping defect and VSD. These reports suggest that PcG proteins play critical roles during heart

development. However, their roles with regards to why CMs lose proliferative capacity after birth have not been explored.

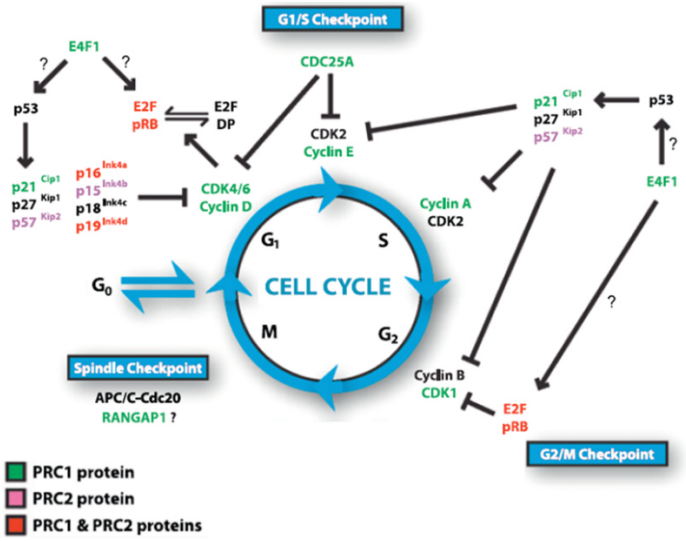

Sauvageau et al, Cell Stem Cell, 2010

Figure 1-6. Cell cycle-related proteins regulated by Polycomb repressive complexes (PRC). Green colored proteins are controlled by PRC1 whereas pink colored proteins are regulated by PRC2. Red colored proteins are governed by both PRC1 and PRC2.

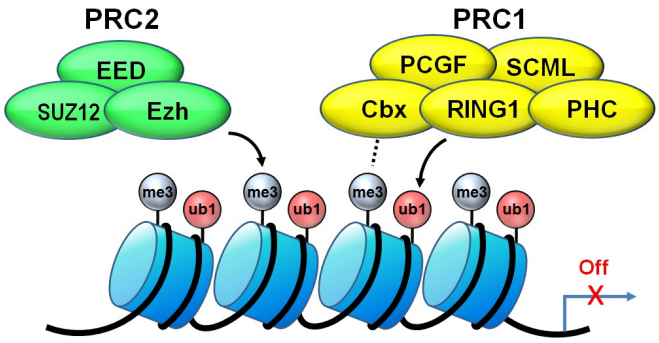

Figure 1-7. Coordinated action of Polycomb repressive complexes (PRC) for epigenetic silencing of genes. Ezh proteins in PRC2 transfer trimethyl groups on K27 residues of H3 (H3K27me3). Then, Cbx proteins in PRC1 recognize H3K27me3 and recruit PRC1. RING1 transfers mono-ubiquitin on H2A (H2Aub) to epigenetically silence target genes. me3, tri-methylation; ub1, mono-ubiquitination; RING1, Really Interesting New Gene 1 Protein.

1.6 Expression, structure, and function of Polycomb group protein CBX7

CBX family proteins are subunits of PRC1 and recognize trimethylated histone tail, thereby they determine target specificity (Figure 1-8). In other words, they recognize different epigenetic signatures and recruit other subunits, leading to silencing of different genes. There are five mammalian orthologues in CBX family: Cbx2, 4, 6, 7 and 8. CBX family members are characterized by chromodomain that binds to trimethylated histone tail (H3K9me3 and H3K27me3) (Figure 1-9). They also have Polycomb repressor (Pc) Box that interacts with other Polycomb proteins.

Among CBX family members, CBX7 is a member with the smallest molecular weight. CBX7 is expressed in various tissues such as brain, lung, liver, skeletal muscle and kidney (55). Diverse functions of CBX7 have been reported. First, CBX7 regulates pluripotency and differentiation in embryonic stem cells (ESCs) and hematopoietic stem cells (HSCs) (56; 57). Developmental genes such as Nrp1, Cdx2, and Dlk1 and progenitor-specific genes such as Bcl11a, Gfi1b, Sfp9, and Ube3c are suppressed by CBX7.

Second, CBX7 has been suggested to regulate cell proliferation, but there has been no consensus on its exact role (Table 1). CBX7 was first identified regarding its function in extending cellular life span (55). Afterwards, several groups claimed that CBX7 functions as an oncogene since it was highly upregulated in lymphoma, prostate cancer, and gastric cancer (Scott et al., 2007; Gil et al., 2004; Zhang et al., 2010). Mechanistically, CBX7 repressed senescence-related genes such as Ink4a/Arf and apoptosis-related genes such as Trail. On the other hand, other groups demonstrated that CBX7 serves as a tumor suppressor gene in various types of cancers including breast cancer, pancreatic cancer, lung cancer, thyroid cancer, colon cancer, bladder cancer and

brain cancer (55; 58-64). It was shown that CBX7 repressed transformation-related genes such as Wnt/β-catenin and cell cycle-related genes such as Cyclin E1.

Divergent observations on CBX7 function suggest that the role of CBX7 could be tissue-specific and context-specific (65). On the other hand, the mechanism of Cbx7-mediated chromatin remodeling is well understood: CBX7 acts as a reader protein for repressive histone code H3K27me3 and mediates stabilization of heterochromatin structure, leading to transcriptional repression of target genes (51; 66).

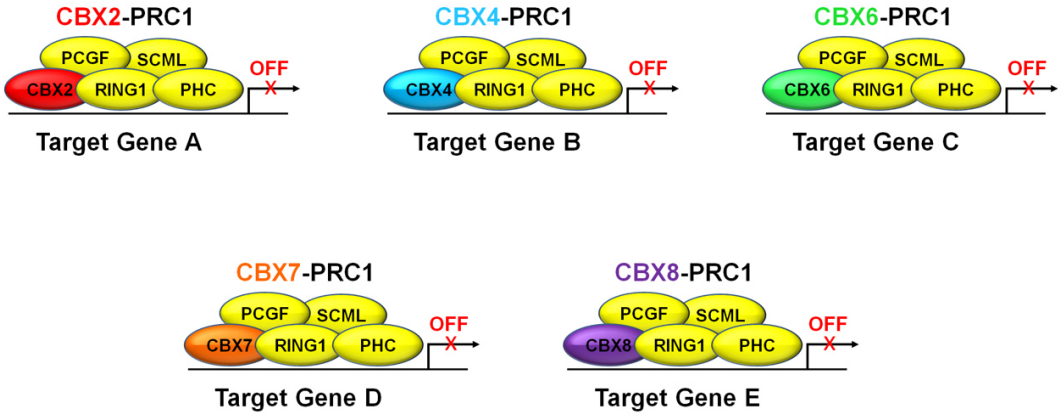

Figure 1-8. PcG target gene specificity determined by CBX family proteins. Each CBX family protein recognizes distinct chromatin context and mediates epigenetic silencing of different genes by recruiting other PRC1 subunits. Thus, target genes to be silenced by PcG proteins are determined by CBX family proteins.

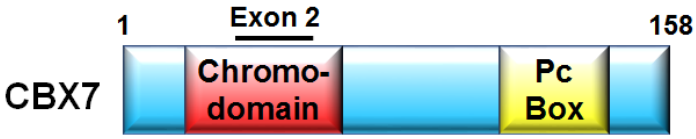

Figure 1-9. Mouse CBX7 protein structure. Exon 2 is located within the chromodomain which recognizes H3K9Me3 and H3K27me3. Polycomb repressor (Pc) Box interacts with other Polycomb proteins.

Table 1. Divergent functions of CBX7 in cell proliferation

Role	Oncogene		Tumor suppressor gene			
Target Gene Class	Senescence	Apoptosis	Transformation	Migration /Invasion	Proliferation	Unknown
Target Example	Ink4a/Arf	Trail	Wnt/β-catenin pathway E-cadherin activation	Wnt/β-catenin pathway CTGF	Cyclin E1 PTEN/Akt Pathway	Downregulation of CBX7
Cancer types	Lymphoma Prostate cancer Gastric cancer	Ovarian cancer	Breast cancer Pancreatic cancer	Glioma Glioblastoma	Glioma Lung cancer Pancreatic cancer	Thyroid cancer Colon cancer Bladder cancer Brain cancer Breast cancer
Reference	Gil, Nat Cell Biol, 2004 Bernard, Oncogene, 2005 Scott, PNAS, 2007 Zhang, J Exp Clin Can Res, 2010 O'Loghlen, Aging Cell, 2015	Shinjo, Int J Cancer, 2014	Kim, FASEBJ, 2014 Federico, Cancer Res, 2009	Bao, Oncotarget, 2017 Nawaz, Sci Rep, 2016	Forzati, JCI, 2012 Yu, Oncotarget, 2017 Hu, Oncol Lett, 2017 Ni, Oncotarget, 2017	Pallante, Cancer Res, 2008 Pallante, Eur J Cancer, 2010 Hinz S, Tumour Biol, 2008 Suarez, Neuro Oncol, 2005 Meseure, Mol Cancer Res, 2016

1.7 The objectives and scope of the dissertation

The overall objective of the current dissertation research is to explore therapeutic strategies targeting CMs for heart regeneration. In Chapter 2, we will discuss purification of ventricular CMs from differentiating mouse embryonic stem cells (ESCs) via molecular beacon technology. In Chapter 3, expression profiling of Polycomb group proteins during cardiac development will be discussed. In Chapter 4, we will discuss loss-of-function analyses of CBX7 in mice in vivo. In Chapter 5, gain-of-function analyses of CBX7 using neonatal mouse CMs in vitro will be illustrated. In Chapter 6, conclusion and future studies will be described.

Chapter 2: Non-genetic purification of ventricular cardiomyocytes from differentiating embryonic stem cells through molecular beacons targeting IRX-4

Ban K*, Wile B*, **Cho KW***, Kim S, Song MK, Kim SY, Singer J, Syed A, Yu SP, Wagner M, Bao G, Yoon YS. Non-genetic purification of ventricular cardiomyocytes from differentiating embryonic stem cells through molecular beacons targeting a ventricle-specific transcription factor. ***Stem Cell Reports***. 2015 Dec 8; 5(6):1239-49. (PMID: 26651608) (***Equal contribution**)

2.1 Introduction

Although not surface markers, several genes are known to be specifically expressed in ventricular hearts or CMs. As a ventricular-specific transcription factor, Iroquois homeobox protein 4 (IRX4) has been reported to be exclusively expressed in the ventricular myocardium while absent from both atria and the outflow tract (67). IRX4 positively regulates ventricular-chamber-specific gene expression by activating the ventricular myosin heavy chain-1 (VMHC1) gene while suppressing the expression of atrial myosin heavy chain-1 (AMHC1) (68; 69). As a structural protein, MYL2 (or MLC-2v), one of the essential MLC-2 isoforms that is important for the contractile function of ventricular CMs, is expressed in ventricular CMs (70). MYL2 expression is mostly restricted to the ventricular segment of the heart with minimal expression in the outflow track during cardiogenesis (71).

Accordingly, we have developed a method targeting an intracellular gene to purify ventricular CMs. We used a molecular beacon (MB)-based method for isolating a pure population of ventricular CMs by targeting the mRNA of the ventricular-specific transcription factor IRX4 (Figure 2-2). MBs are 20- to 30-bp oligonucleotide probes with a fluorophore and a quencher at the 50 and 30 ends, respectively (72). They are designed to form a stem-loop (hairpin) structure so that the fluorophore and quencher are within close proximity and fluorescence is quenched. Hybridization of the MBs with the target mRNA opens the hairpin structure and physically separates the fluorophore from the quencher, allowing a fluorescence signal to be emitted upon excitation (73). It has been demonstrated that cellular delivery of MBs does not alter the expression level of the target genes (74-76), and MBs can be used to isolate mESCs by directly targeting specific intracellular mRNAs such as Oct4 (74). Further, we demonstrated that MBs enable the enrichment of general CMs from differentiating mouse and human PSCs (77).

In the present study, we developed a sophisticated approach using MBs targeting transcription factor mRNAs, which, due to their low copy numbers compared to structural protein mRNAs, are highly challenging and were not previously attempted. By designing specific MBs targeting Irx4 mRNA, we show here that functional ventricular CMs derived from differentiating mouse ESCs could be isolated with high purity. The MB-based cell isolation method is quite versatile; a wide range of specific intracellular mRNAs could be targeted to achieve high specificity, including mRNAs encoding structural proteins and transcription factors.

2.2 Results

2.2.1 Ventricular cardiomyocyte-specific gene selection and generation of IRX4 MBs

Through an extensive literature search, we selected Irx4 as a target gene for generating ventricular CM-specific MBs (67-69). First, we measured mRNA expression levels of Irx4 via qRT-PCR analysis in CMs isolated from either ventricles or atria of mouse adult hearts. We also measured Myl2, which is a well-defined ventricular CM-specific gene, as a positive control. The results showed that Irx4 was robustly expressed in ventricular CMs, but not atrial CMs (Figure 2-1). The expression levels of both Irx4 and Myl2 mRNAs were substantially higher in mouse ventricular CMs compared to atrial CMs, indicating that Irx4 is a viable target for MB selection.

We designed three IRX4 MBs targeting distinct sites in the mouse Irx4 mRNA using design rules validated in our previous publications (Figure 2-2) (73; 74; 77). In addition, we used mFold (78) and the RNA Composer Webserver (79) to model the IRX4 MB designs and to predict the accessibility of hybridization sites in the target mRNAs. These IRX4 MBs were synthesized with a Cy3 fluorophore on the 50 end and a Black Hole Quencher 2 (BHQ2) on the 30 end as specified in Table 2. We quantified MB fluorescence signals when hybridized to perfectly complementary or mismatched synthetic DNA targets by incubating 500-nM MBs in solution with increasing concentrations (60–500 nM) of DNA targets. IRX4 MB signals were recorded using a microplate reader and normalized by the background signals in wells with MBs only. All IRX4 MBs displayed a linear response to increasing concentrations of complementary targets and low signal levels when mismatched targets were used (Figure 2-1).

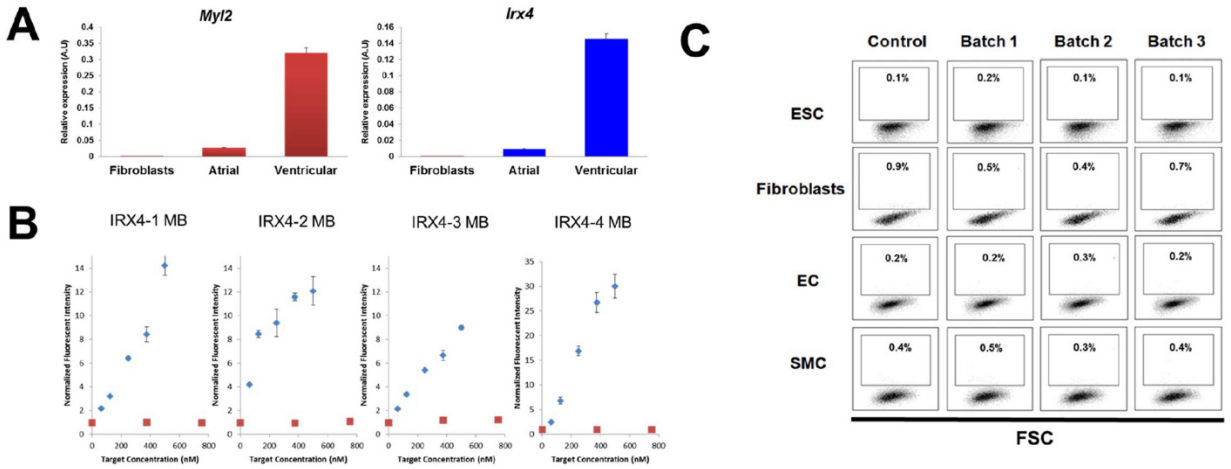

Figure 2-1. Verification of *Irx4* mRNA as a target for ventricular CM specific MB generation. (A) qRT-PCR analysis was performed for *Irx4* and *Myl2* (also known as *Mlc2v*) mRNAs extracted from mouse cardiac fibroblasts and adult mouse atrial or ventricular CMs to determine optimal candidate genes for generating CM-specific MBs. Y axis represents relative mRNA expression of target genes to GAPDH. *P < 0.001. Data are represented as mean ± SEM. All experiments were performed on three independent biological replicates. (B) Hybridization specificity of IRX4 MBs. Each IRX4 MB was incubated with its synthetic 20-30 bp complementary sequence (blue) in PBS solution at 37°C to verify that they would respond to increases in target concentration in a linear fashion. MB fluorescence was measured within 10 minutes to ensure quick signal response and robust signal maintenance. The MBs were also tested against synthetic targets with 6 bp mismatches (red) under identical conditions. All experiments were performed on three independent biological replicates. (C) Specificity of IRX4-2 MBs on several types of non-cardiomyocyte cells. Flow cytometry analysis demonstrated that IRX4-2 MB detected non-cardiomyocyte cells such as SMCs, mECs, mCFs and mESCs at a very low rate. FSC indicates forward scatter.

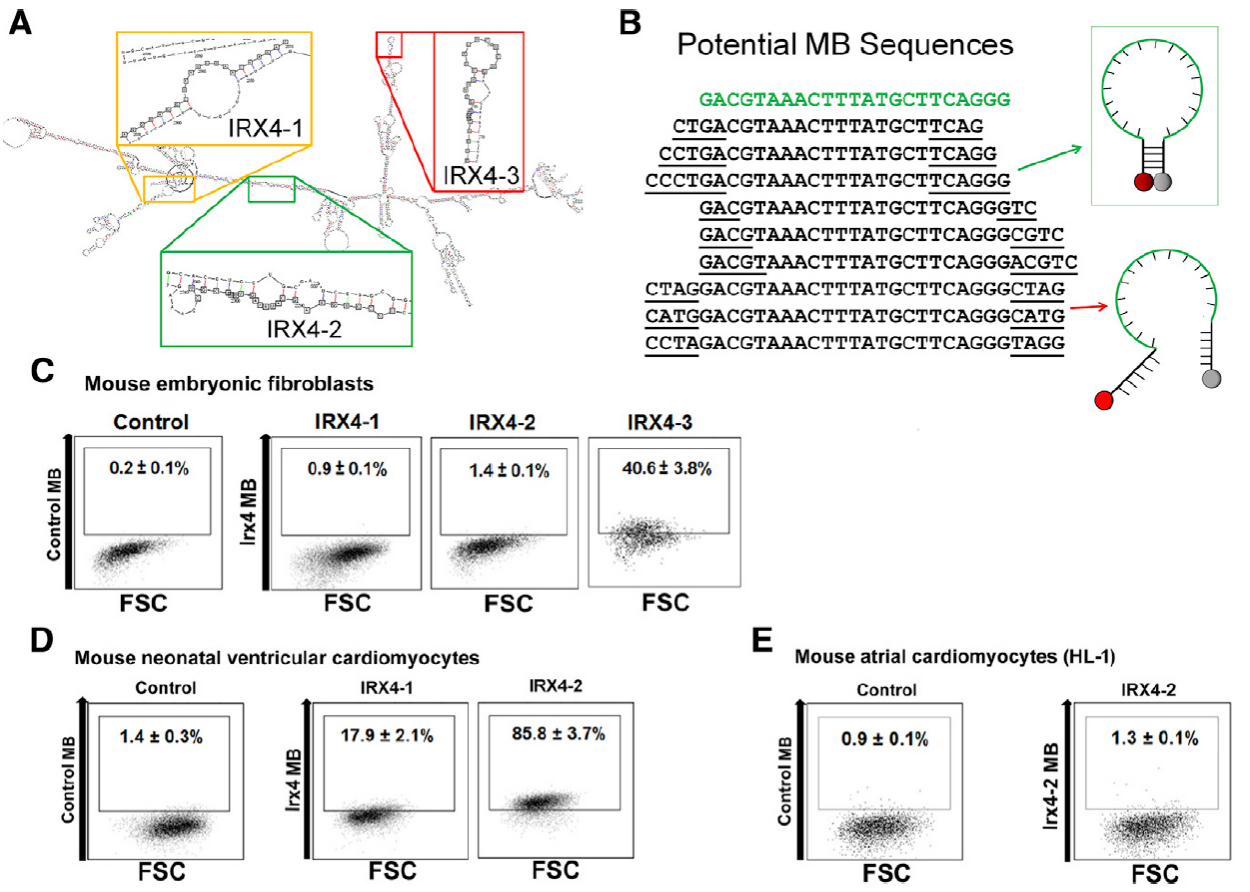

Figure 2-2. Selection of optimal ventricular cardiomyocyte-specific IRX4 molecular beacons. (A) Irx4 mRNA structure was predicted using the RNAfold web server. Three unique target sequences were identified in Irx4 mRNA that maximized the number of predicted unpaired bases as well as the binding affinity of a complementary probe. (B) Stem sequences were appended to the complementary sequence and evaluated using QUIKFOLD to minimize the free energy that causes the oligonucleotide to assume a hairpin structure in solution. (C–E) Flow cytometry results after delivering various IRX4 MBs designed to identify Irx4 mRNAs, or control MB, into mouse embryonic fibroblasts (C), eonatal mouse ventricular CMs (D), and HL-1 CMs (E). The number in each panel represents the percentage of fluorescent cells. FSC indicates forward scatter. All experiments were performed on three independent biological replicates (C–E).

Table 2. IRX-4 MB designs

Beacon Design	Beacon Sequence (5′–3′)[a]	Target Sequence (5′–3′)
IRX4-1	*Cy3*-CACCTAGTTTTGTTATATTAGCCTCCCTAGGTG-*BHQ2*	AGGGAGGCTAATATAACAAAAC
IRX4-2	*Cy3*-CCCTGACGTAAACTTTATGCTTCAGGG-*BHQ2*	CCCTGAAGCATAAAGTTTACGTC
IRX4-3	*Cy3*-CAGGCAGAGAGTAGAAAGCAGATGCCTG-*BHQ2*	AGGCATCTGCTTTCTACTCTCTG
Control MB	*Cy3*-ACGACGCGACAAGCGCACCGATACGTCGT-*BHQ2*	GTATCGGTGCGCTTGTCGCG

[a]Underlined bases indicate the arms forming the stem.

2.2.2 Delivery of MBs into different cell types

After testing several different methods for cellular delivery of MBs, we found that the use of a Nucleofector (Lonza) with Nucleofection Solution V and program A033 was an efficient method (up to 99%) to deliver MBs to a variety of cell types (77). To further refine this approach, we also designed two distinct MBs as controls. The first was a non-specific interaction indicator MB (RQ) that contained a 20-bp loop sequence given by random walk, which did not have any perfect matches in the entire mouse genome. Therefore, any fluorescence resulting from this control MB would be non-specific signal. The second was a delivery control MB (UQ) with the same random sequence, but it did not contain a quencher, so it fluoresced at all times. Both RQ and UQ MBs were delivered to cells to ensure that delivery was efficient and that MB signal was specific to the target mRNA sequence.

2.2.3 Selection of optimal IRX4 MB for isolating ventricular-like CMs

In order to select the best MB to efficiently identify and isolate ventricular CMs, we examined the specificity, sensitivity, and reliability of each IRX4 MB in three separate systems. To determine the specificity of MBs, we used nucleofection to deliver each of the three IRX4 MBs into mouse embryonic fibroblasts (mEFs), which do not express IRX4, and analyzed the cells that showed false-positive signals using flow cytometry. We found that among the three MB designs (IRX4-1, IRX4-2, and IRX4-3) examined, IRX4-1 and IRX4-2 MBs yielded significantly fewer false-positive cells from mEFs (IRX4-1: 0.9% ± 0.1%, and IRX4-2: 1.4% ± 0.1%) than IRX4-3 MB (40.6% ± 3.8%). Hence, only IRX4-1 and IRX4-2 MBs were selected for further experiments (Figure 2-2). To evaluate the detection sensitivity of IRX4-1 and IRX4-2 MBs, each was delivered into mouse neonatal ventricular CMs and analyzed with flow cytometry. IRX4-2 MBs resulted in a substantially higher percentage of ventricular CMs (85.8% ± 3.7%) compared to IRX4-1 MBs (17.9% ± 2.1%). On the basis of these results, we selected IRX4-2 MB as the probe for enriching mESC-derived ventricular CMs (Figure 2-2).

To further confirm detection specificity, we delivered the IRX4-2 MB to HL-1 CMs, an immortalized mouse atrial CM cell line known to retain atrial CM characteristics (80; 81). Flow cytometry analysis showed that less than 2% of HL-1 CMs displayed a positive signal from IRX4-2 MBs, providing additional support for the high specificity of IRX4-2 MB in isolating ventricular CMs (Figure 2-2). We also tested the IRX4-2 MB against the most likely contaminating cell types in cardiomyogenically differentiated PSC cultures: mouse smooth muscle cells (SMCs), mouse aortic endothelial cells (mECs), mouse cardiac fibroblasts (mCFs), and mESCs (Figure 2-1). Flow cytometry analysis showed that less than 3% of those cells displayed detectable fluorescence

signals. These results clearly demonstrated that the IRX4-2 MB is specific for identifying ventricular CMs.

2.2.4 Generation of ventricular CMs from mESCs

To ensure stable production of mESC-derived ventricular CMs, we first established an embryoid body (EB)-mediated CM differentiation system (Figure 2-3). Undifferentiated mouse ESCs (J1) maintained on STO feeder cells were enzymatically detached to form EBs. Since EB-induced differentiation alone is not sufficient to produce a high percentage of CMs, we plated day-4 EBs into a fibronectin-coated dish and added ascorbic acid (50 mg/ml) to enhance CM differentiation. Spontaneously beating clumps began to appear 3–4 days after plating (82). After 7 days of CM differentiation on monolayer cultures, we enzymatically dissociated the cells and applied them to a discontinuous Percoll gradient (40.5% to 58.5%) to enrich mESC-derived CMs (83). Percoll-mediated separation typically produces three layers of cells, and the bottom layer was reported to include a higher percentage of CMs. Thus, the cells in the bottom layer were collected and cultured for another 7 days in the presence of cyclosporine A (30 mg/ml) to further induce CM differentiation (84). Finally, we applied IRX4 MBs to these 18-day cultured mESC-derived CMs. qRT-PCR analysis revealed dynamic changes in the expression of CM-specific genes in our differentiation system, indicative of efficient CM differentiation. Expression of cardiac contractile genes (Tnnt2 and Myh7) and genes for atrial (Myl7) and ventricular (Myl2 and Irx4) CMs began to appear 7 days after culture. Expression of Myl2 and Irx4 continuously increased until day 18 (Data not shown). We next carried out immunocytochemistry and flow cytometry to further characterize the cell population at day 18. Immunocytochemistry demonstrated that day-18 cells significantly expressed CM-specific proteins, including ACTN2 (a-sarcomeric actinin), TNNT2 (cardiac troponin T), and MYH6/7 (a and b myosin heavy chain), confirming their CM nature (Data not shown). A substantial number of cells that were positive for ACTN2, TNNT2, and MYH6/7 concomitantly expressed MYL2 (or MLC2V), which is a specific protein for ventricular

CMs. At day 18, the percentages of cells expressing TNNT2 or MYL2 were 67.9% ± 4.5% and 39.2% ± 3.8%, respectively, and 35.5% ± 4.1% of cells expressed both TNNT2 and MYL2. These results clearly indicate efficient generation of CMs, with a significant percentage of ventricular CMs, through our CM differentiation system.

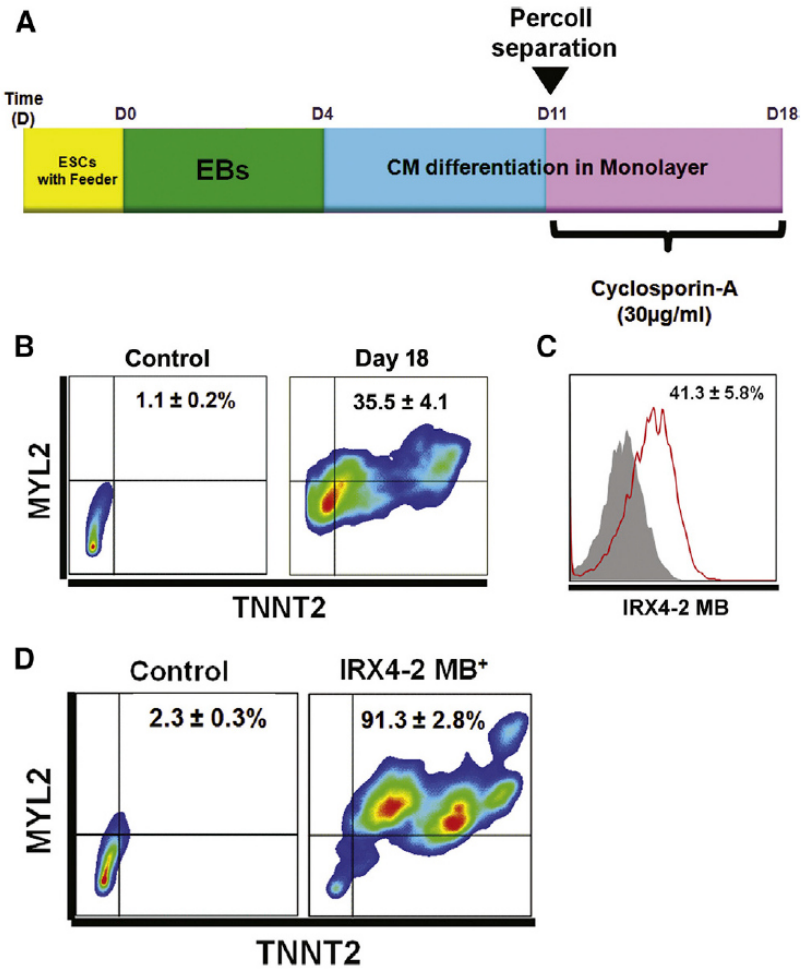

Figure 2-3. Purification of ventricular CMs from differentiating mESCs through IRX4-2 MBs. (A) A schematic of the protocol to differentiate mESCs to the cardiac lineage. ESCs, mouse embryonic stem cells; EBs, embryoid bodies. (B) Flow cytometric scattergrams showing the percentages of cells expressing both TNNT2 and MYL2 at differentiation day 18. (C) A flow cytometry plot showing IRX4-2-MB-positive cells at differentiation day 18. (D) Flow cytometric scattergrams showing the percentages of cells expressing both TNNT2 and MYL2 after FACS sorting with IRX4-2 MB. All experiments were performed on three (B and D) or six (C) independent biological replicates.

2.2.5 Purification of mESC-derived ventricular CMs through IRX4-2 MBs

After establishing the CM differentiation system, we delivered IRX4-2-MB to the 18-day differentiated cells to isolate ventricular CMs.We used a pre-validated nucleofection protocol to deliver MBs and sorted the cells by fluorescence-activated cell sorting (FACS). Flow cytometry results showed that 41.3% ± 5.8% of cells were positive for fluorescence signal from IRX4-2 MB (Figure 2-3). This number is similar to the detection rate (39.2% of Myl2-positive cells) of ventricular CMs using antibody-based methods. We then conducted FACS sorting based on IRX4-2-MB signal, and the MB-positive CMs were seeded onto fibronectin-coated plates for further experiments. The IRX4-2-MB-positive CMs began to beat spontaneously within 48 hr and continued to beat vigorously for up to 2 weeks. Only a small number of IRX4-2-MB negative cells showed beating (data not shown). To determine the cell viability after IRX4-2-MB-based cell sorting, we performed a propidium iodide (PI)-based cell viability assay (85; 86). To this end, two groups of cells were treated with PI: one group that underwent FACS sorting with IRX4-2 MB transfection and the other without IRX4-2 MB transfection. Then, we performed flow cytometry to measure the PI-negative, or viable, cells. Flow cytometry analyses showed that ~55.5% of the IRX4-2-MB-transfected group was PI negative as was ~63.4% of the group without IRX4-2 MB transfection (Data not shown), suggesting ~8% cell damage caused by MBs. Two days after FACS sorting, we conducted flow cytometry analyses using TNNT2 and MYL2 antibodies to quantify the percentage of CMs and ventricular-like CMs in IRX4-2-MB-positive cells. The percentage of cells expressing either TNNT2 or MYL2 was 97.2% ± 3.4% or 91.6% ± 5.1%, respectively, and that expressing both TNNT2 and MYL2 was 91.3% ± 2.8% (Figure 2-3). Together, these results indicate efficient enrichment of mESC-derived ventricular CMs by IRX4-MB-based cell sorting.

2.2.6 Electrophysiological characteristics of IRX4 MB^+ ventricular-like CMs

To investigate the electrophysiological characteristics of IRX4-2-MB-positive and -negative CMs, we performed whole-cell patch clamp analyses (Figure 2-4). It is known that the action potential duration (APD) is longer in mouse fetal ventricular CMs than in atrial CMs (Figure 2-4) (87). Similarly, we found that IRX4-2-MB positive CMs displayed substantially longer APDs than IRX4-2-MB-negative cells (Figure 2-4). APD50 was also longer in IRX4-2-MB-positive cells than in IRX4-2-MBnegative cells (159 ± 21.7 ms versus 35 ± 7.8 ms, $p < 0.01$) (Figure 2-4B). On the basis of these results, we found that 98% of IRX4-2-MB-positive cells possessed ventricular type action potentials (APs) (49 out of 50 cells), which showed electrical synchronism, whereas atrial- or nodaltype APs were not observed in these cells (Figure 2-4). Due to the small number of contracting cardiomyocytes in the IRX4-2-MB-negative cells, we were unable to appropriately measure the APs. Alternatively, we performed immunostaining to verify the identity of the IRX4-2-MB-negative cells with CM-specific antibodies. Immunocytochemistry demonstrated that none of the IRX4-2-MB-negative cells expressed the ventricular CM marker MYL2, and less than 20% of them expressed ACTN2, suggesting that there are some CMs, but no ventricular CMs, in the IRX4-2-MBnegative population (Data not shown). Next, we performed multielectrode arrays (MEAs) to investigate the synchronous activities of the purified CMs. While IRX4-2-MB-negative cells showed limited and nonsynchronous electrical activities, IRX4-2-MB-positive CMs demonstrated regular and synchronous APs, suggesting a well-coupled syncytium of cells with appropriate CM electrophysiological characteristics in the IRX4-2-MB-positive population. Lack of electrical activity measured in the IRX4-2-MB-negative cells may be due to a higher proportion of non-CM cell types in this population (Data not shown). Last, we performed real-time intracellular calcium [Ca2+]i imaging analysis with IRX4-2-MB-sorted ventricular CMs in

comparison to fetal mouse atrial and ventricular CMs (Figure 2-4D). In this analysis, all three types of CMs showed automaticity, but the patterns of calcium transients of IRX4-2-MB-positive CMs were similar to ventricular CMs, but not to atrial CMs; the frequency was slower and the amplitude was larger in IRX4-2-MB-positive CMs and ventricular CMs compared to atrial CMs (Figure 2-4E). Collectively, these results demonstrated that the IRX4-2-MB-positive cells possess ventricular-CM-like electrophysiological properties.

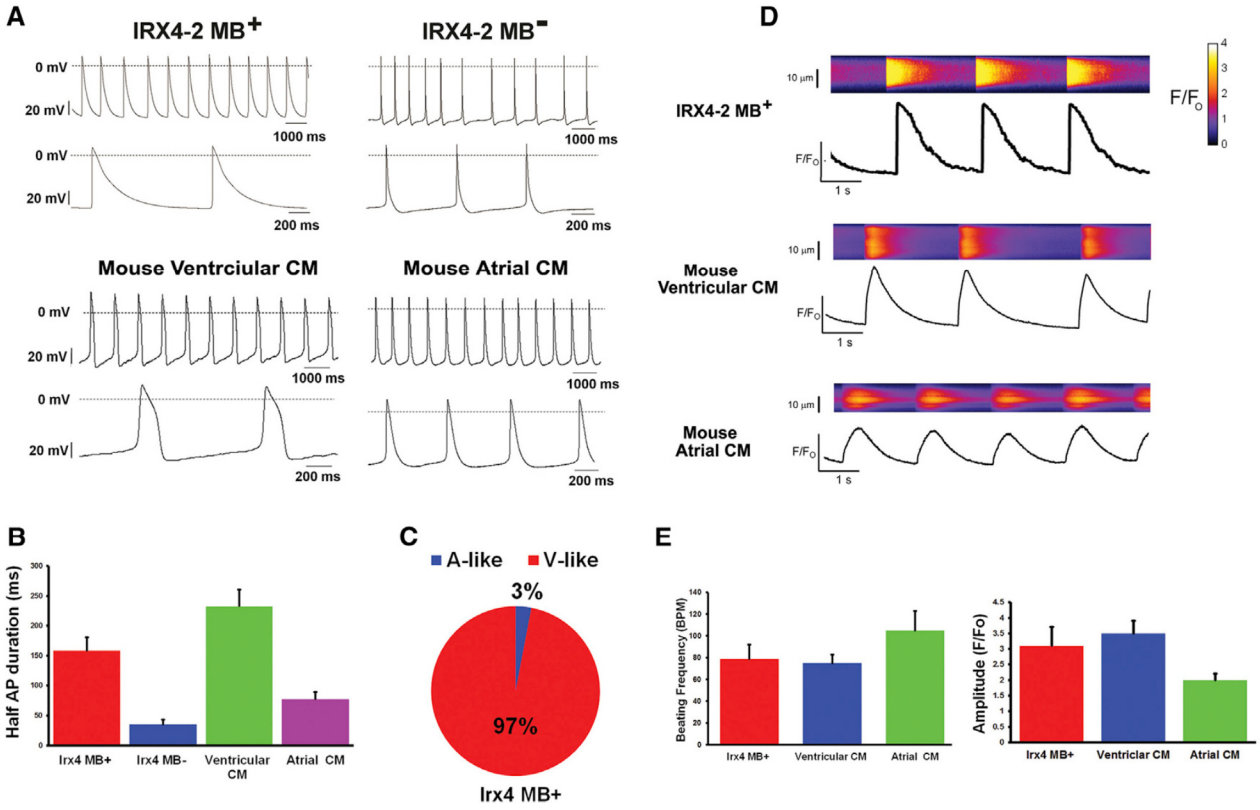

Figure 2-4. Electrophysiological characteristics of IRX4-2-MB-purified ventricular CMs. (A) Representative action potentials of IRX4-2-MB-positive and -negative cells (upper panel) and primarily isolated mouse fetal ventricular and atrial cardiomyocytes (lower panel). (B) Half action potential duration (APD50) of IRX4-2-MB-positive and -negative cells and mouse fetal ventricular and atrial cardiomyocytes. (C) The percentages of the action potential types recorded from IRX4-2-MB-positive cells. A-like, atrial-like AP; V-like, ventricular-like AP. Action potentials were measured from 50 cells in each group (A–C). (D) Representative spontaneous calcium transients in IRX4-2-MB-positive cardiomyocytes (upper panel), mouse primary fetal ventricular cardiomyocytes (middle panel), and mouse primary fetal atrial cardiomyocytes (lower panel). In each panel, calcium transients were recorded in the upper section, where increasing calcium is indicated by the change in color from dark blue to light blue, and fluorescence intensity was normalized to the baseline measured at time 0 (Fo). (E) The averages of the beating frequency

(BPM) and calcium amplitude (F/F0) of IRX4-2-MB-positive cells and mouse fetal ventricular and atrial cardiomyocytes. Calcium transient experiments were performed on 15 cells in each group (D and E).

2.2.7 Cellular characterization of FACS-sorted ventricular-like CMs

To examine the cardiac identity and homogeneity of the ventricular CMs purified with IRX4-2 MB, immunocytochemistry was conducted with antibodies against various CM-specific markers (ACTN2, TNNT2, and MYH6/MYH7 and MYL2) and a ventricular CM marker (MYL2) 2–3 days after FACS sorting and cell culture. As shown in Figure 2-5A, immunocytochemistry demonstrated that almost all IRX4-2-MB-isolated ventricular CMs exhibited ACTN2, TNNT2, and MYH6/MYH7. Furthermore, a positive immunoreactivity for MYL2 was found in all of the IRX4-2-MB-positive CMs (Figure 2-5A). Importantly, these IRX4-2-MB-positive CMs abundantly expressed GJA1 (known as connexin 43), an important connexin isoform in the formation of gap junctions between ventricular CMs, indicating that these enriched ventricular CMs possess the functional capability of forming cardiac junctions (Figure 2-5B). qRTPCR analyses further demonstrated that expression of ventricular CM genes Irx4 and Myl2 was substantially increased in IRX4-2-MB-positive cells compared to the IRX4-2-MBnegative cells (Figure 2-5C). Furthermore, these IRX4-2-MB-positive cells showed a significant increase in the expression of general CM-specific genes (Tnnt2 and Myh6/Myh7) compared to the IRX4-2-MB-negative cells (Figure 2-5C). Genes representing atrial-specific CMs (Myl7) or other cell types were either expressed at negligible levels (Acta2, Ddr2, and MyoD) or were non-detectable (Pecam1 and Neuro D) in the IRX4-2-MB-positive cells (Figure 2-5C and data not shown). Taken together, our results clearly demonstrated that IRX4-2 MBs targeting ventricular CM-specific mRNA in living cells enabled the isolation of functional ventricular CMs from differentiating mESCs with high specificity and efficiency.

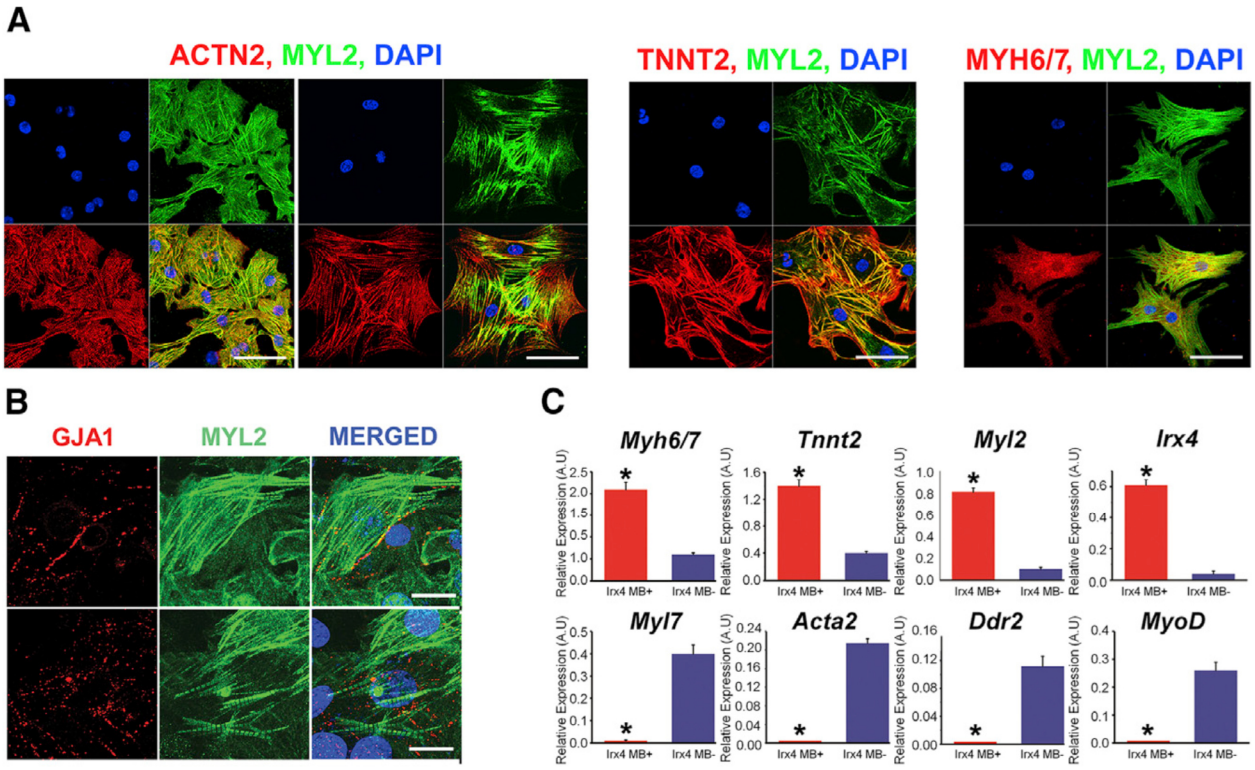

Figure 2-5. Characterization of purified ventricular CMs through IRX4-2 MBs. (A) Immunocytochemistry for ACTN2, TNNT2, and MYH6/MYH7 on IRX4-2-MB-positive cells isolated from cardiomyogenically differentiated mESCs. Scale bars, 20 mm. (B) Expression of GJA1 determined by immunocytochemistry on IRX4-2-MB-positive cells isolated from cardiomyogenically differentiated mESCs. Scale bars, 50 mm. (C) mRNA expression of cardiac (Myh6/Myh7 and Tnnt2), ventricular (Myl2 and Irx4), atrial (Myl7), and non-cardiac genes (Acta2, Ddr2, and MyoD) in IRX4-2-MB-positive and -negative cells measured by qRT-PCR. y axis represents relative mRNA expression of target genes to GAPDH. *$p < 0.05$ compared to in IRX4-2-MB-negative cell group. Data are represented as mean ± SEM. All experiments were performed on three independent biological replicates.

2.3 Discussion

Our study demonstrates that specific cells could be isolated with high specificity by targeting the mRNA of a transcription factor using MBs. This marks a significant advance of the method we developed recently, where the use of MBs targeting the mRNA of a structural protein (MYH) allowed sorting of general CMs from differentiating human and mouse PSCs (77). Since the mRNA expression of a transcription factor is usually much less abundant than that of a structural protein, it was very challenging to apply the MB-based method for the isolation of these specific cells. In fact, we initially designed MBs targeting another transcription factor, NKX2.5, but the MB signal level was not high enough for isolating CMs using FACS. Another major challenge was to identify an optimal delivery method to internalize a large amount of MBs (e.g., > 2,000 per cell) in order to generate a sufficiently high fluorescence signal when hybridized to target mRNAs. We tested quite a few different methods to deliver MBs into living cells, including the use of Streptolysin O, Lipofectamin 2000, Lullaby, microinjection, and nucleofection, and found that nucleofection with a specific buffer solution induced the maximal target mRNA detectability with minimal cytotoxicity (data not shown). We and others have found that after delivery into living cells, MBs do not affect the expression of the target mRNA or other mRNAs (74), and they degrade within a few hours so that their effects on cell viability and cell functionality are negligible (74-77; 88). Even with repetitive delivery of MBs, we did not observe phenotypic or functional changes of cells, as evidenced by the unaffected spontaneous contraction and the results of immunocytochemistry assays shown in this study.

Other RNA detection methods, such as the SmartFlare system (89-91) and ratiometric bimolecular beacons (RBMB) (92; 93), have recently been developed. According to the published reports, both systems can generate sufficient and specific signals to be able to identify less

abundant mRNA transcripts (90; 92). In addition, the cellular delivery of the SmartFlare systemisgenerally easydueto the natural cellular uptake of the nanoparticles (89-91). Nevertheless, the major advantages of an MB-based method over these two methods are the entropic bonus of a single molecule systemand the ability to rapidly iterate design parameters. Since a standard MB is a single-molecule system, the enthalpy of the stemcan be significantly lower than the SmartFlare or RBMB systems while still generating similar binding affinities for the target mRNA (72; 94). In addition, there are a multitude of online software tools that predict single-stranded RNA structure. The RBMB system equires a more complicated two-molecule simulation, and the SmartFlare systemrequires both a competitive binding calculation to be performed and the effect of steric hindrance to be considered due to the relatively large delivery particle.

We believe that the production of homogeneous and functional PSC-derived ventricular CMs using a non-transgenic approach will open new avenues for basic research and clinical applications. First, a pure population of ventricular CMs generated by the MB-based method offers a safer and more effective option for cell therapy and tissue engineering compared to the use of mixed populations of PSC-derived CMs, which are more likely to cause abnormal electrical activity (24) or less efficient contractile function (95). From a research perspective, the MB-purified ventricular CMs represent a powerful in vitro tool for disease investigation and drug discovery. They can be used as better-defined in vitro model systems for genetic or idiopathic cardiac diseases such as long QT syndrome (96; 97). They can also serve as an in vitro model to test chamber-specific effects of candidate cardiac drugs (98). These purified CMs will yield more accurate genetic and epigenetic information through high throughput sequencing techniques. We anticipate that this MB-based cell-sorting method can be adopted for isolating other cardiac cells,

such as nodal cells and atrial CMs, and has the potential to be used in isolating other cell types from differentiating PSCs, such as neuronal cells and pancreatic β cells.

2.4 Materials and Methods

MB Synthesis and Characterization

Three IRX4 MBs were synthesized by MWG Operon with high pressure liquid chromatography (HPLC) purification (Table 2) (77). IRX4 MBs were re-suspended in nuclease-free PBS buffer (pH 7.4) to minimize buffer incompatibility with cells. IRX4 MBs were tested against synthetic 20- to 30-bp complementary sequences in PBS solution to verify their activity. To demonstrate specificity, MBs were also tested against synthetic targets with 6-bp mismatches. Mouse ESC Culture and Differentiation mESCs (J1) were maintained as described previously (77). To differentiate mESCs into cardiac lineage, an embryoid body method was used with some modifications.

Flow Cytometry

After nucleofection, cells were centrifuged at 1,500 rpm for 2 min, re-suspended in DMEM/F12 basal media, and maintained on ice for 20 min to recover. Cells were then analyzed by C6 Flow Cytometer (BD Biosciences) or sorted using a BD FACS Aria II cell sorter (BD Biosciences). MB signal was recorded using a 561-nm laser with a 585/15-nm emission filter to optimally excite and detect Cy3. For MB experiments, negative control MB (Table 2), whose loop sequence was generated using ‘‘random walk’’ and does not match with any mRNA sequence in the entire mouse genome, was used as a negative control for gating. For intracellular flow cytometry (TNNT2 and MYL2) analyses, isotype control antibodies were used as negative controls for gating. Data were analyzed using FlowJo software (Treestar).

Cell Viability Assay

FACS-sorted cells were resuspended in 1 ml of flow cytometry staining buffer and 5 ml of PI staining solution (Sigma) to each sample just prior to analysis. Then it was mixed gently and incubated for 1 min in the dark. PI fluorescence was determined by C6 Flow Cytometer (BD Biosciences) using the FL-2 channel at 488-nm laser illumination. Finally, the obtained results were compared to unstained cells and single-color positive controls.

Immunocytochemistry

Cells were fixed with 4% paraformaldehyde for 10 min at room temperature, washed twice with PBS, and permeabilized with 0.1% or 0.5% Triton X-100 in PBS for 10 min. Samples were then blocked with 1% BSA in PBS for 60 min at room temperature and incubated with anti-Actn2 (Sigma, #A7811; 1:100), mouse anti-Tnnt2 (Thermo, #MS295P1; 1:100), anti-Myl2 (Proteintech Group, #55462-1-AP; 1:100) or Gja1 (BD, #610062; 1:100) at 4ºC overnight. The cells were washed three times with 1% Tween 20 in PBS and incubated with anti-mouse immunoglobulin G (IgG)-Alexa Fluor 594 (Thermo, #A-11005; 1:1,000) or anti-rabbit IgGAlexa Fluor 488 (Thermo, # A-11008; 1:1,000) in PBS for 1 hr at room temperature. DAPI was used for nuclear staining. The samples were visualized under a fluorescent microscope (Nikon) and a Zeiss LSM 510 Meta confocal laser scanning microscope and LSM 510 Image software (CLSM, Carl Zeiss).

qRT-PCR

Total RNA was prepared with the RNeasy Plus Mini Kit (Qiagen) according to the manufacturer's instructions. The extracted RNA (100 ng to 1 mg) was reverse transcribed into cDNA (reverse transcription) via Taqman reverse transcription reagents, including random hexamers, oligo (dT),

and MultiScribe MuLV reverse transcriptase (Applied Biosystems). qPCR was performed on a 7500 Fast Real-Time PCR system (Applied Biosystems) using Fast SYBR Green master mix (Applied Biosystems). All annealing steps were carried out at 60ºC. Relative mRNA expression of target genes was calculated with the comparative CT method. All target genes were normalized to Gapdh in multiplexed reactions performed in triplicate. Differences in CT values (DCT = CT gene of interest ΔCT Gapdh in experimental samples) were calculated for each target mRNA by subtracting the mean value of GAPDH (relative expression = 2–DCT).

Intracellular Calcium Imaging

For calcium (Ca2+) imaging, IRX4-2-MB-based purified cells ESCCMs were plated on glass coverslips and were loaded with 5 mM fluo4 AM for 15 min in culture medium. Coverslips with cells were transferred to a temperature-controlled chamber on an Olympus Fluoview 1000 confocal microscope and washed with physiologic salt solution (Tyrode's) for 20 min for de-esterification of the dye. Experiments were done at 35ºC. Linescan images were taken for cells showing calcium cycling. Calcium transients were analyzed using Clampfit software (Molecular Devices), and measures parameters such as amplitude, rise time from half amplitude to peak, and decay time from peak to half amplitude were averaged for 5–10 beats for each cell.

Action Potential Measurement

For intracellular AP recording, both IRX4-2-MB-positive and -negative cells were transferred and cultured on 0.1% fibronectin-coated glass bottom microwell dishes for 7 to 14 days. Next, the 35-mm dishes were mounted on an inverted microscope (Olympus IX71) and heated by a heating/cooling bath temperature controller (DTC-200, Dagan Corporation). The cells were

perfused with Tyrode's solution containing (mmol/L) 140 NaCl, 5.4 KC1, 1 MgCl2, 10 HEPES, 10 glucose, 1.8 $CaCl_2$ (pH 7.4) with NAOH 37 ºC. Glass microelectrodes were fabricated from borosilicate glass (PG52151-4, World Precision Instruments) and pulled on a P-87 Flaming/Brown puller (Sutter Instrument Company). The tip resistance of the microelectrode was 40–80 MU when filled with a 3 mol/L KCl solution. Intracellular recordings of membrane potential were performed using an EPC 7 amplifier (List Medical) in current clamp mode at 37 ± 0.5 ºC. The junction potential between the microelectrode solution and the bath solution was adjusted to zero, and the microelectrodes' capacitance was compensated. Individual cells were impaled with the sharp microelectrodes, and the spontaneous APs were filtered at 10 kHz and digitized on a computer at 10 kHz. APs were analyzed using Origin 6.0 software (Microcal).

MEA Recordings

Both IRX4-2-MB-positive and -negative cells were examined using a MEA data acquisition system, a 64-channel Muse MEA system (Axion Biosystems). Thirty thousand cells were plated onto fibronectin-coated MEA chambers, and 3–5 days later, when cells were stabilized, MEA recording was performed. After recording, the data were analyzed using the AxIS software. Statistical Analyses All data were expressed as mean ± SEM. Kruskal-Wallis ANOVA test was used for the statistical analysis for a small number of samples. Values of $p < 0.05$ were considered to denote statistical significance. All statistical analyses were conducted using SPSS 20.0 (SPSS).

Chapter 3: Expression profiling of Polycomb group proteins during cardiac development

3.1 Introduction

CMs have a very limited proliferative capacity which limits heart regeneration (99). Rodent data indicate that CM cell cycle exit is accompanied by coherent repression of cell cycle activators during the postnatal period, particularly early after birth (88; 100-106). Despite extensive investigations (33-36; 107-109), it is still largely unknown what silences cell cycle activators in mammalian postnatal CMs.

It is highly likely that the silencing of cell cycle activators is mediated by epigenetic mechanisms, because chromatin is actively reorganized during the cell cycle (47-49) and epigenetic changes play critical roles in cardiac development (37-43; 45).

However, the identity of the chromatin modifying enzymes which mediate the silencing of cell cycle activators in the postnatal heart remains unknown. It was well eastablished that multiple cell cycle regulators are epigenetically controlled by Polycomb group (PcG) proteins which transcriptionally silence genes by modifying chromatin structure (110).

In this chapter, we analyzed the expression profile of PcG proteins to assess potential involvement of PcG genes in the regulation of CM proliferation. First, we selected 18 PcG genes which were reported to regulate cell cycle. Their expression patterns were compared between neonatal and adult CMs via qRT-PCR. In addition, we determined time-course changes in CBX family gene expression level by collecting mouse hearts at different developmental stages and performing qRT-PCR. Furthermore, we examined expression pattern of CBX family genes between remote and border zone of injured hearts. Finally, we confirmed protein expression of CBX7 and its downstream chromatin modification in the postnatal mouse hearts.

3.2 Results

3.2.1 Polycomb group subunits are differentially expressed in neonatal and adult mouse cardiomyocytes

To assess potential involvement of PcG proteins in the regulation of CM proliferation, expression patterns of 18 PcG genes, which were reported to regulate cell cycle, were examined in primary neonatal (P0) and adult (3 months) CMs by quantitative real time PCR (qRT-PCR) (Figure 2-1). Distinct expression patterns were observed such as upregulated (Cbx7, Cbx8, Cbx2, Ring1a and Pcgf5), downregulated (Cbx4, Ezh2, Pcgf2 and Ring1b), and unchanged (Scmh1, Pcgf6, Yy1 and Cbx6).

Interestingly, CBX family members showed distinct expression profiles. Cbx7, Cbx8, and Cbx2 were upregulated whereas Cbx4 was downregulated in the adult mouse CMs compared to neonatal ones. There was no significant change in the level of Cbx6. Since CBX proteins recruit other PRC1 subunits, this result suggests that PcG-mediated transcriptional regulation is dynamic during different developmental stages. Among all PcG genes, Cbx7 had the highest fold difference (about 27-fold) between adult and neonatal CMs.

In addition, Ring1 isoforms, ubiquitin transferases, showed differential expression pattern. Ring1a was upregulated while Ring1b was downregulated in the post-mitotic CMs. Although Ring1a and Ring1b have functional redundancy, phenotypic characteristics of each knockout mice are distinct (111; 112), suggesting their divergent functions. Our data imply that Ring1a is the major PRC1 ubiquitin transferase in adulthood whereas Ring1b plays a central role during neonatal period.

A

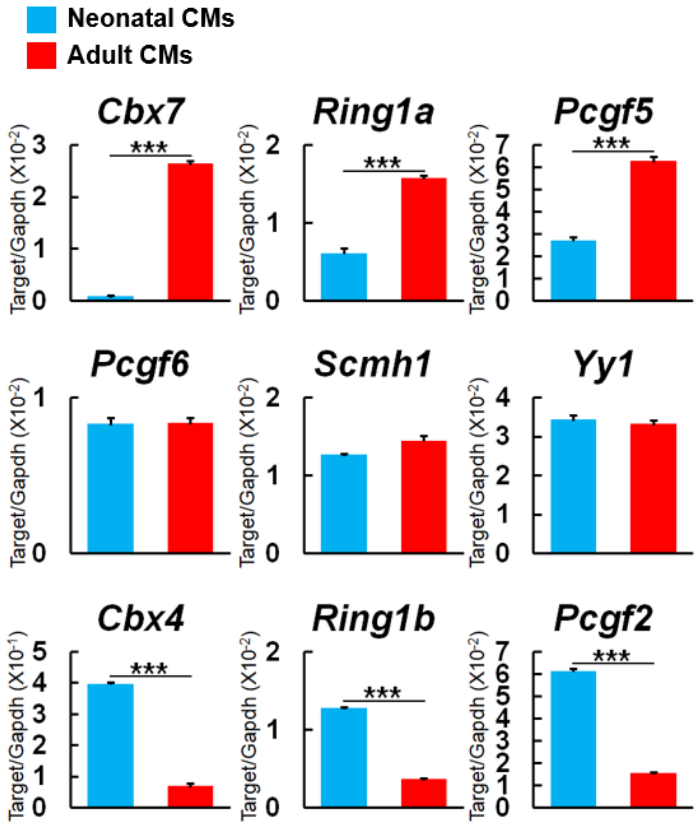

B

Adult / Neonate	
Gene	Fold Change
Cbx7	27.32
Cbx8	6.48
Cbx2	2.86
Ring1a	2.56
Pcgf5	2.32
Pcgf1	1.93
Pcgf4	1.40
Scmh1	1.13
Pcgf6	1.00
Yy1	-1.04
Cbx6	-1.04
Phc1	-1.22
Pcgf3	-1.81
Suz12	-1.97
Ring1b	-3.48
Pcgf2	-3.93
Ezh2	-4.79
Cbx4	-5.67

Figure 3-1. Gene expression profiling of Polycomb group proteins in mouse CMs. A. Representative qRT-PCR results. Expression patterns of 18 *PcG* genes were examined in primary neonatal (P0) and adult (3 months) mouse CMs by qRT-PCR. B. qRT-PCR results of 18 PcG genes expressed as ratio of adult CMs vs. neonatal CMs. Error bars: standard error of mean. Standard unpaired Student's t test. N=3, *** $P < 0.001$.

3.2.2 CBX family proteins are dynamically regulated during cardiac development

Since Cbx family genes determine specificity of target gene (113), their expression patterns were further examined in the heart at different time points via qRT-PCR (Figure 3-2). Cbx2 decreased from fetal to juvenile period and fluctuated up and down during adulthood. Cbx6 and 8 showed a similar pattern. Cbx4 increased until preadolescent stage and decreased afterwards with a little fluctuation.

Interestingly, among five mammalian orthologues of CBX proteins, only CBX7 showed exponential up-regulation during the perinatal period. Cbx7 was induced right after birth and highly maintained in the postnatal heart. To be specific, 6 days after birth, expression Cbx7 increased by 10 folds when compared to fetal period. The slope started to become gentle beginning postnatal day 20 and plateaued a month after birth. Compared to prenatal period, mRNA level of Cbx7 in the adult heart was much higher with 27-57 fold change.

Previously, it was reported that CBX family members repress each other (56; 114). For example, CBX7 inhibits expression of CBX2, 4, and 8 in embryonic stem cells. On the other hand, CBX2, 4, and 8 repress expression of CBX7 during differentiation. Similarly, in the adult mouse hearts, postnatal upregulation of CBX7 was correlated with downregulation of CBX2, 4, and 8.

To examine the quality of RNA samples from mouse heart, expression of cell cycle-related genes and Myh7 gene was analyzed. Consistent with previous reports, multiple cell cycle activator genes including Cdk1, Ccnb1, Ccnb2, and Ccna2 were downregulated in the postnatal mouse hearts. Immature isoform of cardiac myosin heavy chain Myh7 was also downregulated as the heart becomes mature. These results confirm the quality of our heart samples and consistency with previous observations.

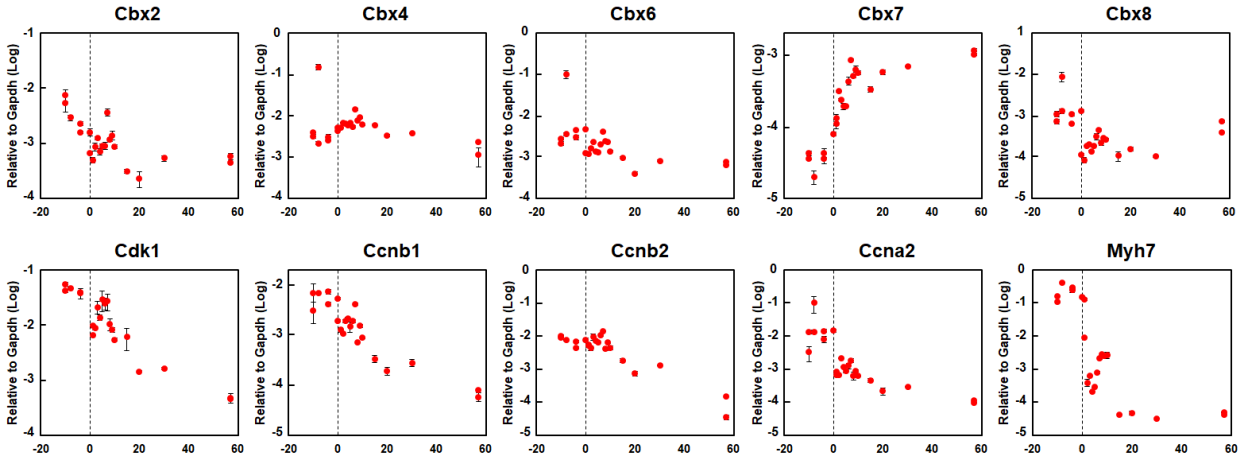

Figure 3-2. Gene expression profiling of CBX family in the mouse hearts. Messenger RNA level of mammalian CBX family members (Cbx2, 4, 6, 7 and 8), cell cycle activator genes involved in G2/M phase transition (Cdk1, Ccnb1, Ccnb2 and Ccna2), and immature isoform of cardiac myosin heavy chain (Myh7) was examined in the mouse hearts at different developmental stages via qRT-PCR. Error bars: standard error of mean. N=22

3.2.3 Expression of CBX7 gene is induced in the perinatal mouse hearts

Figure 3-2 showed exponential upregulation of Cbx7 in the postnatal heart. To define when Cbx7 expression is induced, fetal (E17.5 and E19.5) and neonatal mouse hearts were subjected to qRT-PCR for Cbx7 gene. As a result, expression of Cbx7 gene was relatively low during the fetal stage until E19.5 (Figure 3-3). However, its expression was doubled right after birth (postnatal day 0). These data suggest that Cbx7 gene was induced by stimuli associated with perinatal physiologic events.

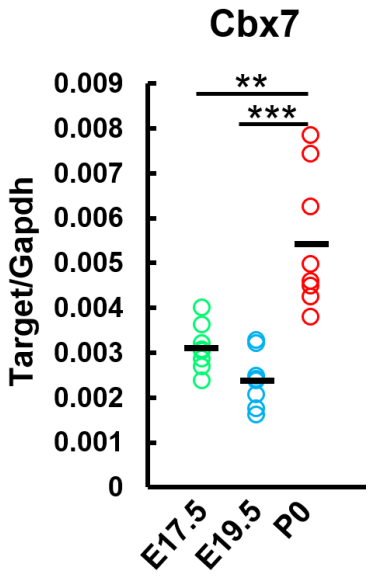

Figure 3-3. Perinatal upregulation of Cbx7 in the mouse hearts. Messenger RNA level of Cbx7 was examined in the mouse hearts on embryonic day 17.5 (E17.5), E19.5, and postnatal day 0 (P0) via qRT-PCR (N=8, each group). ** $P < 0.01$, *** $P < 0.001$, Standard unpaired Student's t test.

3.2.4 CBX7 protein is expressed in the adult mouse cardiomyocytes

To determine protein expression of CBX7 in adult mouse CMs, we performed western blot using anti-CBX7 antibody (Figure 3-4). Isolated adult mouse CMs were subjected to western blot (Figure 3-4A). Human embryonic kidney-293 cell line infected with adenoviral particles inducing overexpression of CBX7 was used as a positive control. Whole protein fraction from adult mouse CMs contained CBX7 protein with the same molecular weight of that ectopically expressed in HEK-293 cells, suggesting that our anti-CBX7 antibody specifically recognize mouse CBX7 protein (Figure 3B).

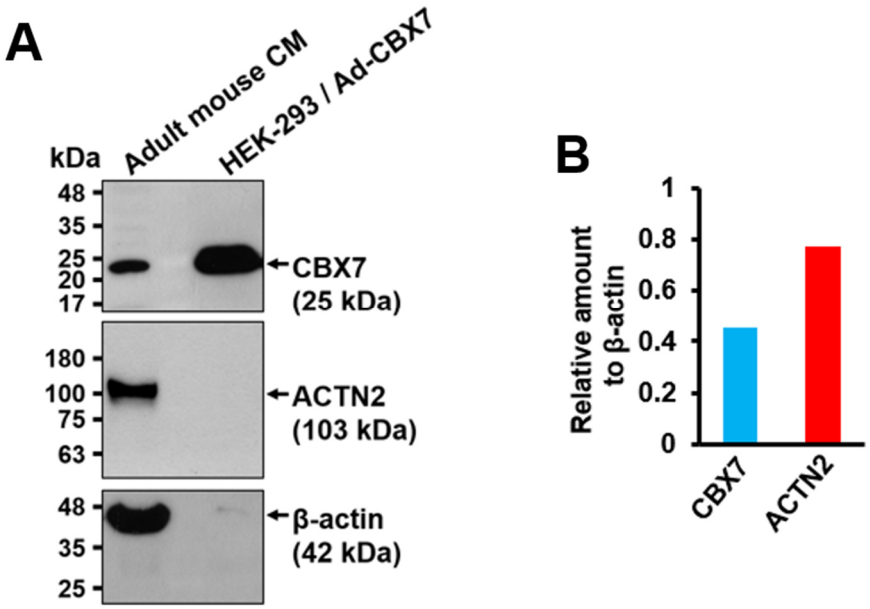

Figure 3-4. Expression of CBX7 protein in the adult mouse CMs. (A) CBX7 protein was detected via western blotting. Wild type (ICR CD-1) adult mouse hearts were dissociated by Larngendorff method and isolated CMs were used for western blot. HEK-293 cells infected with adenoviral particles inducing overexpression of CBX7 was used as a positive control. (B) Relative protein amount of CBX7 and ACTN to β-actin in adult mouse CMs (panel A) was quantified by using Image J.

3.2.5 Cbx7 is downregulated in the border zone of infarcted heart

Mammals display a cardiac regenerative response, although limited (115). In fact, DNA synthesis and proliferation of adult mouse CMs in the border zone is stimulated by myocardial infarction (MI) although not substantially (5; 116; 117). We hypothesized that the limited regenerative capacity of the mammalian adult heart is attributed to high expression of CBX7. Therefore, expression levels of Cbx7 transcript were compared between control and infarcted hearts. While Cbx7 mRNA level was not different at the whole heart level, it was profoundly lower in the border zone when the MI-induced heart was dissected into remote and border zone (Figure 3-5). Overall, other CBX genes did not show as much difference (less than 1.5 fold). This result suggests that Cbx7 may serve as a therapeutic target to rescue the regenerative capacity of the adult heart.

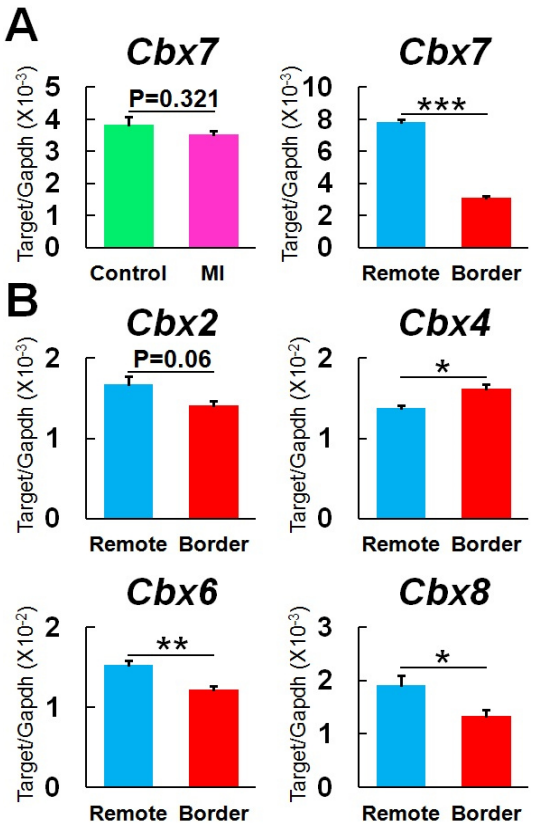

Figure 3-5. Downregulation of Cbx7 in the border zone after MI. A. Whole hearts from control and MI-induced mouse were subjected to qRT-PCR to measure Cbx7 mRNA level (Left). Remote and border zone dissected from MI heart were subjected to qRT-PCR (Right). B. Same as the right panel of A. Error bars: standard error of mean. * $P < 0.05$, ** $P < 0.01$, *** $P < 0.001$, Standard unpaired Student's t test, N=3.

3.2.6 Downstream chromatin modifications of CBX7 are detected in the adult mouse cardiomyocytes.

CBX7 mediates chromatin modifications including H3K9me3 and H2Aub1 (118; 119). To check whether CBX7-mediated chromatin modifications are present in the adult mouse CMs, we performed IHC for CBX7 protein (Figure 3-6) using Myh6-mCherry transgenic mouse line. As a result, both chromatin modification marks were observed in adult mouse CMs. Interestingly, both H3K9me3 and H2Aub1 were detected in non-CMs. This result is consistent with our previous result that CBX7 was expressed in non-CMs.

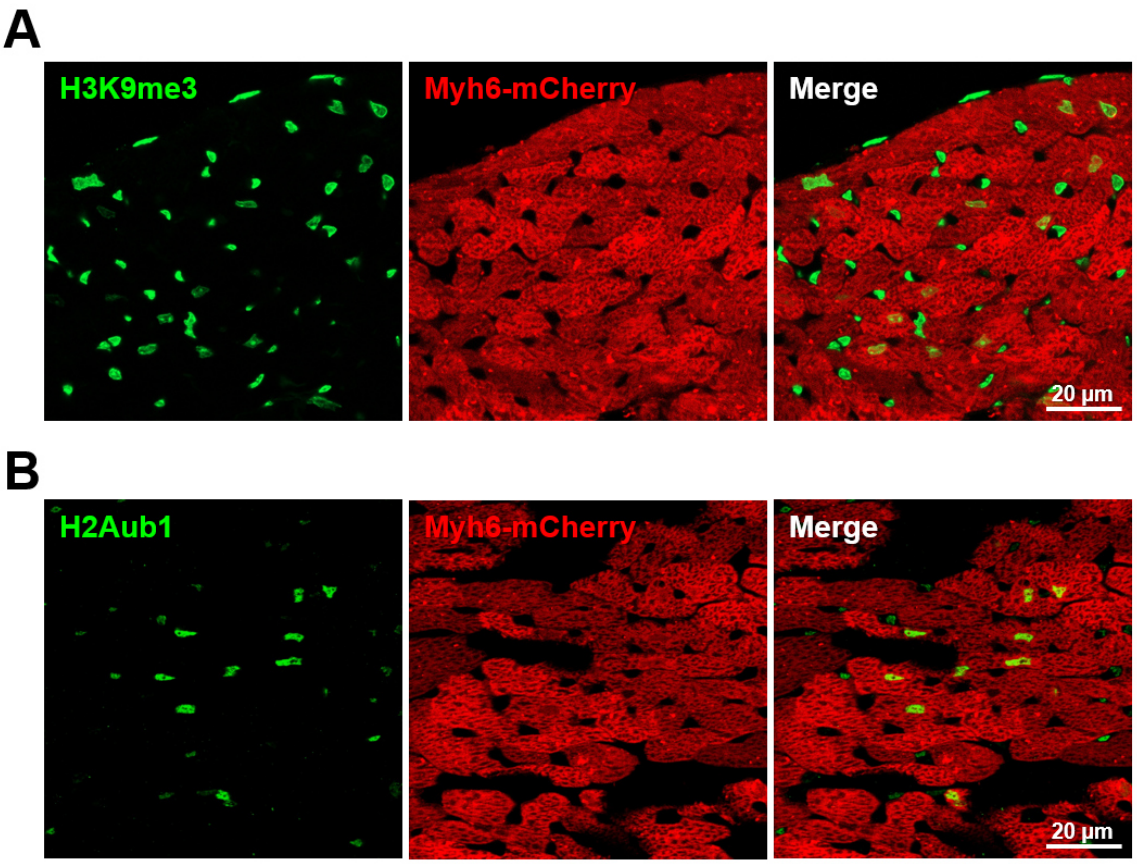

Figure 3-6. Detection of H2Aub1 and H3K9me3 in the adult mouse hearts. Adult (3 months-old) Myh6-mCherry mouse hearts were subjected to IHC for H3K9me3 (A) and H2Aub1 (B).

3.3 Discussion

Polycomb group proteins have been known as epigenetic regulators of the cell cycle (110). However, their behavior during cardiac development is still unclear. In particular, the role of CBX family in PRC1 in CM proliferation is unknown. Expression profiling of PcG genes identified CBX7 as one of the major PRC1 subunits in the postnatal heart. Previously, the role of CBX7 in stem/progenitor cells and cancer cells were illustrated (56; 57; 120), but its behavior in postnatal somatic cells were poorly understood. In particular, it has been controversial whether CBX7 inhibits or promotes cell proliferation. Due to divergent observations, it has been claimed that CBX7 functions in a tissue- and context-specific manner (65).

Previous reports implied perinatal reduction of CM proliferative capacity with downregulation of cell cycle regulators such as Cyclin A and Cyclin B (100; 101; 106). Because CBX7 gene was upregulated between E19.5 and P0 and highly expressed in post-mitotic CMs, we speculate that CBX7 would play anti-proliferative roles in CMs. Since CBX7 mediates epigenetic repression, it is likely that cell cycle-promoting genes could be repressed by CBX7 during perinatal period. Perinatal downregulation of multiple cell cycle activators supports such notion (Figure 3-2).

Gene expression profiling of PcG genes also revealed their dynamic changes between neonatal and adult mouse CMs (Figure 3-1). Among Cbx family members, Cbx7, Cbx8, and Cbx2 were upregulated whereas Cbx4 was downregulated in adult mouse CMs. It was previously reported that Cbx7 and Cbx8 share ~95% of their targets in hematopoietic stem cells (57). On the other hand, Cbx7 and Cbx8 exhibited antagonistic effect to each other in embryonic stem cells. This discrepancy implies the relationship between Cbx7 and Cbx8 could be cell type- and context-

specific. Thus, defining interaction between Cbx7 and Cbx8 in CMs would be a potential future direction.

Expression pattern of some CBX family members were not consistent between CM and heart samples (Figure 3-1 and 3-2). For instance, Cbx2 was upregulated in adult mouse CMs, but not in adult mouse heart. This could be due to heterogeneous cellular composition of the heart: Cbx2 could be downregulated in adult non-CMs. However, expression pattern of Cbx7 was consistent between CM and heart samples, suggesting that postnatal upregulation of Cbx7 in the heart would be due to its increase in postnatal CMs. This observation leads us to ask questions about the role of Cbx7 in CMs.

Gene expression profiling of PcG proteins identified Cbx7 as the most highly upregulated gene in the postnatal heart. Cbx7 gene was induced in the heart during perinatal period. Protein expression of CBX7 in adult mouse CMs was further confirmed via WB. Border zone of injured adult heart showed decreased expression of Cbx7. CBX7-mediated chromatin modifications were detected in adult mouse CMs. These data suggest that CBX7 may play a role in perinatal physiologic process in the heart.

In summary, Polycomb group proteins are epigenetic regulators of the cell cycle, but their role in CM proliferation is unclear. Gene expression profiling revealed that CBX7, a subunit of Polycomb Repressive Complex 1, was upregulated in the postnatal heart. Expression of CBX7 gene was induced at P0. Protein expression of CBX7 in adult mouse CMs were confirmed by western blot.

3.4 Materials and Methods

Mice

B6;D2-Tg(Myh6*-mCherry)2Mik/J mice were purchased from the Jackson Laboratories. ICR CD-1 mice were purchased from Charles River. Following primers were used for PCR genotyping. Myh6-mCherry (288 bp) forward: 5'-AGGACGGCGAGTTCATCTAC-3', reverse: 5'-TGGTGTAGTCCTCGTTGTGG-3'.

Mouse CM isolation

For neonatal mouse CM isolation, we modified a previously reported protocol (121). Briefly, neonatal hearts from P0 mice were minced with scissors and incubated in HBSS containing 0.0125% trypsin overnight at 4ºC for pre-digestion. On the following day, the tissue fragments were further digested in oxygenated HBSS containing 1.5 mg/ml Collagenase/Dispase mix (Roche) at 37 ºC for 30 min with gentle agitation. After filtering with 100 µm strainer, cells were plated and cultured in the Plating medium (84% DMEM high glucose, 10% horse serum, 5% FBS, 1% anti-anti) at 37 ºC for 1.5 hrs, allowing the preferential attachment of fibroblasts. Non-adherent cells were subjected to percoll-based separation (83) and MACS using feeder removal microbeads (Miltenyi Biotec 130-095-531) for the further purification of neonatal CMs. Enriched neonatal CMs were used for RNA extraction and qRT-PCR. Adult mouse CMs were isolated via conventional Langendorff method as described previously (122).

Generation of recombinant adenovirus particles

cDNA of mouse CBX7 (NM_144811.3) was cloned into pCR2.1-TOPO vector via TA cloning method using the following primers. Forward: 5'-ATGGAGCTGTCAGCCATAGG-3' and Reverse: 5'-TGTCCGGATGTGTTCATGGG-3'. Cloned mouse CBX7 cDNA was subcloned into adenoviral shuttle plasmid pDC316 (Microbix Biosystems). Both adenoviral genomic and shuttle plasmids were transfected to HEK-293 cells using Lipofectamine 3000 (Thermo Fisher Scientific). Recombinant adenoviral particles were extracted from cell lysates and the relative titer of Ad-Mock and Ad-CBX7 viral particles was determined via qRT-PCR for adenovirus serotype 5 (Ad5) genome (123).

Histological analysis

After euthanasia, mouse heart tissues were removed, fixed in 2% paraformaldehyde (PFA) at 4°C for 16 hours, and submerged in 30% sucrose solution at 4°C for 24 hours. Frozen heart sections prepared with OCT compound (Tissue-TeK 4583) were washed with PBS. Then samples were permeabilized/blocked with PBS containing 0.5% Triton X-100 and 2.5% BSA at room temperature for 1hour. Slides were then incubated with anti-ACTN2 (Sigma A7811, 1:100), anti-CBX7 (Abcam ab21873, 1:100), anti-Ki67 (Cell Marque 275R-14, 1:100), anti-phospho-Histone H3 (Ser10) (Millipore 06-570, 1:100), anti-Cyclin B1 (Cell Signaling Technology 12231, 1:100), anti-Ubiquityl-Histone H2A (Lys119) (Cell Signaling Technology 8240, 1:100), and anti-H3K9me3 (Abcam ab8898, 1:100) at 4°C overnight. The slides were washed three times with PBS containing 0.1% Tween 20 and incubated with appropriate secondary antibodies at room temperature for 1-2 hours. DAPI was used for nuclear staining. The samples were visualized under a Zeiss LSM 510 Meta confocal laser scanning microscope (Carl Zeiss).

Quantitative Real-time PCR

Total RNAs from mouse CMs and hearts were isolated using a guanidinium extraction method (124) combined with RNA extraction kit (Qiagen). Extracted RNA was reverse-transcribed using Taqman Reverse Transcription Reagents (Applied Biosystems 4304134) according to the manufacturer's instructions. The synthesized cDNA was subjected to qRT-PCR using specific primers and probes (see Table 3). Quantitative assessment of RNA levels was performed using an ABI PRISM 7500 Sequence Detection System (Applied Biosystems). Relative mRNA expression was normalized to Gapdh gene.

Western blot

Cells were lysed with RIPA buffer, supplemented with PMSF, phosphatase-inhibitor cocktail (Sigma) and protease-inhibitor cocktail on ice for 1 h and the lysates were clarified by centrifugation. Equal amounts of lysates were subjected to SDS-PAGE, transferred onto a nitrocellulose membrane, and blocked for 1 h at room temperature in Tris-buffered saline with 0.05% Tween-20 (TBST) and 5% non-fat milk. The membrane was subsequently incubated with anti-CBX7 (Abcam ab21873, 1:1000), anti-β-actin (Cell Signaling Technology 4967, 1:1000), anti-ACTN2 (Sigma A7811, 1:1000) at 4ºC overnight. After washing with TBST, blots were incubated with the appropriate secondary antibodies for 1 h at room temperature and developed using ECL detection reagent (Thermo Fisher Scientific).

Statistical analyses

All data were expressed as mean ± SEM. Values of $P < 0.05$ were considered to denote statistical significance.

Chapter 4: Loss-of-function analyses of CBX7 in mice in vivo

4.1 Introduction

At present, the role of Cbx7 in cell proliferation is controversial (55; 58-64; 125) and was suggested to be tissue-specific and context-specific (65). But its role in CM proliferation is unknown. Mechanistically, Cbx7 acts as a reader for H3K27me3 and mediates stabilization of heterochromatin structure, leading to transcriptional repression of target genes (51; 66).

In Chapter 3, gene expression profiling of PcG genes revealed that Cbx7 expression was induced at perinatal stage and exponentially upregulated in the postnatal heart. The expression pattern of Cbx7 was negatively correlated with those of cell cycle activator genes. Furthermore, Cbx7 gene was downregulated in border zone of injured hearts where CMs exhibit mitotic activity. These results argue that Cbx7 can play an anti-proliferative role in the adult heart through transcriptional repression of cell cycle promoting genes. Thus, we hypothesize that Cbx7 represses proliferative capacity of perinatal CMs.

To test this hypothesis, we generated a mutant mouse line with targeted inhibition of Cbx7 for the loss-of-function analyses in vivo. In this chapter, we will discuss characterization of the mutant mice to see if targeted inhibition of Cbx7 leads to enhanced proliferative capacity of perinatal/postnatal CMs in vivo. Phenotypic characterization of the mutant mice will be analyzed at the organ, cellular, and molecular levels.

4.2 Results

4.2.1 Generation of mutant mice with cardiac haploinsufficiency of CBX7

To investigate the function of CBX7 in CMs, a Tnnt2-cre mouse was crossed with a $Cbx7^{floxed}$ mouse to generate Tnnt2-cre;$Cbx7^{floxed/+}$ mice (Figure 4-1). In $Cbx7^{floxed}$ mice, exon 2 of CBX7 gene was replaced by a targeting plasmid encoding a gene trap cassette that consisted of an EN2 splice acceptor, LacZ reporter gene, internal ribosomal entry site (IRES), neomycin selection marker, and SV40 polyA signal. The replacement is mediated by homologous recombination since the 5' and 3' arms of the targeting plasmid are complementary to intergenic regions flanking exon 2 in the Cbx7 allele.

The targeted allele was confirmed by conventional PCR genotyping method in which primers were designed to specific indicated regions (Figure 4-1 A&B). Through this method, we were able to successfully genotype all the different mutant mouse lines. When Cbx7 transcript was amplified by primers specific to full length cDNA via RT-PCR, the cardiac Cbx7 haplodeficient mice expressed a shorter transcript which seemed to be a truncated version of Cbx7 (Figure 4-1 C). Lack of bands corresponding to full length Cbx7 in the haplodeficient mice suggests that a single copy of Cbx7 is not enough for producing wild-type transcript.

To quantify and compare Cbx7 transcript level between wild type and the mutant line hearts, qRT-PCR was performed (Figure 4-1D). As a result, mRNA level of Cbx7 gene was reduced by more than half in the cardiac Cbx7 haplodeficient mice compared to wild type mice at postnatal day 0 (P0). This result suggests that Cbx7 gene was successfully targeted in the mutant mouse line.

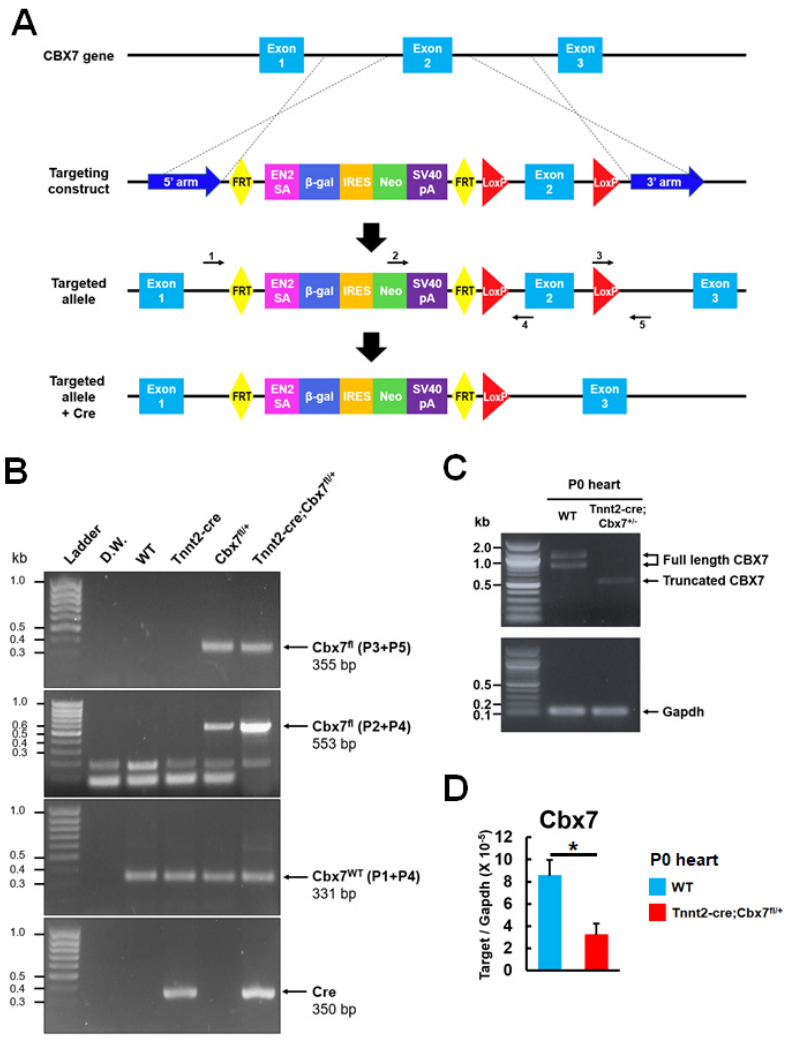

Figure 4-1. A schematic and validation of targeted allele. A. Cbx7 allele, targeting construct, and targeted allele are shown in a schematic. Arrows with numbers represent primers specifically designed to indicated regions. B. Genomic DNAs from indicated mice were subjected to conventional PCR for the detection of targeted allele. C. cDNA from wild type and Tnnt2-cre;$Cbx7^{fl/+}$ neonatal hearts (P0) were subjected to RT-PCR with primers amplifying full length Cbx7. D. cDNA from wild type and Tnnt2-cre;$Cbx7^{fl/+}$ neonatal hearts (P0) were subjected to qRT-PCR for Cbx7. Error bars: standard error of mean. * $P < 0.05$, Standard unpaired Student's t test, N=3.

4.2.2 Cardiac haploinsufficiency of CBX7 causes cardiomegaly and cardiac remodeling during perinatal period

All the progenies from the crossbreeding died before Postnatal day 2 (P2), suggesting that cardiac-specific haploinsufficiency of Cbx7 leads to embryonic or perinatal lethality. Viable progenies showed abnormal behaviors and lethargy; overall increased inactivity, even when laid on their backs, followed by repeated convulsions. All the viable mutant pups succumbed to death within a day. Considering a relatively low expression level of CBX7 in the embryonic heart compared to the adult heart and the previous report of viable adult Cbx7 knockout mice (62), perinatal lethality of cardiac Cbx7-haplodeficient mice was an unexpected result. Nonetheless, these results clearly indicate that CBX7 is critical for heart development.

To assess the defects in cardiac Cbx7-haploinsufficient mice, hearts were harvested from live mice at P0. The mutant mice exhibited cardiomegaly and increased weight to body ratio by 38% (Figure 4-2). Postmortem samples were excluded because their dehydrated body could exaggerate this ratio.

To examine cardiac structure, heart tissues were subjected to H&E staining in a four-chamber view. The mutant hearts showed variable structures and were categorized into 4 groups based on structural features. Group A features substantially increased thickness of ventricular walls. Group B gives prominence to enlarged atrium in addition to ventricle. In Group C, heart size is bigger, but there is no substantial difference in wall thickness compared to wild type. Group D presents dilation of myocardial walls. The highest proportion of mice was categorized as Group A in which all the hearts showed increased wall thickness in RV, IVS and LV, compared to WT.

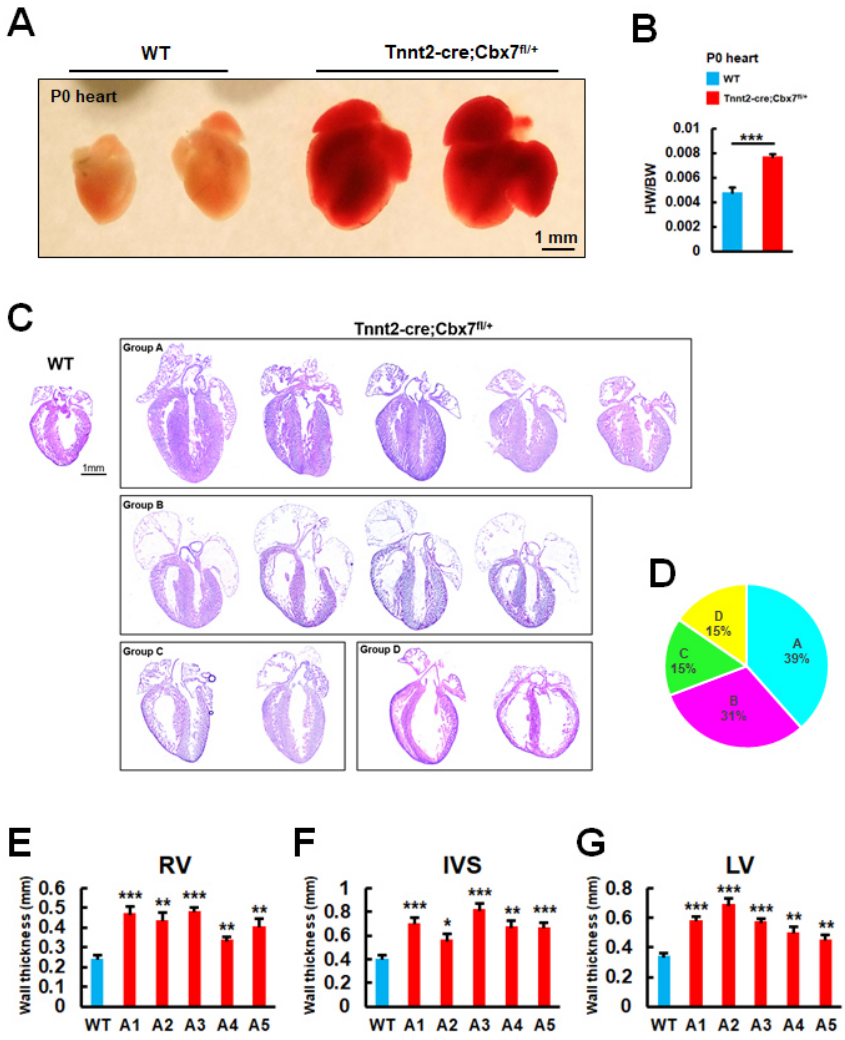

Figure 4-2. Cardiomegaly and cardiac remodeling caused by cardiac haploinsufficiency of CBX7. A. The picture of neonatal (P0) mouse heart tissues from wild type and Tnnt2-cre;Cbx7$^{fl/+}$. B. The heart to body weight ratio (Control N=3, Mutant N=10). Post mortem samples were excluded. C. H&E staining of the wild type and Tnnt2-cre;Cbx7$^{fl/+}$ hearts in a four chamber view. The mutant hearts were categorized into four groups based on structural features. D. Percentage of each group that were categorized in panel C. E-G. RV, IVS, and LV wall thickness of wild type and Group A Tnnt2-cre;Cbx7$^{fl/+}$. Error bars: standard error of mean. * $P < 0.05$, ** $P < 0.01$, *** $P < 0.001$, Standard unpaired Student's t test, N=5.

4.2.3 Cardiac haploinsufficiency of CBX7 sustains proliferative capacity of perinatal cardiomyocytes

To examine the role of CBX7 in CM proliferation, heart tissues were subjected to IHC for proliferation markers such as Ki67 and phospho-histone H3 (pH3) (Figure 4-3). Ki67 has been widely used as a marker for cellular proliferation. Its function is associated with ribosomal RNA synthesis (126). Ki67 is localized to nucleus during interphase but it moves to the chromosomal surface during mitosis (127). In addition, Ki67 is expressed in cells with active cell cycle progression, but disappears in quiescent cells (128). On the other hand, phosphorylation of histone H3 at Ser10 by AURKB is linked to mitotic chromosome condensation (129).

We were able to observe cardiac expression of Ki67 and pH3 in the neonatal mouse heart (Figure 4-3). Double positive cells for ACTN2 and either Ki67 or pH3 represent proliferative CMs. There were higher percentage of $Ki67^+$ CMs than $pH3^+$ CMs because pH3 is specific to mitotic cells whereas Ki67 can be expressed in all active cell cycle stages except for resting phase. Strong pH3 expression was correlated to sarcomere disassembly which is one of the major hallmarks of proliferating CMs.

On E17.5 and E19.5, the percentage of $Ki67^+$ or $pH3^+$ CMs was similar between control and mutant mice (Fig 3-4). In both groups, $Ki67^+$ CMs took up about 40 % of total CMs. On the other hand, the proportion of $Ki67^+$ CMs was much higher in CBX7 haploinsufficient heart (25%) compared to wild type heart (10%) on P0. Wide view images of control and mutant hearts stained for $Ki67^+$ or $pH3^+$ are shown in Figure 4-5 and Figure 4-6.

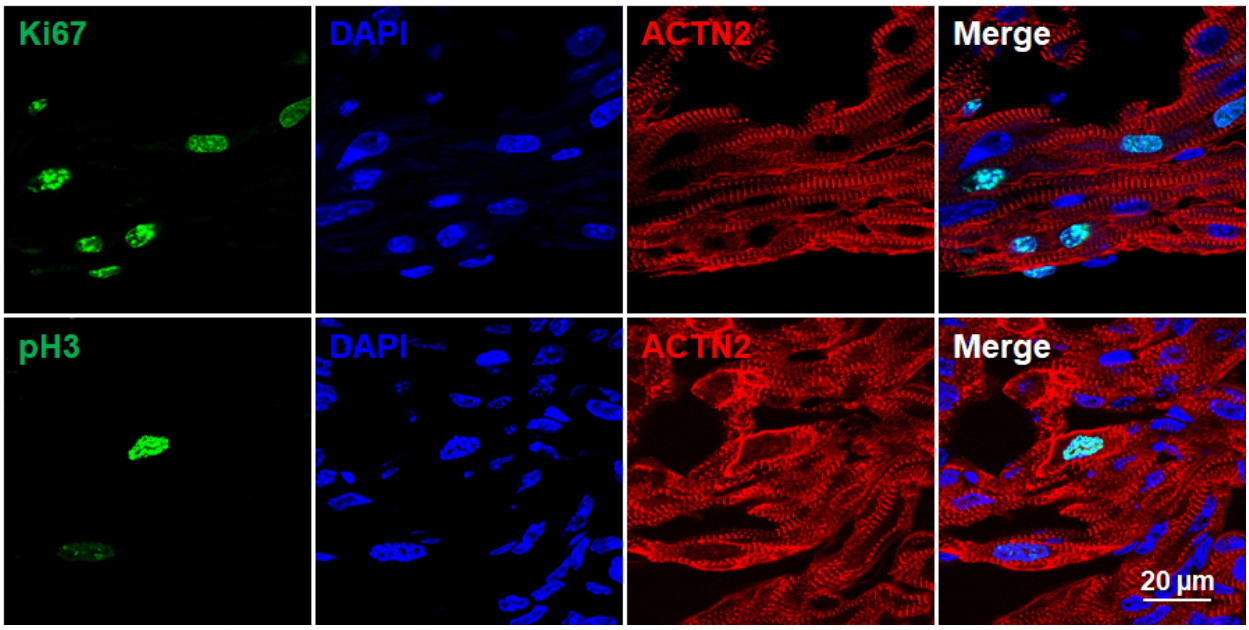

Figure 4-3. Measurement of CM proliferative capacity via Ki67 and pH3 staining. Wild type neonatal (P0) mouse hearts were subjected to IHC for Ki67 (upper row) and pH3 (lower row). ACTN2 was used as a marker for CMs.

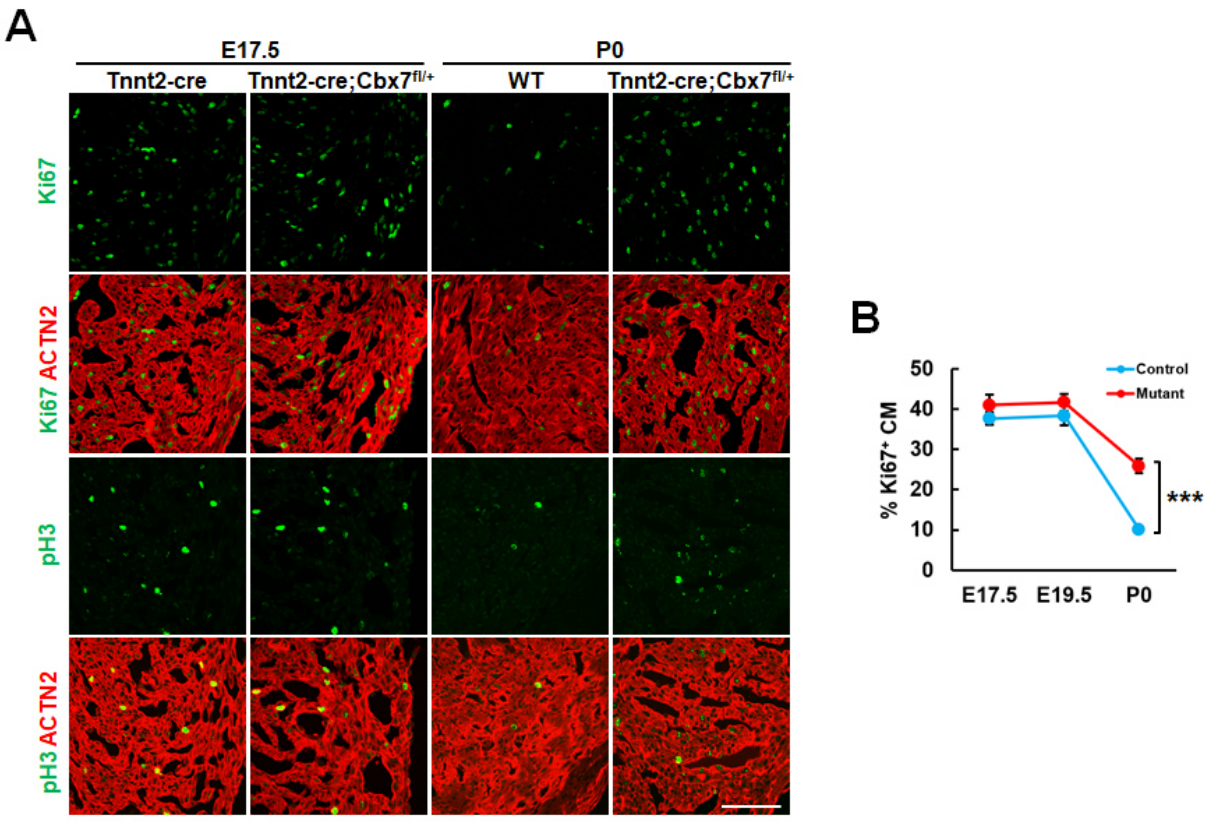

Figure 4-4. Sustained proliferative capacity of perinatal CMs by targeted inhibition of CBX7.

A. Representative IHC images stained for ACTN2 and either Ki67 or pH3 on E17.5 and P0 from wild type and Tnnt2-cre;Cbx7$^{fl/+}$. Bar = 50μm B. Quantification of percentage of Ki67^{+} CMs (double positive for ACTN2 and Ki67) out of total CMs (single positive for ACTN2). Quantification was performed by two individuals in a blinded setting. Error bars: standard error of mean. *** $P < 0.001$, Standard unpaired Student's t test, N=3.

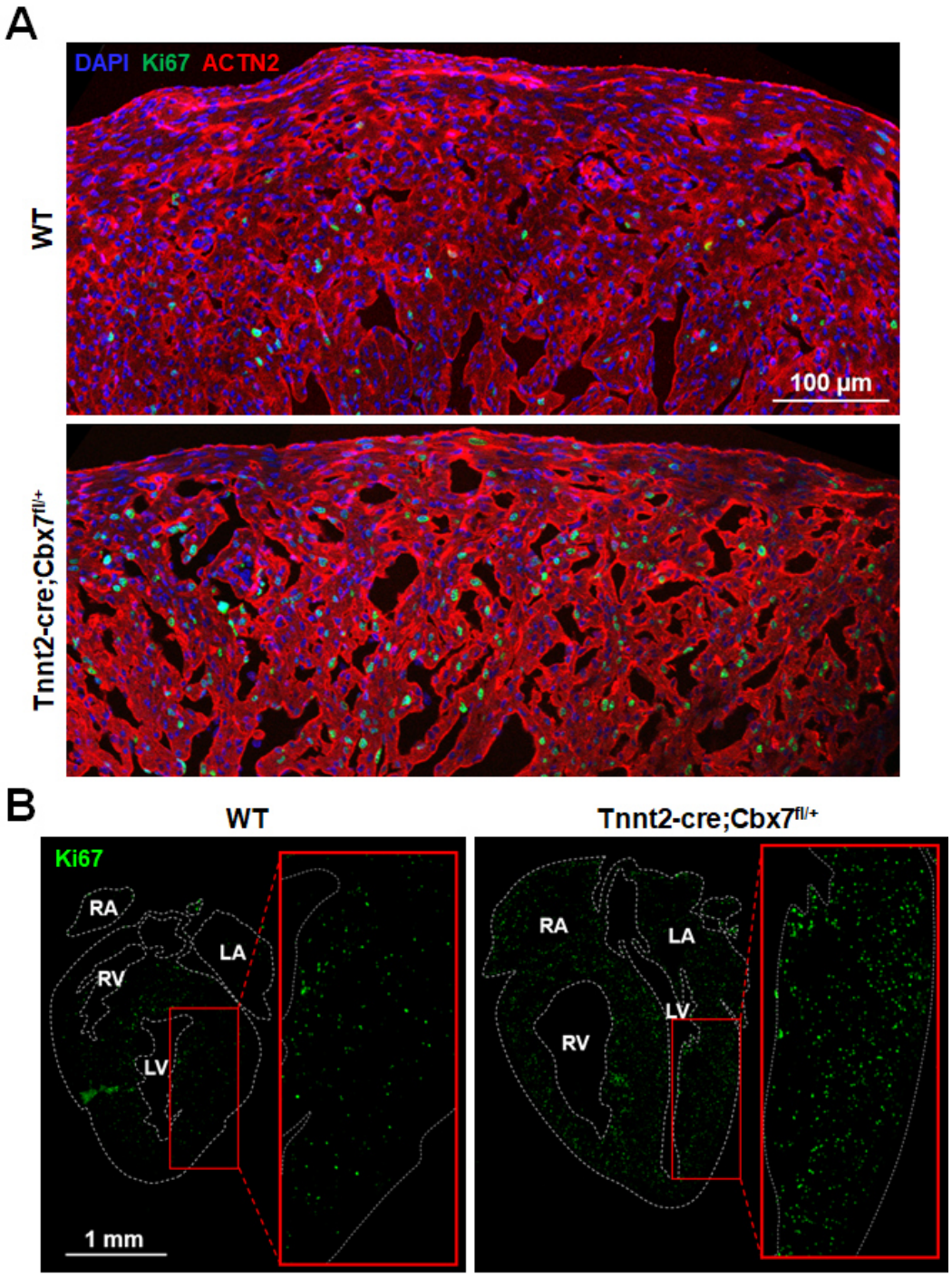

Figure 4-5. Wide view images showing increased number of Ki67^{+} neonatal CMs by CBX7 haploinsufficiency. A. IHC for ACTN2 and Ki67 in the left ventricle of control and Tnnt2-cre;Cbx7$^{fl/+}$ mice. B. Whole heart images for Ki67 staining of control and Tnnt2-cre;Cbx7$^{fl/+}$ mice.

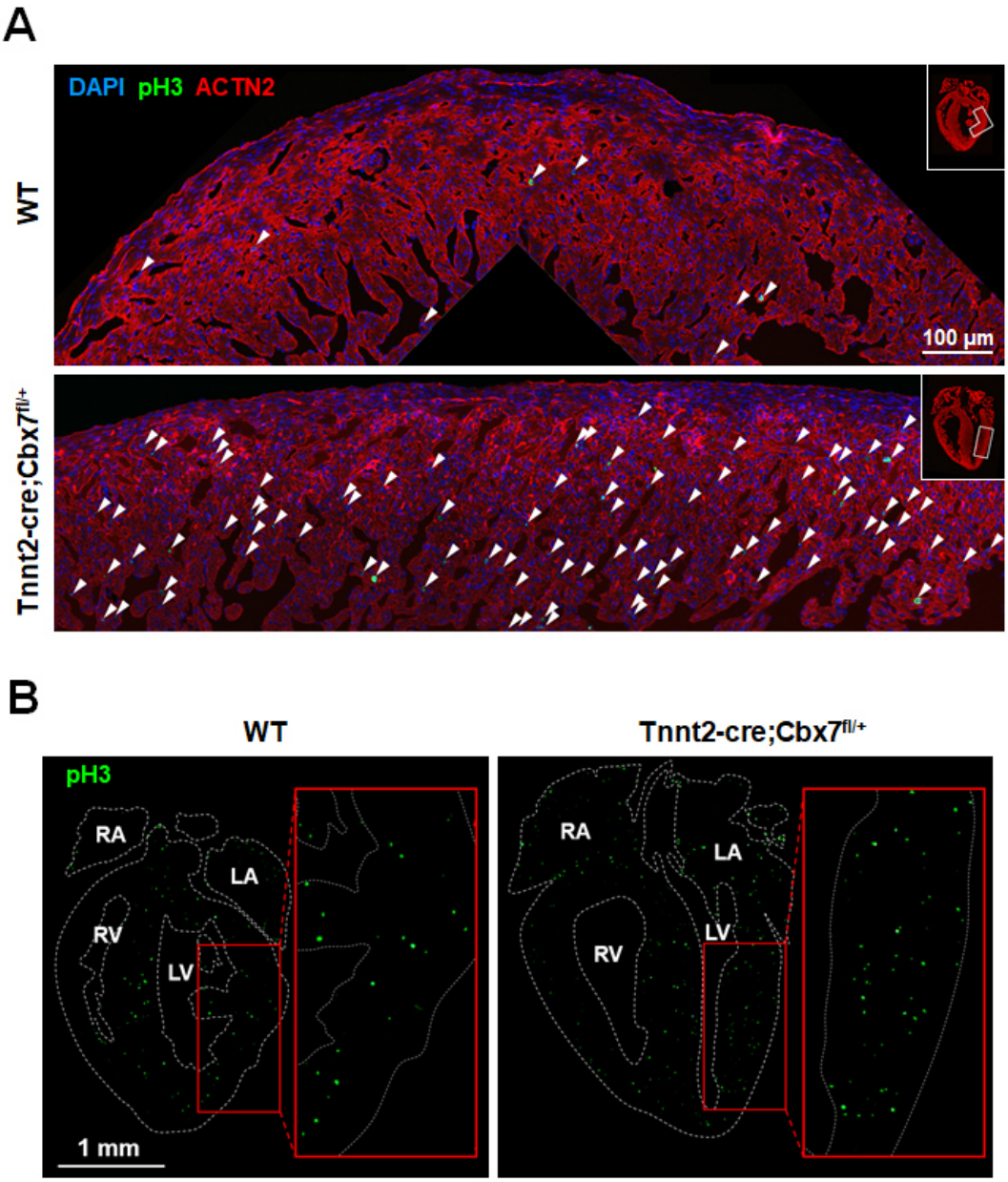

Figure 4-6. Wide view images showing increased number of pH3^{+} neonatal CMs by CBX7 haploinsufficiency. A. IHC for ACTN2 and pH3 in the left ventricle of control and Tnnt2-cre;Cbx7$^{fl/+}$ mice. B. Whole heart images for pH3 staining of control and Tnnt2-cre;Cbx7$^{fl/+}$ mice.

4.2.4 Cardiac haploinsufficiency of CBX7 causes reduced cell size of perinatal cardiomyocytes

Relatively immature proliferative CMs tend to have smaller cellular volume. Induction of Neuregulin1/ErbB4 signaling resulted in reduced CM volume along with increased CM proliferation (33). Inhibition of neonatal heart regeneration by overexpression of miR-195 lead to increased CM size (130). Hypoxia-induced CM mitosis was associated with decreased CM size (131; 132). Furthermore, the mean cellular volume of CMs increases as the human heart matures (133). For instance, human CM volume increases by 8.6 folds from infant period (0-1 year) to adolescent period (10-20 years).

To investigate the effect of targeted inhibition of CBX7 on CM size, control and mutant neonatal hearts were subjected to IHC for wheat germ agglutinin (WGA) and ACTN2 staining (Figure 4-7). Compared to wild type, cross-sectional size of neonatal CMs was reduced by 2.3 folds in Tnnt2-cre;$Cbx7^{fl/+}$ mice compared to control. This result supports previous result that proliferative capacity of perinatal CMs was enhanced by targeted inhibition of CBX7.

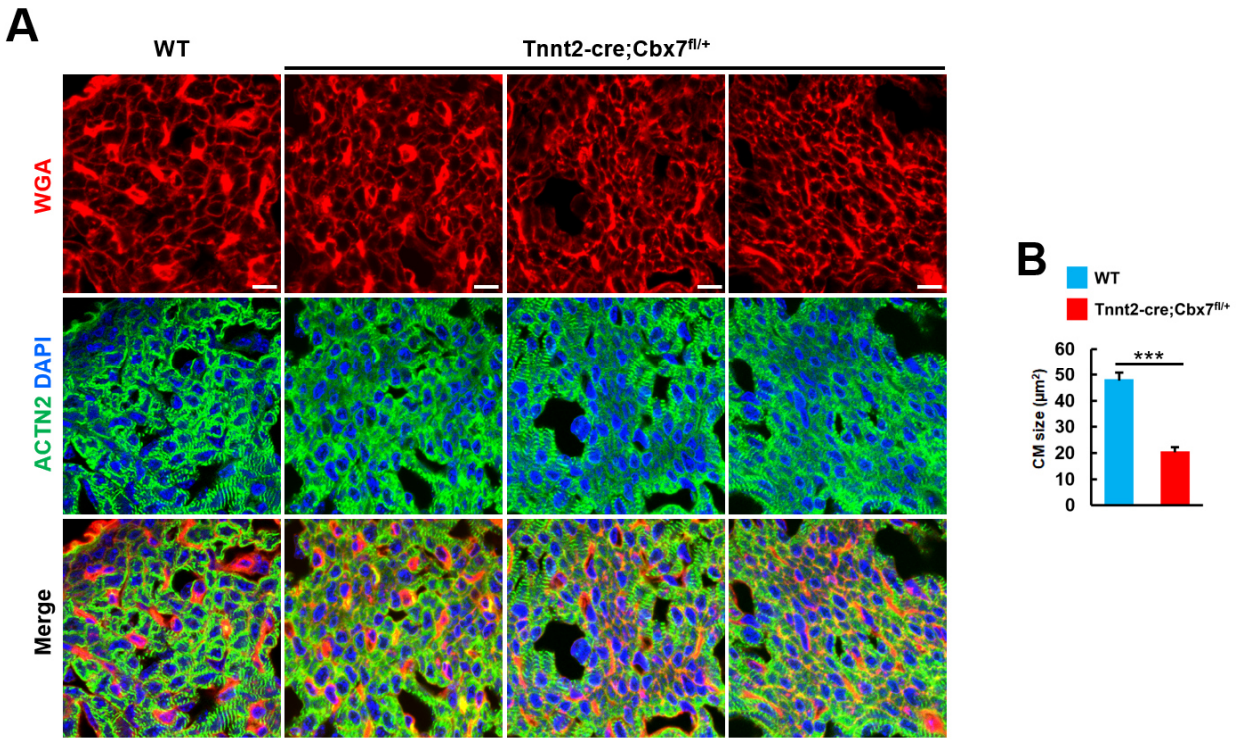

Figure 4-7. Reduced CM size by targeted inhibition of CBX7. A. Representative IHC images stained for ACTN2 and WGA on P0 from wild type and Tnnt2-cre;Cbx7$^{fl/+}$. Bar = 10μm B. Quantification of CM size (double positive for ACTN2 and WGA). Error bars: standard error of mean. *** $P < 0.001$, Standard unpaired Student's t test, N=5.

4.2.5 Cardiac haploinsufficiency of CBX7 causes upregulation of mitotic signaling and downregulation of cardiac maturation-related genes

As the heart matures, cell cycle activator genes are suppressed in CMs, leading to reduced proliferative capacity of CMs. On the other hand, genes involved in cardiac maturation are upregulated to meet the metabolic demands of fully functional CMs in the adult heart.

To define mechanisms of how CBX7 limits proliferative capacity of perinatal CMs, we performed gene expression profiling of wild type and CBX7-haploinsufficient heart via qRT-PCR (Figure 4-8). As a result, cell cycle activator genes for G_2/M phase including Ccna2, Ccnb1, Ccnb2, and Cdk1 were upregulated by targeted inhibition of CBX7 in CMs. Downregulated genes include cardiac cytoskeletal/gap junction genes such as Myl7, Myl2, Tnnt2, and Gja1, and cardiac ion transporting genes such as Kcnj2, Scn5a, and Atp2a2. As for cardiac myofibril maturation, mature isoform of myosin heavy chain (Myh6) was downregulated whereas immature isoform myosin heavy chain (Myh7) was upregulated by targeted inhibition of CBX7 in the neonatal heart. This result indicates that mitotic signaling was upregulated whereas cardiac maturation-related genes were downregulated by targeted inhibition of CBX7.

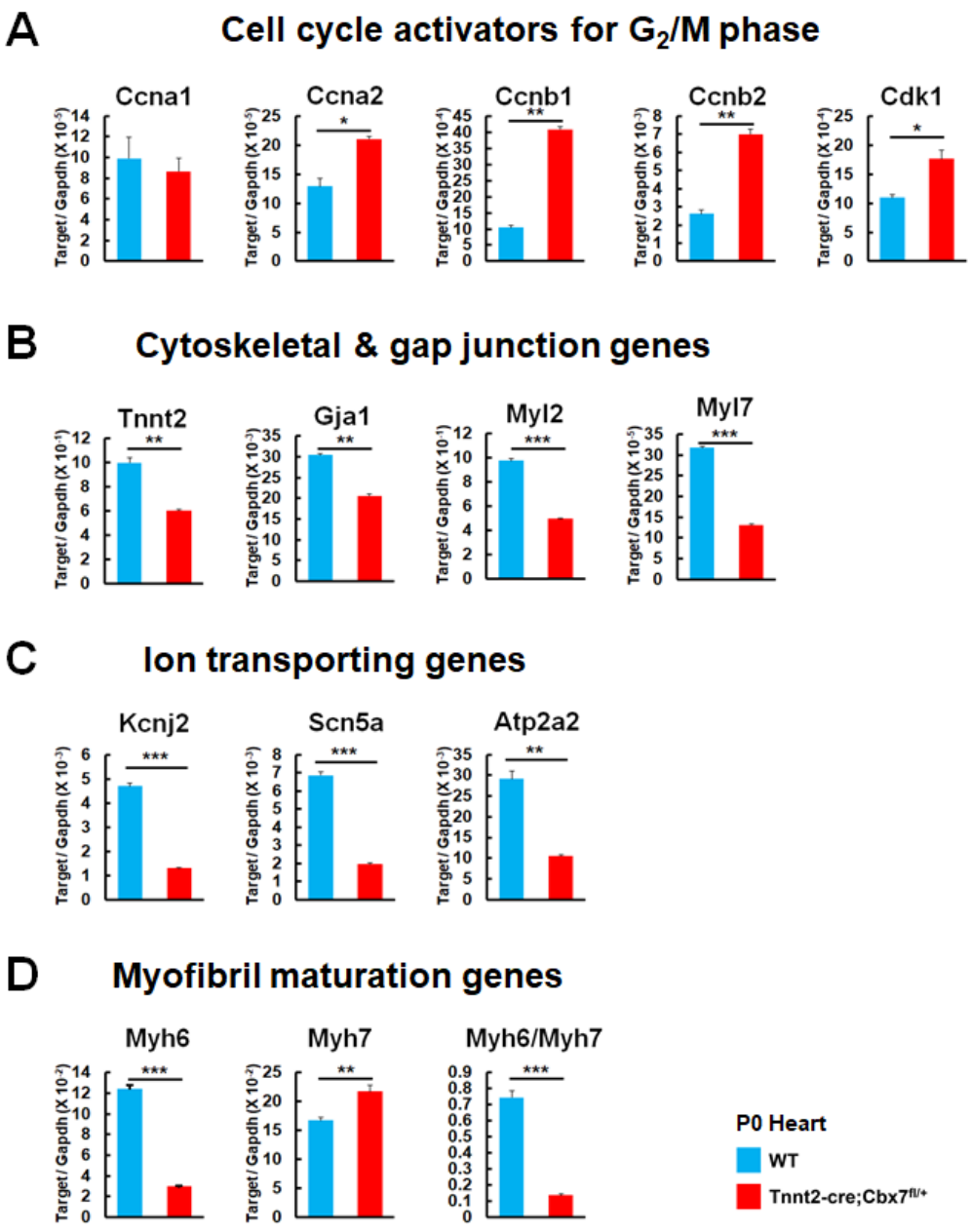

Figure 4-8. Upregulation of mitotic signaling and downregulation of cardiac maturation-related genes by CBX7 haploinsufficiency. Whole neonatal hearts from wild type and Tnnt2-cre;Cbx7$^{fl/+}$ mice were subjected to RNA extraction followed by cDNA synthesis and qRT-PCR. Error bars: standard error of mean. * $P < 0.05$, ** $P < 0.01$, *** $P < 0.001$, Standard unpaired Student's t test. N=3 from Group C.

4.2.6 Cardiac haploinsufficiency of CBX7 results in increased number of Cyclin B1+ cardiomyocytes

Cyclin B1 functions as a "molecular switch" for mitotic entry. Cyclin B1 is accumulated in the cytoplasm during the whole cell cycle but it is degraded at the end of mitotic activity. Upon its phosphorylation, it enters nucleus and binds to CDK1 to form a functional complex, called "maturation-promoting factor (MPF)". The Cyclin B1/CDK1 complex remains active via positive feedback loops. This complex controls multiple mitotic events such as chromosome condensation, disintegration of nuclear membrane, and assembly of spindle pole.

Since gene expression of Cyclin B1 (Ccnb1) was upregulated by targeted inhibition of CBX7 in the neonatal mouse heart, its protein expression level was confirmed via IHC (Figure 4-9 & 3-10). Targeted inhibition of CBX7 resulted in 2.75-fold increase of the percentage of Cyclin $B1^+$ CMs in the neonatal mouse heart.

Interestingly, we observed 3 different staining patterns of Cyclin B1 in terms of its subcellular localization, such as cytoplasmic, partial nuclear localization, and full nuclear localization. In all three localization patterns, Cyclin $B1^+$ CM populations were increased by targeted inhibition of CBX7. This result supports the previous qRT-PCR result in Figure 4-8.

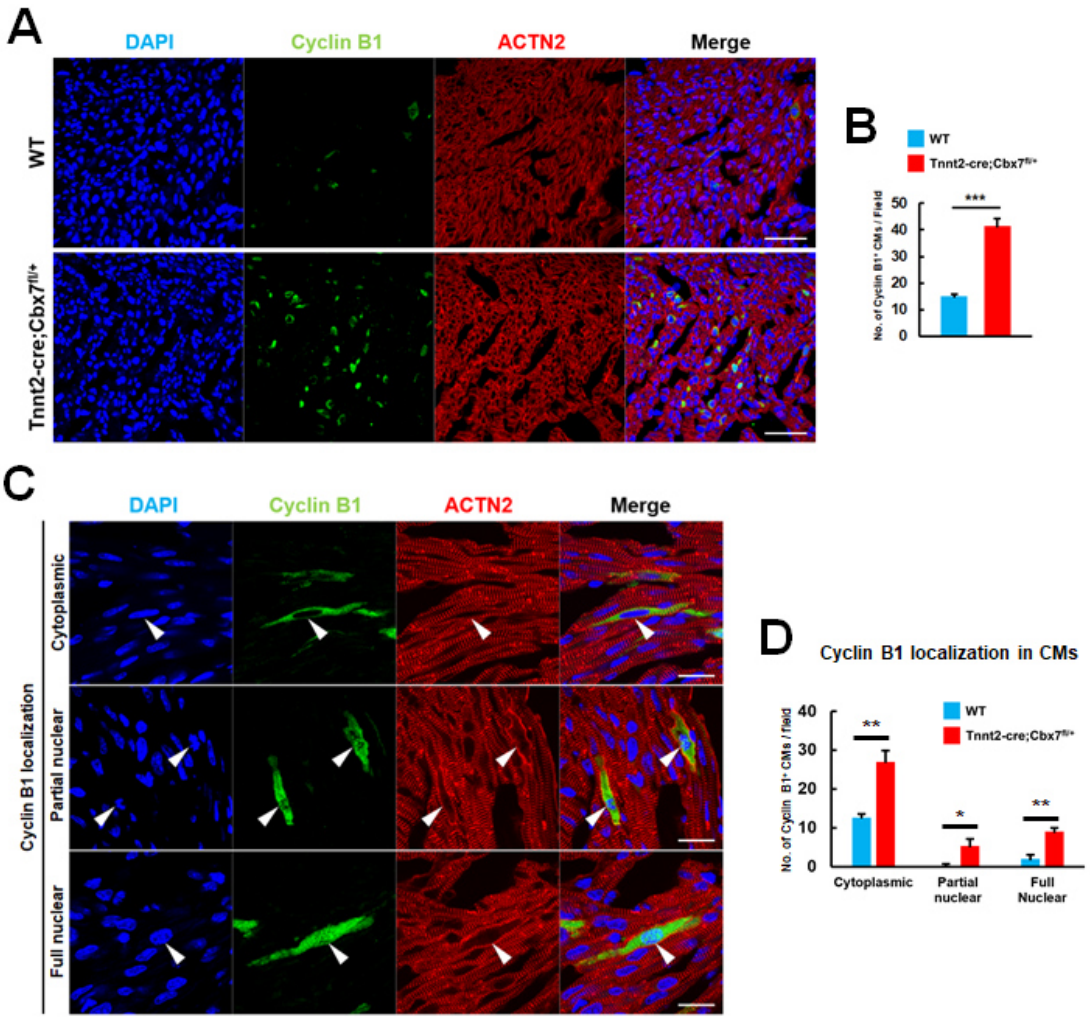

Figure 4-9. Increased number of Cyclin B$^+$ CMs in the neonatal heart by targeted inhibition of CBX7. Neonatal hearts from wild type and Tnnt2-cre;Cbx7$^{fl/+}$ mice were subjected to IHC for Cyclin B1 and ACTN2. A. Low magnification images stained for Cyclin B1 and ACTN2. Bar = 50 µm B. Quantification of A. Error bars: standard error of mean. *** P < 0.001, Standard unpaired Student's t test. C. Higher magnification images showing three different subcellular localizations of Cyclin B1 in CMs. Bar = 20 µm D. Quantification of C. Error bars: standard error of mean. * P < 0.05, ** P < 0.01, *** P < 0.001, Standard unpaired Student's t test. 170 Cyclin B$^+$ CMs in 5 different fields were counted.

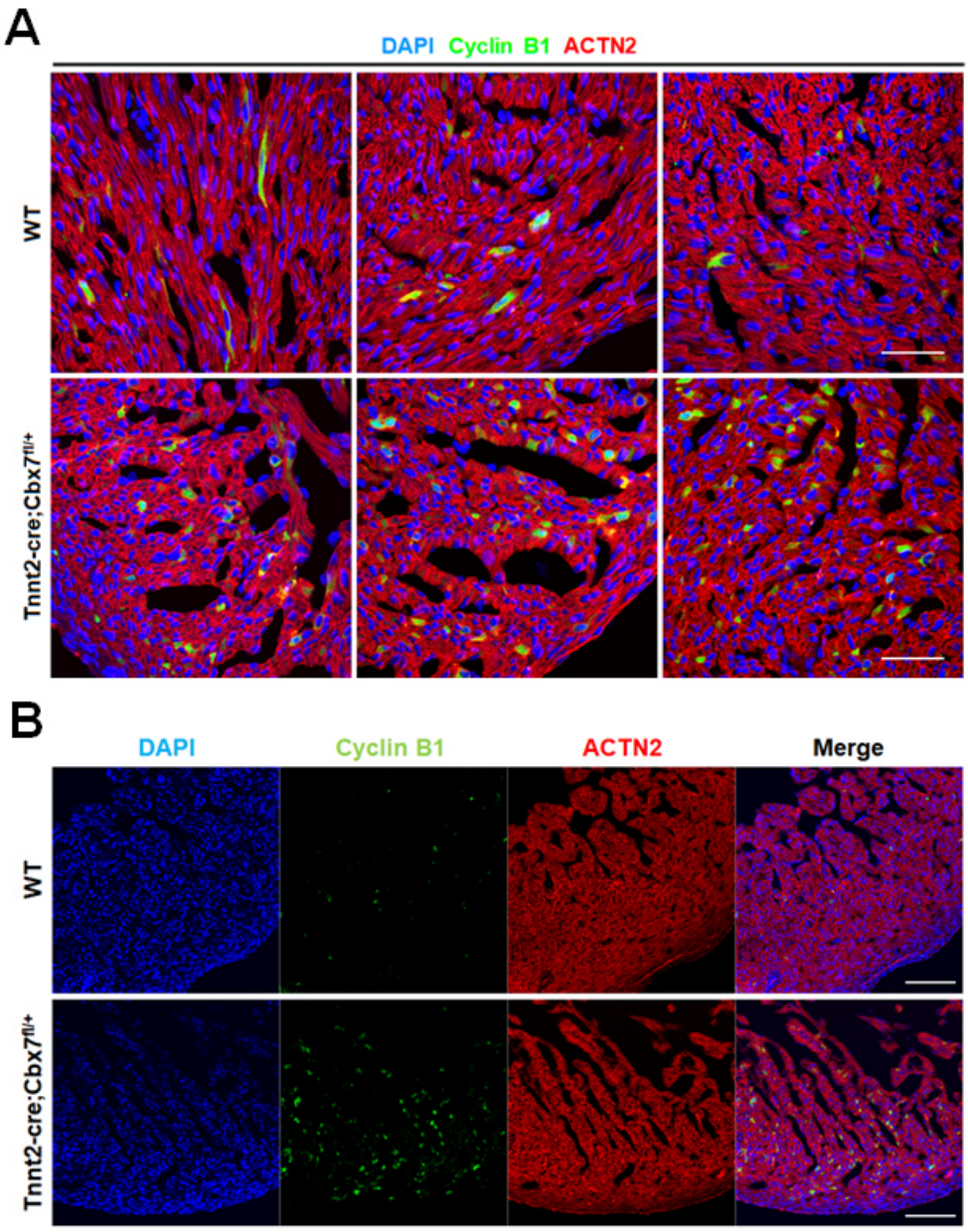

Figure 4-10. Low magnification IHC images stained for Cyclin B1 and ACTN2 in wild type and Tnnt2-cre;Cbx7$^{fl/+}$ mouse hearts. Neonatal hearts (P0) from wild type and Tnnt2-cre;Cbx7$^{fl/+}$ mice were subjected to IHC for Cyclin B1 and ACTN2. A. Bar = 50μm B. Bar = 100μm

4.2.7 Cardiac haploinsufficiency of CBX7 decreases cardiac connexin 43

Connexin 43, whose official name is Gap junction alpha-1 protein (GJA1), is an important protein that mediates intercellular communication. It is ubiquitously expressed in most cell types. In the heart, Connexin 43 is the major gap junction protein and controls coordinated myocardial contraction.

Since gene expression of Connexin 43 was downregulated by targeted inhibition of CBX7 in the neonatal mouse heart, its protein expression level was further confirmed via IHC (Figure 4-11). Targeted inhibition of CBX7 resulted in decreased expression of Connexin 43 protein in the neonatal mouse heart. This result implies that intercellular communication between CMs was impaired, leading to unsynchronized myocardial contraction and lethality. It is speculated that proliferative and immature CMs in the CBX7-haploinsufficient heart fail to establish communication networks with nearby cells.

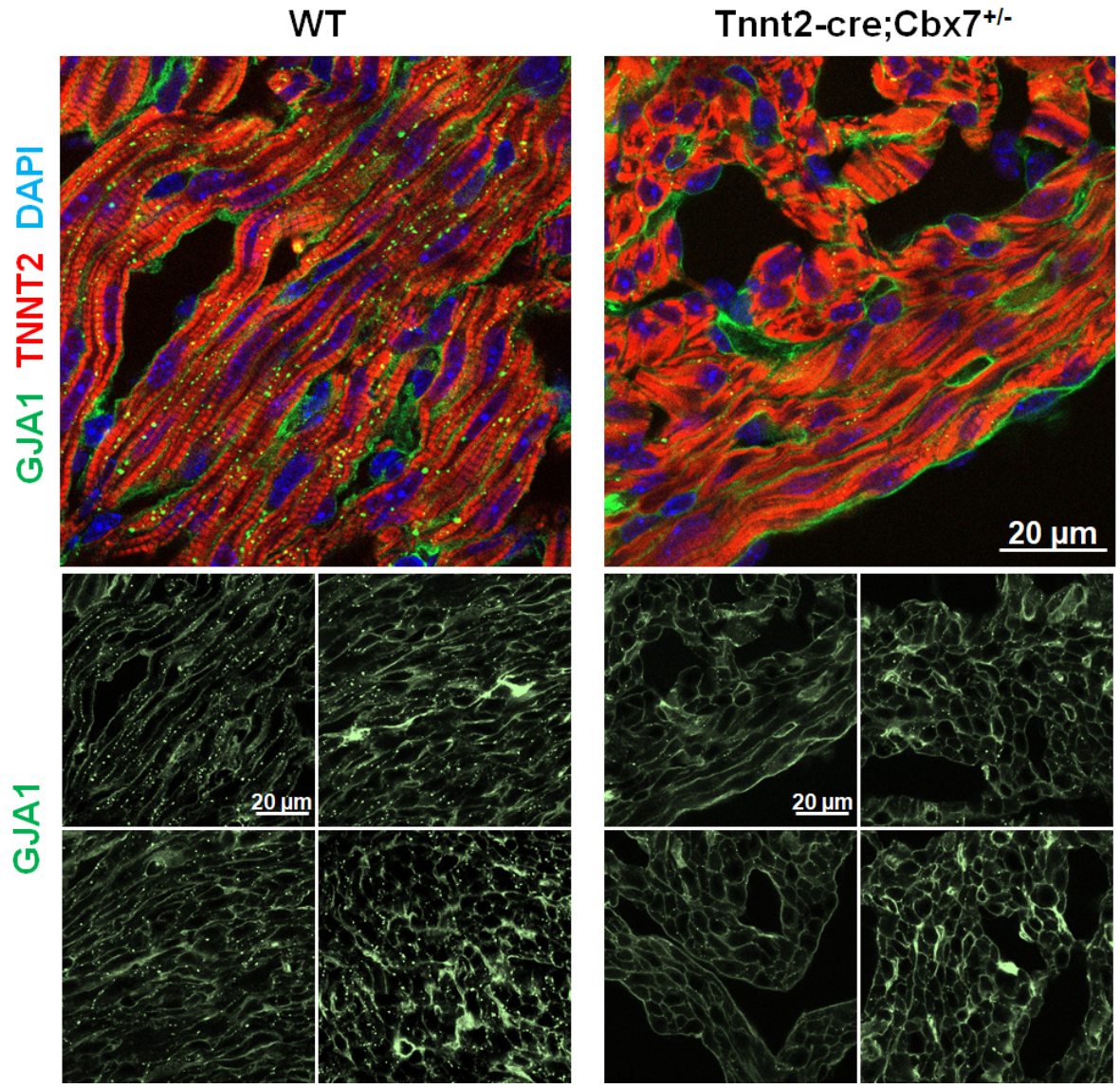

Figure 4-11. Downregulation of Connexin 43 in the neonatal heart by CBX7 haploinsufficiency. Neonatal hearts (P0) from wild type and Tnnt2-cre;Cbx7$^{fl/+}$ mice were subjected to IHC for Connexin 43 (GJA1) and ACTN2.

4.2.8 CBX7 does not affect expression of senescence-related genes in the neonatal mouse heart

CBX7 has been known to epigenetically represses cyclin-dependent kinases inhibitors (CDKIs) such as Cdkn2a, Cdkn2b, and Cdkn2d in certain types of cells. To examine whether CBX7 inhibits these CDKIs in CMs, we measured gene expression level of Cdkn2a, Cdkn2b, and Cdkn2d in whole neonatal hearts from wild type and the mutant mice via qRT-PCR (Figure 4-12). As a result, targeted inhibition of CBX7 did not affect gene expression level of Cdkn2a, Cdkn2b, and Cdkn2d, suggesting tissue- and context-specific role of CBX7.

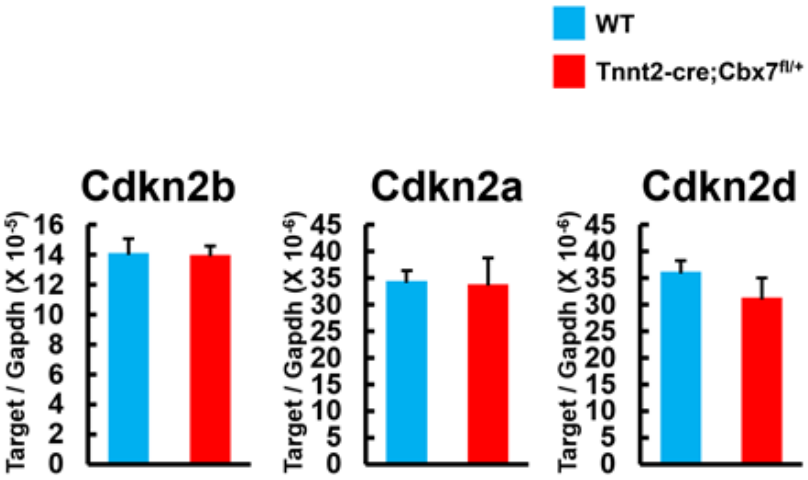

Figure 4-12. Minimal role of CBX7 in the regulation of senescence-related genes in the neonatal heart. Whole neonatal hearts from wild type and Tnnt2-cre;Cbx7$^{fl/+}$ mice were subjected to RNA extraction followed by cDNA synthesis and qRT-PCR. Error bars: standard error of mean, N=3.

4.3 Discussion

Despite previous investigations on cardiac functions of Polycomb group proteins, those of CBX7 have remained unknown. Increased thickness of myocardial walls and heart to body weight ratio of cardiac CBX7-haplodeficient mice indicate critical roles of CBX7 during heart development.

Perinatal lethality of cardiac CBX7-haplodeficient mice suggests the importance of controlled proliferation and terminal differentiation of perinatal CMs in the normal heart development. At birth, cardiac workload is increased by elevated systemic vascular resistance and circulatory transitions. Thus, perinatal myocardium must be capable of dealing with augmented workload during functional adaptation of the heart to a new environment. The cardiac CBX7-haplodeficient myocardium might have reduced contractility due to immature and proliferative natures of CMs. Cardiomegaly and dilated myocardium of the CBX7-haplodeficient heart reflect their failure to handle elevated afterload and hemodynamic stress associated with perinatal physiologic events.

Immunohistochemical analyses revealed that targeted inhibition of CBX7 resulted in sustained proliferation of CMs during perinatal period between E19.5 and P0. There have been few reports illustrating perinatal kinetics of CM proliferative capacity. In wild type mice, percentage of $Ki67^{+}$ CMs decreased from ~40% to ~15% between E18.5 and P1 (134). In addition, substantial reduction of CM proliferative capacity before birth was also observed in sheep (135).

Gene expression profiling revealed CBX7-mediated repression of fetal cardiac gene programs during perinatal period. Previously, it was shown that the neonatal heart exhibited downregulation of multiple cell cycle-related proteins such as Cyclin A, Cyclin B, Cyclin D1-3, CDK1, CDK2, CDK4, and CDK6, compared to the fetal heart (88; 100; 101; 103-106). Among

them, Cyclin A and Cyclin B were repressed a during narrow perinatal period between E19.5 and P1 (102). In the cardiac CBX7-haplodeficient myocardium, multiple cell cycle activators including CDK1, Cyclin A2 and Cyclin B1/2 were upregulated, suggesting that CBX7 blocks G_2/M transition by silencing of cell cycle activator genes. CBX7 did not repressed CDKI genes including Cdkn2a, Cdkn2b, Cdkn2d which were reported to be silenced by CBX7 in several types of cancers, suggesting tissue- and context-specific roles of CBX7 in terms of cell proliferation.

On the other hand, repression of early developmental genes seems to be a general function of CBX7. In the neonatal heart, CBX7 repressed early/fetal cardiac genes, suggesting that CBX7 is required for terminal differentiation of immature CMs. Consistently, key developmental genes were epigenetically silenced by CBX7 in stem/progenitor cells (56; 57; 114). It would be interesting to explore the potential of ectopic expression of CBX7 in immature CMs (such as iPSC-derived CMs) to enhance cardiac maturation.

We found Cyclin B1 protein as a useful marker for CM proliferation. Cytoplasmic accumulation and subsequent nuclear entry of Cyclin B1 are critical for mitotic entry (105; 136). Despite its critical roles in the mitotic process, Cyclin B1 has never been utilized as a marker for mitotic CMs. We found that protein expression and nuclear entry of Cyclin B1 in CMs were correlated to sarcomere disassembly which is one of the hallmarks of proliferative CMs (137), and here we first report its usefulness (utility or suitability) in analyzing CM proliferation. Increased number of Cyclin $B1^+$ CMs in the mutant heart suggests that CBX7 represses mitotic entry of perinatal CMs. The effect of targeted inhibition of CBX7 on the mitotic activity of adult CMs will be one of our future investigations.

Downregulation of Connexin 43 protein in the CBX7 haploinsufficient heart implies that impaired cardiac conduction system might cause the perinatal lethality. Connexin 43 plays critical

roles in cardiac intercellular communication and its genetic deletion lead to ventricular arrhythmias (138; 139). Sustained fetal cardiac gene program by targeted inhibition of CBX7 might result in failure to build cell-to-cell communication networks, ending up with unsynchronized myocardial contraction.

In contrast to our data, Forzati et al showed that CBX7 knockout mice were viable and reached adulthood (62). This apparent discrepancy between the previous report and our data could be due to the different knockout strategies; Forzati et al deleted exon 5, 6, and 3'UTR whereas we targeted deletion of exon 2 encompassing the chromodomain that recognizes H3K27me3. Interestingly, we observed a transcriptional variant of CBX7 in the mouse heart via qRT-PCR. Molecular cloning of CBX7 variant revealed that it had longer coding sequence in exon 5, compared to the original mouse CBX7 (Data not shown). This data suggests that expression of truncated CBX7 variant with intact chromodomain in the fetal organ might enable viability of the knockout mice in Forzati et al. In contrast, our mutant mice were lacking exon 2, leading to functional disruption of both CBX7 and its variant in the developing heart.

In summary, the mutant mice with cardiac CBX7 haplodeficiency displayed perinatal lethality with cardiomegaly. Targeted inhibition of CBX7 increased proliferative capacity of perinatal CMs in vivo. Mitosis-related genes and proteins were derepressed whereas cardiac maturation genes were downregulated by targeted inhibition of CBX7. On the other hand, CBX7 did not play a role in the expression of senescence-related genes in CMs.

4.4 Materials and Methods

Mice, Breeding and Genotyping

Tg(Tnnt2-cre)5Blh/JiaoJ and B6;D2-Tg(Myh6*-mCherry)2Mik/J mice were purchased from the Jackson Laboratories. Cbx7$^{tm1a(KOMP)Wtsi}$ mouse was generated by the trans-NIH Knock-Out Mouse Project (KOMP). Its sperms were obtained from the KOMP Repository and rederived via IVF and transplantation to B6 wildtype donor female mice by the Mouse Transgenic and Gene Targeting Core (TMF) at Emory University. Following primers were used for PCR genotyping. Cre (350 bp) forward: 5'-ATTTGCCTGCATTACCGGTC-3', reverse: 5'-ATCAACGTTTTCTTTTCGG-3'; Myh6-mCherry (288 bp) forward: 5'-AGGACGGCGAGTTCATCTAC-3', reverse: 5'-TGGTGTAGTCCTCGTTGTGG-3'; Cbx7 floxed (355 bp) forward: 5'-GAGATGGCGCAACGCAATTAATG-3', reverse: 5'-CAGAATCACTGAACTGTACGGTGGC-3'; Cbx7 pre-cre (553 bp) forward: 5'-GGGATCTCATGCTGGAGTTCTTCG-3', reverse: 5'-TGCTGCCACCCTTTAATACAGTTCC-3'; Cbx7 wildtype (331 bp) forward: 5'-ACCTGAGTCTCCCACAAGAGCAGC-3', reverse: 5'-CAGAATCACTGAACTGTACGGTGGC-3'. Purchased or rederived mice were crossed with B6 wildtype mice. Heterozygotes for either Tg(Tnnt2-cre)5Blh/JiaoJ or Cbx7$^{tm1a(KOMP)Wtsi}$ allele were selected from F1 progenies and outcrossed each other to generate cardiac Cbx7-heplodeficient mice (*Tnnt2-cre;Cbx7$^{floxed/+}$*).

Histological analysis

After euthanasia, mouse heart tissues were removed, fixed in 2% paraformaldehyde (PFA) at 4°C for 16 hours, and submerged in 30% sucrose solution at 4°C for 24 hours. Frozen heart sections prepared with OCT compound (Tissue-TeK 4583) were washed with PBS. Then samples were permeabilized/blocked with PBS containing 0.5% Triton X-100 and 2.5% BSA at room temperature for 1hour. Slides were then incubated with anti-ACTN2 (Sigma A7811, 1:100), anti-Ki67 (Cell Marque 275R-14, 1:100), anti-phospho-Histone H3 (Ser10) (Millipore 06-570, 1:100), anti-Cyclin B1 (Cell Signaling Technology 12231, 1:100), at 4°C overnight. WGA staining was performed by following the manufacturer's instruction (ThermoFisher W32466). The slides were washed three times with PBS containing 0.1% Tween 20 and incubated with appropriate secondary antibodies at room temperature for 1-2 hours. DAPI was used for nuclear staining. The samples were visualized under a Zeiss LSM 510 Meta confocal laser scanning microscope (Carl Zeiss). H&E staining was performed as described previously and examined under Olympus IX71 bright field microscope and Zeiss Axioskop 2 Plus.

Quantitative Real-time PCR

Total RNAs from mouse CMs and hearts were isolated using a guanidinium extraction method (124) combined with RNA extraction kit (Qiagen). Extracted RNA was reverse-transcribed using Taqman Reverse Transcription Reagents (Applied Biosystems 4304134) according to the manufacturer's instructions. The synthesized cDNA was subjected to qRT-PCR using specific primers and probes (see Table 3). Quantitative assessment of RNA levels was performed using an

ABI PRISM 7500 Sequence Detection System (Applied Biosystems). Relative mRNA expression was normalized to Gapdh gene.

Statistical analyses

All data were expressed as mean ± SEM. Values of $P < 0.05$ were considered to denote statistical significance.

Chapter 5: Gain-of-function analyses of CBX7 using neonatal mouse cardiomyocytes in vitro

5.1 Introduction

CMs undergo robust DNA synthesis in two distinct phases (104). The first phase takes place during proliferation of fetal CMs whereas the second phase is associated with binucleation and polyploidization of neonatal/juvenile CMs. In mice, binucleation and polyploidization account for 57% and 13% of the second phase of DNA synthesis respectively (140). Binucleated CMs are generated through DNA synthesis followed by nuclear mitosis (karyokinesis) without cytokinesis. This process is called “acytokinetic mitosis”.

The physiological meaning of CM binucleation and polyploidization is unclear. However, increased DNA content in the second phase is considered to be closely linked to proliferative capacity of CMs for the following reasons. First, the rodent heart loses regenerative capacity within the first postnatal week which coincides with increased DNA content in the second phase. In addition, most proliferative CMs in the embryonic heart across all species are mononuclear diploid cells whereas most mammalian CMs undergo binucleation or polyploidization, leading to increased total DNA content. Furthermore, the frequency of mononuclear diploid CMs was correlated with the regenerative response of the adult mouse heart (141). Lastly, adult CMs in zebra fish and newt, which have regenerative hearts, remain mononuclear diploid throughout life.

Both multinucleation and polyploidization are indications of cardiac maturation. Increased DNA content for the sake of loss of mitotic capacity in mammalian CMs would be beneficial to meet the augmented metabolic demand of mature CMs where more DNAs can be transcribed and thus more RNAs can be translated into proteins.

In the previous Chapter, the loss-of-function of CBX7 in CMs was investigated using mutant mouse lines. In this Chapter, the gain-of-function of CBX7 in CMs will be discussed. The effects of CBX7 overexpression on proliferative capacity, binucleation, and total DNA content

were examined via adenoviral transduction into wild type neonatal mouse CMs. Furthermore, the potential role of CBX7 in non-CMs was explored.

5.2 Results

5.2.1 CBX7 overexpression decreases proliferative capacity and promotes binucleation of neonatal mouse cardiomyocytes

For CBX7 gain-of-function analyses, the recombinant Adenovirus particles inducing overexpression of mouse CBX7 were generated and validated by western blot and qRT-PCR (Figure 5-1). Endogenous CBX7 protein was not detected in both HEK-293 cells and mouse embryonic fibroblasts (MEFs). Ad-Mock virus induced expression of CBX7 in HEK-293 cells, but not in MEFs. Ad-CBX7 induced overexpression of CBX7 protein in both cell types. To confirm this result in CMs, isolated neonatal (P0) mouse CMs were infected with these viruses. As a result, Ad-CBX7 adenoviral particles induced 254-fold increase in CBX7 transcript level compared to Ad-Mock virus.

To examine the effect of CBX7 overexpression on CM proliferation, neonatal mouse CMs were treated with these viruses and subjected to ICC for Ki67. CBX7 overexpression caused a ~15% decrease in $Ki67^{+}$ CMs compared to Ad-Mock group. Interestingly, the percentage of binucleated CMs was increased by ectopic expression of CBX7. These results indicate that CBX7 represses proliferative capacity and promotes maturation of neonatal CMs.

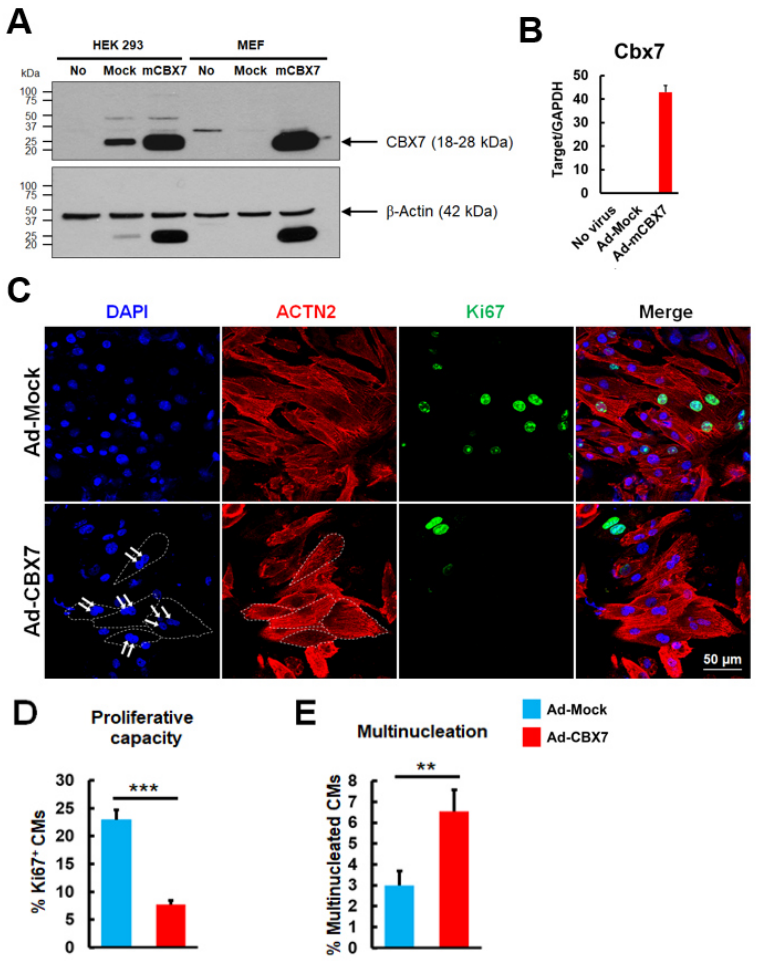

Figure 5-1. Decreased proliferative capacity and increased binucleation of neonatal mouse CMs by CBX7 overexpression. A. HEK-293 and MEFs were treated with either nothing (No), empty adenoviral particles (Mock), and adenoviral particles inducing mouse CBX7 overexpression (mCBX7). Three days after transduction, whole cell lysates were subjected to western blot. B. Neonatal (P0) mouse CMs were infected with adenoviral particles for 3 days and subjected to qRT-PCR for Cbx7 gene. C. Three days after adenoviral transduction, neonatal mouse CMs were subjected to ICC for ACTN2 and Ki67. D. Quantification of percentage of $Ki67^+$ CMs. E. Quantification of percentage of multinucleated CMs. Error bars: standard error of mean. * $P < 0.05$, ** $P < 0.01$, *** $P < 0.001$, Standard unpaired Student's t test. 1,200 cells in each group were examined.

5.2.2 CBX7 overexpression increases DNA content of neonatal mouse cardiomyocytes

In Chapter 4, CBX7-haplodeficient CMs showed increased level of Ki67, pH3 and Cyclin B1, and reduced cell size. On the other hand, CBX7 overexpression lead to decreased proliferative capacity and increased binucleation, suggesting CBX7 promotes cardiac maturation. Increased DNA content (via either polyploidization or binucleation) is one of the major characteristics of mature CMs. Thus, we hypothesized that CBX7 overexpression leads to increased DNA content in CMs.

To test this hypothesis, wild type neonatal mouse CMs were transduced with adenoviral particles inducing overexpression of CBX7, followed by Propidium Iodide (PI) & TNNT2 staining and flow cytometry (Figure 5-2). Live cells were gated for selecting singlet and further gated for $TNNT2^{+}$ CMs. These cells were further analyzed for PI staining. The left peak indicates 2N, and the right peak represents 4N, cells in between are 2-4N. Compared to mock control, 2N population was decreased, and 4N population was 10% increased by CBX7 overexpression.

This data suggests that CBX7 promotes increase in DNA content. However, we cannot define whether increased DNA content was due to polyploidization or binucleation. In order to define this, CM nuclei will be isolated and subjected to staining for PCM1 (pericentriolar material 1) and PI, followed by flow cytometry analyses in the future (142). PCM1 marks nuclear membrane of CMs, enabling specific detection or isolation of CM nuclei.

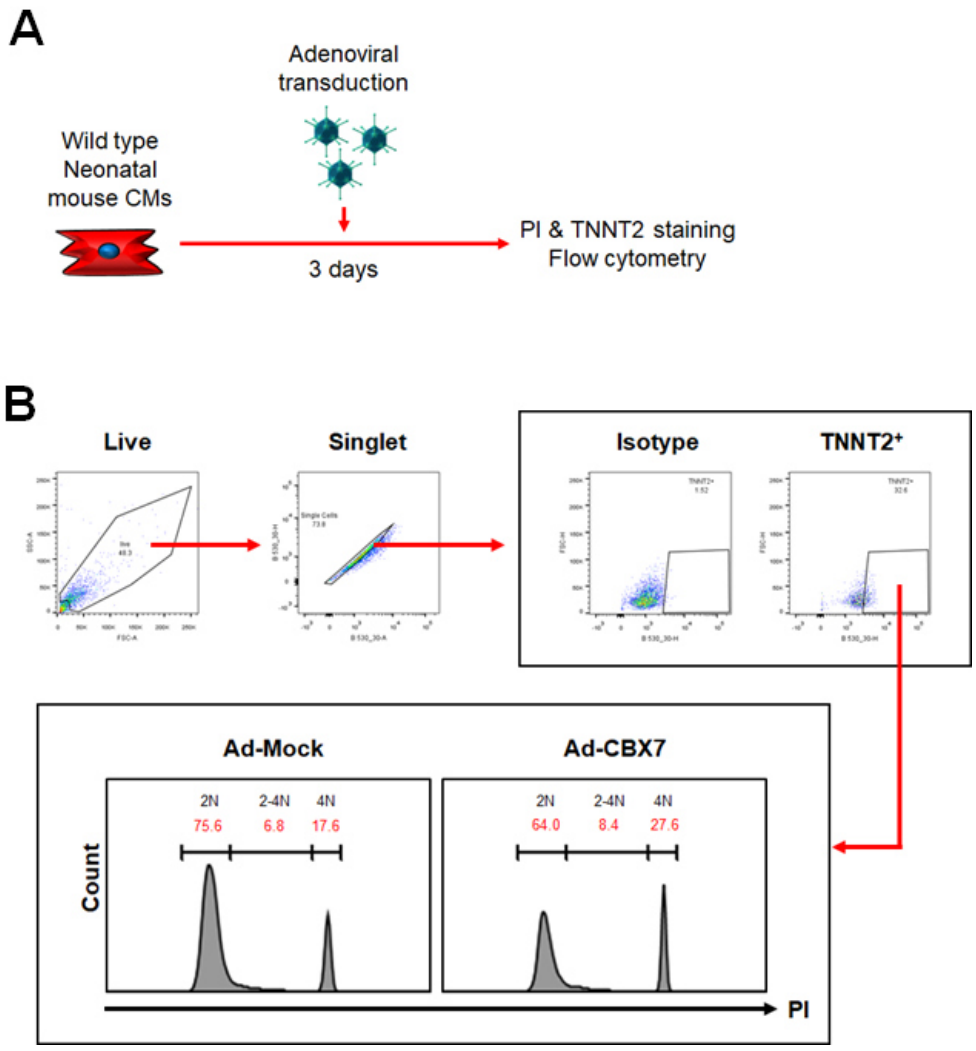

Figure 5-2. Increased DNA content of neonatal mouse CMs by CBX7 overexpression. A. A schematic of experimental design. wild type neonatal mouse CMs were transduced with adenoviral particles inducing overexpression of CBX7, followed by Propidium Iodide (PI) & TNNT2 staining and flow cytometry. B. Flow cytometry analysis of neonatal mouse CMs treated with Ad-Mock and Ad-CBX7 viral particles.

5.2.3 CBX7 represses proliferation of cardiac fibroblasts

Immunohistochemical analyses of the mouse adult heart revealed that CBX7 was expressed in other types of cardiac cells as well as CMs (Figure 3-4). This result lead us to ask a question about the role of CBX7 in non-CMs. To answer this question, isolated neonatal cardiac fibroblasts were treated with adenoviral particles inducing overexpression of CBX7 and subjected to MTT assay to measure proliferation. CBX7 overexpression inhibited proliferation of neonatal mouse cardiac fibroblasts (Figure 5-3). Since Adenovirus have cytolytic effects, higher amount of Ad-Mock viral particles reduced cell viability (Blue dots). Viability of neonatal mouse cardiac fibroblasts was even more decreased by the treatment of Ad-CBX7 viral particles. This data indicates that CBX7 represses proliferation of cardiac fibroblasts and implies that the role of CBX7 is similar between CMs and cardiac fibroblasts.

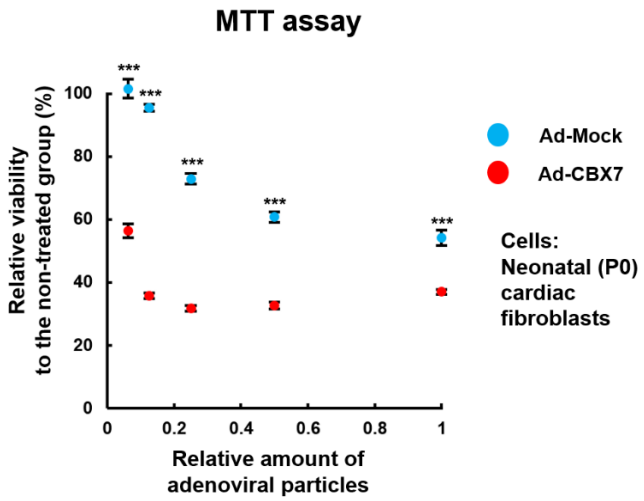

Figure 5-3. Repressed proliferation of cardiac fibroblasts by CBX7 overexpression. Neonatal mouse cardiac fibroblasts were treated with either Ad-Mock and Ad-CBX7 viral particles at different amounts for 3 days and subjected to MTT assay. Error bars: standard error of mean of quintuplicate. *** $P < 0.001$, Standard unpaired Student's t test.

5.3 Discussion

In this Chapter, the cardiac role of CBX7 was characterized by adenovirus-mediated gene delivery to neonatal mouse CMs and cardiac fibroblasts. It was revealed that CBX7 repressed proliferative capacity and promoted increase in DNA content in neonatal mouse CMs. This result was consistent with the previous result where targeted inhibition of CBX7 increased CM proliferative capacity and decreased cardiac maturation.

During embryonic and fetal stages, cardiac mass increases via proliferation of CMs. After birth, such hyperplastic growth starts to decline as most CMs undergo cell cycle arrest. Postnatal reduction of CM proliferative capacity is mediated by oxidative DNA damage response which is initiated by exposure to oxygen-rich environment right after birth (131). However, it is unknown how this environmental cue induces epigenetic changes that shut down fetal cardiac gene program and promote postnatal cardiac maturation. Perinatal upregulation of CBX7 implies that it might be a responsive epigenetic factor to oxygen-rich environmental cues, remodeling epigenomic landscape of perinatal CMs.

However, the mechanism whereby CBX7 represses proliferative capacity and promotes maturation of perinatal CMs is unknown. Since multiple cell cycle activators are downregulated during the perinatal stage, those genes could be epigenetically silenced by CBX7. It is also possible that CBX7 silences genes related to cardiac growth factor signaling such as Nrg1, IGF1, and FGF1. In order to identify genome-wide direct targets of CBX7 in CMs, systems biology approaches such as ATAC-seq, ChIP-seq, and RNA-seq will be employed in the future.

Whether CBX7 directly promotes cardiac maturation or indirectly via suppression of proliferation remains unclear. Proliferation and differentiation have inverse relationship and are regulated by distinct signaling pathways antagonistic to each other (143). For instance, MAPK p38

promotes cardiac differentiation and the targeted inhibition of p38 resulted in enhanced proliferative capacity of adult rat CMs (108). Thus, it is possible that CBX7 promoted cardiac maturation via repression of proliferation-related signaling pathways.

In summary, overexpression of CBX7 in the neonatal CMs resulted in reduced proliferation of $Ki67^{+}$ CMs and increased multinucleation. Increased DNA content by CBX7 GOF was further confirmed by PI staining. Overexpression of CBX7 in cardiac fibroblasts resulted in reduced cell proliferation, suggesting similar role of CBX7 in both CMs and fibroblasts.

5.4 Materials and Methods

Immunocytochemistry

Cells were fixed in 4% PFA at room temperature for 10 minutes. Then samples were permeabilized/blocked with PBS containing 0.1% Triton X-100 and 2.5% BSA at room temperature for 1hour. Slides were then incubated with anti-ACTN2 (Sigma A7811, 1:100), anti-CBX7 (Abcam ab21873, 1:100), or anti-Ki67 (Cell Marque 275R-14, 1:100) at 4°C overnight. The slides were washed three times with PBS containing 0.1% Tween 20 and incubated with appropriate secondary antibodies at room temperature for 1-2 hours. DAPI was used for nuclear staining. The samples were visualized under a Zeiss LSM 510 Meta confocal laser scanning microscope (Carl Zeiss).

Isolation and culture of neonatal mouse CMs and cardiac fibroblasts

We modified a previously reported protocol (121). Briefly, neonatal hearts from P0 mice were minced with scissors and incubated in HBSS containing 0.0125% trypsin overnight at 4ºC for pre-digestion. On the following day, the tissue fragments were further digested in oxygenated HBSS containing 1.5 mg/ml Collagenase/Dispase mix (Roche) at 37 ºC for 30 min with gentle agitation. After filtering with 100 µm strainer, cells were plated and cultured in the Plating medium (84% DMEM high glucose, 10% horse serum, 5% FBS, 1% anti-anti) at 37 ºC for 1.5 hrs, allowing the preferential attachment of fibroblasts. Adherent cells were sub-cultured and used for cardiac fibroblasts which were cultured in DMEM high glucose media containing 10% FBS. Non-adherent cells were subjected to percoll-based separation (83) and MACS using feeder removal microbeads

(Miltenyi Biotec 130-095-531) for the further purification of neonatal CMs. Enriched neonatal CMs were plated onto collagen-coated dishes and cultured in the Plating medium. On the following day, the medium was changed to the Culture medium (78% DMEM high glucose, 17% M-199, 4% horse serum, 1% anti-anti, 1% ITS). Growth factors including 50 ng/ml IGF1 and 25 ng/ml FGF1 were added to both Plating and Culture media. Two days after the treatment of recombinant adenoviral particles, cells were subjected to ICC.

Generation of recombinant adenovirus particles

cDNA of mouse CBX7 (NM_144811.3) was cloned into pCR2.1-TOPO vector via TA cloning method using the following primers. Forward: 5'-ATGGAGCTGTCAGCCATAGG-3' and Reverse: 5'-TGTCCGGATGTGTTCATGGG-3'. Cloned mouse CBX7 cDNA was subcloned into adenoviral shuttle plasmid pDC316 (Microbix Biosystems). Both adenoviral genomic and shuttle plasmids were transfected to HEK-293 cells using Lipofectamine 3000 (Thermo Fisher Scientific). Recombinant adenoviral particles were extracted from cell lysates and the relative titer of Ad-Mock and Ad-CBX7 viral particles was determined via qRT-PCR for adenovirus serotype 5 (Ad5) genome (123).

Western blot

Cells were lysed with RIPA buffer, supplemented with PMSF, phosphatase-inhibitor cocktail (Sigma) and protease-inhibitor cocktail on ice for 1 h and the lysates were clarified by centrifugation. Equal amounts of lysates were subjected to SDS-PAGE, transferred onto a nitrocellulose membrane, and blocked for 1 h at room temperature in Tris-buffered saline with

0.05% Tween-20 (TBST) and 5% non-fat milk. The membrane was subsequently incubated with anti-CBX7 (Abcam ab21873, 1:1000) and anti-β-actin (Cell Signaling Technology 4967, 1:1000) at 4 ºC overnight. After washing with TBST, blots were incubated with the appropriate secondary antibodies for 1 h at room temperature and developed using ECL detection reagent (Thermo Fisher).

Flow cytometry

Neonatal mouse CMs were detached using Accutase (Thermo Fisher). Cells were incubated with anti-TNNT2 antibody (Thermo Fisher MS-295) and Propidium iodide (BD Biosciences) at 4 ºC for 20 min. After washing twice with ice-cold PBS, cells were subjected to reading. Flow cytometry was performed using BD LSRII Flow Cytometer and gained data were analyzed using FLOWJO software.

MTT assay

Neonatal cardiac fibroblasts were seeded on 96 well plate at 5 x 10^3 cells per well. DMEM high glucose media supplemented with 10% FBS, 1% glutamine, 1% non-essential amino acid (NEAA) was used for culture. Two hours after seeding, cells were treated with adenoviral particles and further incubated for three days. MTT reagent was added to cell culture at the final concentration of 0.5 mg/ml. The plate was incubated at 37ºC for 30 min in the darkness. After removal of culture media, cells were lysed by DMSO and color was measured at 570 nm.

Statistical analyses

All data were expressed as mean ± SEM. Values of $P < 0.05$ were considered to denote statistical significance.

Table 3. Primers used in qRT-PCR

Primer name	Sequence (5'->3')
Ad5_F	CAGCGTAGCCCCGATGTAA
Ad5_R	TTTTTGAGCAGCACCTTGCA
Atp2a2_F	TGGAACAACCCGGTAAAGAGT
Atp2a2_R	CACCAGGGGCATAATGAGCAG
Cbx2_F	CTATGGCGACCCCAGAGAAC
Cbx2_R	GCGTCCTCACTTTCAGGTCTA
Cbx4_F	AAGAAGCGGATACGCAAGGG
Cbx4_R	GGAGGAGTCTTGAAGCCCAG
Cbx6_F	TGGCACATTTGCGCTCTACAA
Cbx6_R	CTCCGGGAGTAGCTTGGGT
Cbx7_F	TGCGGAAGGGCAAAGTTGAAT
Cbx7_R	ACAAGGCGAGGGTCCAAGA
Cbx8_F	ACCAGCCGTGTAGACGACA
Cbx8_R	GGTCACACCATATTGCACCAG
Ccna1_F	AAGAACCTGAGAAGCAGGGC
Ccna1_R	CTAGCACGGTTCTCTGTGGG
Ccna2_F	GGTCCTAACGCTCCCATCTC
Ccna2_R	TTCATGGGCAGTCCTGGTAG
Ccnb1_F	GCGAAGAGCTACAGGCAAGA
Ccnb1_R	ATGTTTCCATCGGGCTTGGA
Ccnb2_F	CTATCCGGCGGGCAGTTTTA
Ccnb2_R	TCTGAGGTTTCTTCGCCACC
Cdk1_F	AGAAGGTACTTACGGTGTGGT
Cdk1_F	GAGAGATTTCCCGAATTGCAGT
Cdkn2a_F	GGGTTTCGCCCAACGCCCCGA
Cdkn2a_R	TGCAGCACCACCAGCGTGTCC
Cdkn2b_F	CAGTTGGGTTCTGCTCCGT
Cdkn2b_R	AGATCCCAACGCCCTGAAC
Cdkn2d_F	GTCCTGGACATTGGGGCT
Cdkn2d_R	AACCGCTTCGGCAAGAC
Ezh2_F	TCCATGCAACACCCAACACAT
Ezh2_R	GGGTCTGCTACTGTTATTCGGAA
Gapdh_F	ATGACCACAGTCCATGCCATC
Gapdh_R	CCTGCTTCACCACCTTCTTG
Gja1_F	ACAGCGGTTGAGTCAGCTTG
Gja1_R	GAGAGATGGGGAAGGACTTGT

Primer name	Sequence (5'->3')
Kcnj2_F	ATGGGCAGTGTGAGAACCAAC
Kcnj2_R	TGGACTTTACTCTTGCCATTCC
Myh6_F	ATGGGCTGGCTGGAAAAGAA
Myh6_R	ATTTTCCCGGTGGAGAGCAG
Myh7_F	ACTGTCAACACTAAGAGGGTCA
Myh7_R	TTGGATGATTTGATCTTCCAGGG
Myl2_F	TGACCACACAAGCAGAGAGG
Myl2_R	CCGTGGGTAATGATGTGGAC
Pcgf1_F	AGATGGACCCACTACGGAAC
Pcgf1_R	GCTGCGTCTCGTGGATCTT
Pcgf2_F	AACGGCGACGGGACTTCTA
Pcgf2_R	CATCTCCATTCTCCGTGAGGT
Pcgf3_F	CAGGTAAGCATCTGTCTGGAATG
Pcgf3_R	GTAACAACCACGAACTTGAGAGT
Pcgf4_F	ATCCCCACTTAATGTGTGTCCT
Pcgf4_R	CTTGCTGGTCTCCAAGTAACG
Pcgf5_F	GTAAGACCTGTATTGTCCAGCAC
Pcgf5_R	TCTCGTAGTCCAGGCACTAATTT
Pcgf6_F	GAGGAGCGCCTGATAAACCTT
Pcgf6_R	TGGTGGACAACTATGTTGCATT
Phc1_F	TAGCACAGATGTCCCTGTATGA
Phc1_R	TTGCTGGAGCATGAACTGGTG
Ring1_F	GATGGTACAGAGATTGCGGTTT
Ring1_R	CCTATGCAGGCACTCCTTGG
Ring2_F	AACACCTCAGGAGGCAATAACA
Ring2_R	GCGCAAAACCGATGTAAACACT
Scmh1_F	CCCTCTAGGATTTCGGCTGAA
Scmh1_R	CGCCTCGAACTTCTCCAATAG
Scn5a_F	ATGGCAAACTTCCTGTTACCTC
Scn5a_R	CCACGGGCTTGTTTTTCAGC
Suz12_F	AGCAACATGGGAGACAATTCTTG
Suz12_R	ACAGCAATAGTTTGTGCAGGTTT
Tnnt2_F	TCACAACCTGGAGGCTGAGAAGTT
Tnnt2_R	TCATCTATTTCCAACGCCCGGTGA
Yy1_F	CAGTGGTTGAAGAGCAGATCAT
Yy1_R	AGGGAGTTTCTTGCCTGTCAT

Chapter 6: Conclusion and Future Directions

Conclusion and Future Directions

The current dissertation research explored two major therapeutic strategies targeting CMs for heart regeneration: PSC-derived CMs and proliferation of pre-existing CMs. We first discussed the purification of ventricular CMs from differentiating mouse embryonic stem cells (ESCs) via molecular beacon technology in Chapter 2. From Chapter 3 to 5, we addressed a possible mechanism that reduces CM proliferation during the perinatal stage.

Over the past decade, there has been notable advancement in the methodologies for generating PSCs (82; 144) and producing CMs from PSCs, raising the prospects of using stem-cell-derived CMs for cardiac repair (17; 145). However, all reported CM differentiation protocols to date can generate only heterogeneous CMs mixed with other cell populations. Although several recent studies reported non-genetic methods for isolating general CMs (146; 147), these methods still generate heterogeneous CMs, not chamber-specific CMs. Given the major role of ventricular CMs for cardiac contractile function, it is important to develop a non-genetic method to isolate ventricular CMs from differentiating PSCs for preclinical and clinical applications.

To address this unmet need, we designed MBs targeting IRX-4, a ventricular CM-specific transcription factor, generated homogeneous ventricular-like CMs from mESCs without altering their genome, and demonstrated that this method yielded functional ventricular CMs with high specificity and efficiency. Specifically, nucleofection-based delivery of MBs targeting the Irx4 mRNA followed by FACS sorting enabled efficient enrichment of ventricular CMs from differentiating mESCs with 92% purity. In electrophysiological studies, approximately 98% of these MB-purified CMs demonstrated ventricular-CM-like action potentials and Ca^{2+} oscillations, indicating that they are functionally intact ventricular CMs. These cells showed coordinated contraction and maintained their phenotype for more than 2 weeks in culture.

To date, attempts to induce robust proliferation of adult CMs have failed. Thus, the field has made extensive efforts to understand regulatory mechanism of CM proliferation over the past several decades. However, it has been largely unknown what causes CMs to exit the cell cycle and lose proliferative capacity. In the current study, we uncovered a novel regulatory mechanism how perinatal CMs lose proliferative capacity and become mature during the functional adaptation of the heart at birth. Through expression profiling, LOF, and GOF analyses, we identified CBX7 as a novel repressor of perinatal CM proliferation. Expression profiling of PcG genes revealed CBX7 as one of the major PRC1 subunits in the postnatal heart. Previously, the role of CBX7 in stem/progenitor cells and cancer cells were illustrated (56; 57; 120), but its behavior in postnatal somatic cells were poorly understood. In particular, its role in CMs has been unknown. Our results indicate that CBX7 plays an anti-proliferative role in CMs during perinatal and postnatal period. It has been controversial whether CBX7 inhibits or promotes cell proliferation. Due to divergent observations, it has been claimed that CBX7 functions in a tissue- and context-specific manner (65).

CBX7 is the first discovered chromatin remodeler that represses proliferative capacity of perinatal CMs. Chromatin remodelers are attractive therapeutic targets for inducing CM proliferation for the following reasons: 1) Profound chromatin changes are necessary for mitosis (47; 48; 129). 2) Proliferative (fetal/neonatal) CMs have distinct epigenetic landscapes from those of post-mitotic (adult) CMs (45; 148). 3) Chromatin remodelers orchestrate multiple gene expression programs (110) AND multiple cell cycle genes are down-regulated in post-mitotic CMs (29; 100; 101; 104; 106; 148; 149).

Perinatal lethality of cardiac CBX7-haplodeficient mice suggests the importance of controlled proliferation and terminal differentiation of perinatal CMs in normal heart development.

At birth, cardiac workload is increased by elevated systemic vascular resistance and circulatory transitions (150). Thus, perinatal myocardium must be capable of dealing with augmented workload during functional adaptation of the heart to a new environment. The mutant myocardium might have reduced contractility due to immature and proliferative characteristics of CMs and delayed myocardial maturation. Cardiomegaly and dilated myocardium of the mutant mice reflect their failure to handle elevated afterload and hemodynamic stress associated with perinatal physiologic events.

However, there are multiple remaining questions that the current study was not able to fully address. We observed lethality of the mutant mice where CMs exhibited enhanced proliferation. How can the enhanced proliferation of CMs cause lethality? We consider that the cause of perinatal death of CBX7-haplodeficient mice would be immature characteristics of CMs. Our data support this notion in several aspects: 1) The mutant neonatal heart showed sponge-form myocardium (Figure 4-4, 4-5, and 4-6) which is a hallmark of fetal heart (151), suggesting that CBX7 deficiency delayed myocardial maturation. 2) CMs in the mutant heart showed increased level of proliferation markers such as Ki-67 and pH3 (Figure 4-4, 4-5, and 4-6). 3) Molecular markers for cardiac maturation were reduced in the mutant heart (Figure 4-8 and 4-11). 4) CM size was reduced (Figure 4-7).

To further prove immature characteristics of mutant CMs, we could assess heart function via fetal echocardiography at the organ level (152). In addition, we could determine CM maturation at the cellular level via traction force microscopy, electron microscopy, calcium signaling imaging, analysis of morphological features such as length-to-width ratio, cell size (by WGA staining), nuclei shape (circular vs. elongated) and multinucleation via immunocytochemistry (ICC). Furthermore, alignment and length of sarcomere could be assessed by staining for ACTN2,

TNNT2, MYH6/7, and MYL2. Presence of Transverse tubules (T-tubules) and the quantity of mitochondrial cristae could be examined through transmission electron microscopy (TEM) imaging. Electrophysiological recordings could be performed to measure upstroke velocity, resting membrane potential, membrane capacitance, and response to β-adrenergic stimulation (no vs. inotropic reaction) via patch clamp techniques. To examine CM maturity at the molecular level, isoform profiling of Titin (N2BA vs. N2B) and Troponin I (ssTnI vs cTnI) could be measured by qRT-PCR. In addition, expression of ion transporters and their regulatory proteins such as Scn5a, Gja1, Hcn4, Kcnj2, and Serca2a could be measured by IHC and ICC. Finally, gene expression of cardiac transcription factors including Nkx2.5, Gata4, Mef2c, Tbx5, Hand, Isl1 and Irx4 could be examined by qRT-PCR.

Another possible explanation for the lethality of the mutant mice is that sarcomere disassembly of proliferative CMs may reduce myocardial contractility for a following reason. Proliferating CMs undergo disassembly of myofibril for successful cytokinesis (137). The sarcomere is the fundamental contractile unit of CMs. Thus, it is highly likely that sarcomere disassembly would reduce contractile force of an individual CM. Large-scale (or global) proliferation of CMs may result in the gross reduction of myocardial contractility, leading to cardiac dysfunction. On the other hand, previous reports showed that the neonatal mouse heart with proliferative CMs can fully regenerate itself, surviving without suffering from cardiac dysfunction or reduced contractility (8). Thus, increased CM proliferation in the mutant mice could be the innate response to overcome or compensate cardiac dysfunction caused by targeted inhibition of CBX7.

Then, why do the mutant mice die at the perinatal stage? What causes perinatal lethality of the mutant mice? We speculate that the failed heart cannot compensate the increased vascular

resistance after birth. Systemic vascular resistance (SVR) is elevated as the low resistance placental circulation is removed at birth (150; 153). Thus, blood pressure tends to peak right after birth, go down to minimum at 3h, and then rise again to the initial levels observed immediately after birth in 4-6 days (150). In addition, systemic blood flow increases to compensate elevated oxygen consumption (by 2-3 folds) due to the work of breathing and feeding (150). Furthermore, as the neonatal mice start to breathe, pulmonary blood flow increases (5 to 10-folds), leading to increased left arterial return (150). As a result, both increases in SVR and left arterial return cause left arterial pressure to rise, closing the foramen ovale (150). This is the reason why left ventricular preload is increased by elevated pulmonary blood flow which is achieved by increased SVR and decreased pulmonary artery pressure (PAP) and pulmonary vascular resistance (PVR) right after birth (150).

Other possible factors that may affect perinatal lethality include: 1) hemodynamic stress caused by circulatory transitions that impose more workload on the left ventricle (150), 2) high cardiac output caused by a substantial increase in metabolic demands (154; 155), 3) oxidative stress due to higher blood oxygenation after birth (131; 156), and 4) volume overload due to increased circulatory blood volume (150). Volume overload is associated with dilated cardiomyopathy which was observed in group D of the mutant mice (Figure 4-2).

However, we still don't know when the cardiac abnormality occurs. There could be cardiac abnormality during fetal stages because fetal wild type hearts still expressed CBX7 mRNA despite at low level (Figure 3-2 and 3-3). CBX7 might play a critical role in cardiac maturation during fetal stage. The mutant mice exhibited delayed myocardial compaction (spongiform myocardium) as early as E17.5 (Figure 4-4), suggesting cardiac maturation was impeded by targeted inhibition

of CBX7. But the timing of onset of cardiac abnormality in the mutant mice needs to be further investigated.

Another remaining question is about when CM proliferation is repressed in nature. Our data indicated reduction of CM proliferative capacity right after birth in terms of $Ki67^+$ or $pH3^+$ CM percentage (Figure 4-4). Also, multiple literatures implied perinatal reduction of CM proliferative capacity. For example, mRNA of Cyclin A was reduced by 60% between E18.5 and P2 (106). In addition, other cell cycle regulators were downregulated in the neonatal heart compared to the fetal heart (29; 149). Furthermore, the percentage of $Ki67^+$ CMs decreased from ~40% to ~15% between E18.5 and P1 in the previous report (134). However, the neonatal heart can fully regenerate itself after injury (8) and neonatal CMs grow robustly on the culture dish in vitro, suggesting that there seems to be no loss of CM proliferative capacity right after birth. Therefore, there is a possibility that CBX7 inhibition unleashed mitogenic signaling rather than it sustained or extended innate CM proliferative capacity. To examine whether mitogenic signaling was unleashed by CBX7 inhibition, the level of ERK in CMs could be compared between the wild type and the mutant heart via IHC or western blot at P0 (157). As an alternative explanation, after perinatal reduction of CM proliferation, there could be transiently sustained downstream signaling of cell proliferation that enables cardiac regeneration during neonatal period.

To measure CM proliferation, we utilized cell proliferation markers such as Ki67 and pH3, but there are other compensatory markers and methods. Counting CM number after dissociation of the heart could be an option (158). This method can directly measure CM proliferation since true CM proliferation would result in increased CM number. However, it is very challenging to dissociate multiple hearts at the consistent efficiency (159). Unexpected difficulties with CM isolation can happen due to multiple factors such as variable cannulation of the aorta, poor

water/buffer quality, pH or temperature of buffers, batch-to-batch variations in collagenase and proteases, incompletely washed or contaminated instruments, and air bubbles during perfusion. Even normal wild type mice at the same age show variability in heart size, suggesting that physiological variability in individual mice could make it challenging to produce reliable and significant data by counting cell number after dissociation of the heart. Measuring incorporation of BrdU or EdU is a reliable method to examine DNA synthesis (104). They are thymidine analogues and incorporated into the newly synthesized DNA. However, DNA synthesis does not always result in cytokinesis (e.g. polyploidization) (140). Detection of AURKB is useful method to examine cytokinesis of CMs (108). AURKB regulates chromosomal segregation during cell division (160). However, mitosis occurs in a very short time so that detection frequency of AURKB is very low (161). Furthermore, AURKB localizes to microtubules at kinetochores so that its staining pattern is a dot. It is difficult to detect these dots and differentiate them from aggregations of secondary antibodies or dye. Ki67 is a reliable marker for cell proliferation since it is expressed at every phase in cells with active cell cycle progression but disappears in quiescent cells (128). Ki67 is localized to nucleus during interphase but it moves to the chromosomal surface during mitosis (127). On the other hand, phosphorylation of histone H3 at Ser10 by AURKB is linked to mitotic chromosome condensation (129). This could be the reason why less number of $pH3^+$ CMs were observed compared to that of $Ki67^+$ CMs in our data (Figure 4-4, 4-5, and 4-6).

The mutant mice showed variable cardiac structure although they had the same genotype (Figure 4-2). The reason might be that CBX7 interacts with other Polycomb group proteins (56). It was previously reported that genetic deletion of Polycomb group proteins resulted in various kinds of cardiac abnormalities (37). For example, deletion of EZH2 in cardiac progenitors resulted in myocardial hypoplasia, excessive trabeculation, septal defects, and RV dilation (He et al., 2012).

EED1 was also reported to be essential for normal cardiac development but its exact role has not been elucidated (53; 54). Loss-of-function of JMJ resulted in excessive trabeculation, double outlet right ventricle (DORV), and ventricular septal defect (VSD) (162). Phc1 knockout mice also exhibited cardiac defects including looping defect and VSD (163). Thus, variability in the cardiac structure of the mutant mice could be due to the influence of CBX7 deficiency on other PcG proteins that play critical roles during heart development. Furthermore, the phenotypic variability of the mutant mice could be due to incomplete penetrance or variable expressivity of the targeted allele (164). Lastly, it could be due to genetic modifiers. Crossbreeding of different inbred mice results in heterogenous genetic background, leading to differential expression of genetic modifiers. Several rounds of backcrossing can minimize the effect of genetic modifiers (165).

So far, extensive attempts have been made toward enhancing proliferation of adult CMs assuming that this may benefit cardiac function after injury (166). But those efforts have failed to induce robust proliferation of adult CMs (4). In the future, we will examine whether targeted inhibition of CBX7 would induce robust proliferation of adult CMs in vivo by using inducible CM-specific Cbx7 conditional knock-out (CKO) mice (Myh6-mercremer;$Cbx7^{fl/fl}$) in the murine model of myocardial infarction.

In addition to issues addressed above, several important questions about mechanistic insights into the role of CBX7 remain unanswered: 1) Which stage of cell cycle is affected by CBX7 in perinatal CMs? 2) What is the upstream regulator of CBX7 for the repression of CM proliferation? 3) What genes are direct targets of CBX7 in perinatal/postnatal CMs? 4) Among direct targets of CBX7, what key genes are involved in the repression of perinatal CM proliferation and promotion of cardiac maturation? 5) Would targeted inhibition of CBX7 in adult CMs enhance

regenerative potential after myocardial injuries? These questions will be addressed one by one below.

Our data suggested that CBX7 overexpression resulted in increased DNA contents and multinucleation in neonatal CMs (Figure 5-1 and 5-2), but it does not tell the exact information about which stage of cell cycle is arrested. Multinucleation occurs after S and G2 phase, and nuclear division but prior to cytokinesis (167). Thus, CBX7 may induce cell cycle arrest between anaphase and telophase by repressing genes related to cleavage furrow formation. However, another possibility is that CBX7 plays a role in polyploidization of CMs. To examine this idea, nuclei of CMs after CBX7 overexpression could be isolated by using PCM1 (pericentriolar material 1) (142) and subjected to DNA content analysis via flow cytometry. If CBX7 induces polyploidization that occurs right after DNA synthesis, cells will be stuck in S phase without going further to G2 phase (167).

Studies reported that Cbx7 expression is regulated by microRNAs (miRNAs) in other types of cells (114; 168; 169). We thus speculate that the postnatal induction of CBX7 in the mouse heart is mediated by miRNAs. Oxygen-rich environment induces DNA damage response and repair right after birth (131). It was reported that DNA damage regulates miRNA expression (170). Thus, we believe that certain miRNAs downregulated during DNA damage response may be responsible for the induction of CBX7. However, there could be other mechanisms for CBX7 induction such as epigenetic regulation by other PcG proteins, transcriptional regulation by transcription factors, and post-transcriptional regulation such as phosphorylation by MAP kinase (171).

To identify genome-wide targets of CBX7, genome-wide occupancy of CBX7 in the adult CMs will be mapped via ChIP followed by high-throughput DNA sequencing (ChIP-seq). The data will show genome-wide direct targets of CBX7 and affected gene networks in the postmitotic

CMs. Some or all of such targets and networks are expected to be linked to cell cycle regulation and their relationship with cell cycle exit of postnatal CMs could be investigated. To narrow down genes that are involved in cell cycle withdrawal of perinatal CMs, transcriptome of CBX7-haplodeficient CMs will be profiled via RNA-seq. Neonatal mouse CMs from wild type and cardiac CBX7 haplodeficient mice will be isolated and subjected to RNA-seq. After transcriptome assembly, differently expressed genes will be identified by using bioinformatic tools such as DESeq and edgeR. Principal Component Analysis (PCA) will be performed to compare the transcriptional profile of each experimental group. Gene Ontology (GO) term enrichment analysis will be performed to better understand the underlying biological processes that CBX7 mediates. Ingenuity Pathway Analysis (IPA) or Kyoto Encyclopedia of Genes and Genomes (KEGG) pathway analysis will be performed to identify major signaling pathways controlled by CBX7 for CM proliferation. Activation Z Score will be determined, to explore upstream regulators in the pathway regulated by CBX7 in CMs.

Integration of ChIP-seq to RNA-seq data would allow identification of critical direct targets of CBX7 in the cardiac transcriptional network for CM proliferation. This systems biology approach would provide comprehensive information regarding how CM proliferation is epigenetically regulated, offering insights into developing novel therapeutic strategies to regenerate injured myocardium via promoting CM generation.

Based upon such investigation, therapeutic potential of CBX7 antagonists for inducing CM proliferation and heart regeneration could be explored. Notably, CBX7 was downregulated in the infarct zone of injured (post-MI) adult mouse heart (Figure 3-5) where CMs exhibit limited regenerative response (5), suggesting that CBX7 may serve as a therapeutic target to rescue the regenerative capacity of the adult heart. Currently, several antagonists for human CBX7 have been

developed for the treatment of cancers (65; 172-176). However, those CBX7 inhibitors have cross-reactivity to other CBX paralogues or other chromodomain-containing proteins, implying their off-target effects (173). Development of specific inhibitors of CBX7 and their application for cardiac regeneration will be an interesting area of research in the future.

Chapter 7: References

References

1. Braunwald E. 2015. The war against heart failure: the Lancet lecture. *Lancet* 385:812-24
2. Velagaleti RS, Pencina MJ, Murabito JM, Wang TJ, Parikh NI, et al. 2008. Long-term trends in the incidence of heart failure after myocardial infarction. *Circulation* 118:2057-62
3. Ezekowitz JA, Kaul P, Bakal JA, Armstrong PW, Welsh RC, McAlister FA. 2009. Declining in-hospital mortality and increasing heart failure incidence in elderly patients with first myocardial infarction. *J Am Coll Cardiol* 53:13-20
4. Cahill TJ, Choudhury RP, Riley PR. 2017. Heart regeneration and repair after myocardial infarction: translational opportunities for novel therapeutics. *Nat Rev Drug Discov* 16:699-717
5. Senyo SE, Steinhauser ML, Pizzimenti CL, Yang VK, Cai L, et al. 2013. Mammalian heart renewal by pre-existing cardiomyocytes. *Nature* 493:433-6
6. Jopling C, Sleep E, Raya M, Marti M, Raya A, Izpisua Belmonte JC. 2010. Zebrafish heart regeneration occurs by cardiomyocyte dedifferentiation and proliferation. *Nature* 464:606-9
7. Kikuchi K, Holdway JE, Werdich AA, Anderson RM, Fang Y, et al. 2010. Primary contribution to zebrafish heart regeneration by gata4(+) cardiomyocytes. *Nature* 464:601-5
8. Porrello ER, Mahmoud AI, Simpson E, Hill JA, Richardson JA, et al. 2011. Transient regenerative potential of the neonatal mouse heart. *Science* 331:1078-80
9. Beltrami AP, Barlucchi L, Torella D, Baker M, Limana F, et al. 2003. Adult cardiac stem cells are multipotent and support myocardial regeneration. *Cell* 114:763-76

10. van Berlo JH, Kanisicak O, Maillet M, Vagnozzi RJ, Karch J, et al. 2014. c-kit+ cells minimally contribute cardiomyocytes to the heart. *Nature* 509:337-41

11. Vagnozzi RJ, Sargent MA, Lin SJ, Palpant NJ, Murry CE, Molkentin JD. 2018. Genetic Lineage Tracing of Sca-1(+) Cells Reveals Endothelial but Not Myogenic Contribution to the Murine Heart. *Circulation*

12. Ieda M, Fu JD, Delgado-Olguin P, Vedantham V, Hayashi Y, et al. 2010. Direct reprogramming of fibroblasts into functional cardiomyocytes by defined factors. *Cell* 142:375-86

13. Chong JJ, Yang X, Don CW, Minami E, Liu YW, et al. 2014. Human embryonic-stem-cell-derived cardiomyocytes regenerate non-human primate hearts. *Nature* 510:273-7

14. Liu YW, Chen B, Yang X, Fugate JA, Kalucki FA, et al. 2018. Human embryonic stem cell-derived cardiomyocytes restore function in infarcted hearts of non-human primates. *Nat Biotechnol* 36:597-605

15. Kehat I, Kenyagin-Karsenti D, Snir M, Segev H, Amit M, et al. 2001. Human embryonic stem cells can differentiate into myocytes with structural and functional properties of cardiomyocytes. *J Clin Invest* 108:407-14

16. Laflamme MA, Murry CE. 2011. Heart regeneration. *Nature* 473:326-35

17. Yang L, Soonpaa MH, Adler ED, Roepke TK, Kattman SJ, et al. 2008. Human cardiovascular progenitor cells develop from a KDR+ embryonic-stem-cell-derived population. *Nature* 453:524-8

18. Zwi L, Caspi O, Arbel G, Huber I, Gepstein A, et al. 2009. Cardiomyocyte differentiation of human induced pluripotent stem cells. *Circulation* 120:1513-23

19. Huber I, Itzhaki I, Caspi O, Arbel G, Tzukerman M, et al. 2007. Identification and selection of cardiomyocytes during human embryonic stem cell differentiation. *FASEB J* 21:2551-63

20. Lian X, Hsiao C, Wilson G, Zhu K, Hazeltine LB, et al. 2012. Robust cardiomyocyte differentiation from human pluripotent stem cells via temporal modulation of canonical Wnt signaling. *Proc Natl Acad Sci U S A* 109:E1848-57

21. Shiba Y, Fernandes S, Zhu WZ, Filice D, Muskheli V, et al. 2012. Human ES-cell-derived cardiomyocytes electrically couple and suppress arrhythmias in injured hearts. *Nature* 489:322-5

22. Tohyama S, Hattori F, Sano M, Hishiki T, Nagahata Y, et al. 2013. Distinct metabolic flow enables large-scale purification of mouse and human pluripotent stem cell-derived cardiomyocytes. *Cell Stem Cell* 12:127-37

23. Ng SY, Wong CK, Tsang SY. 2010. Differential gene expressions in atrial and ventricular myocytes: insights into the road of applying embryonic stem cell-derived cardiomyocytes for future therapies. *Am J Physiol Cell Physiol* 299:C1234-49

24. Liao SY, Liu Y, Siu CW, Zhang Y, Lai WH, et al. 2010. Proarrhythmic risk of embryonic stem cell-derived cardiomyocyte transplantation in infarcted myocardium. *Heart Rhythm* 7:1852-9

25. Bizy A, Guerrero-Serna G, Hu B, Ponce-Balbuena D, Willis BC, et al. 2013. Myosin light chain 2-based selection of human iPSC-derived early ventricular cardiac myocytes. *Stem Cell Res* 11:1335-47

26. Muller M, Fleischmann BK, Selbert S, Ji GJ, Endl E, et al. 2000. Selection of ventricular-like cardiomyocytes from ES cells in vitro. *FASEB J* 14:2540-8

27. Bergmann O, Bhardwaj RD, Bernard S, Zdunek S, Barnabe-Heider F, et al. 2009. Evidence for cardiomyocyte renewal in humans. *Science* 324:98-102

28. Bergmann O, Zdunek S, Felker A, Salehpour M, Alkass K, et al. 2015. Dynamics of Cell Generation and Turnover in the Human Heart. *Cell* 161:1566-75

29. Ahuja P, Sdek P, MacLellan WR. 2007. Cardiac myocyte cell cycle control in development, disease, and regeneration. *Physiological reviews* 87:521-44

30. Pasumarthi KB, Nakajima H, Nakajima HO, Soonpaa MH, Field LJ. 2005. Targeted expression of cyclin D2 results in cardiomyocyte DNA synthesis and infarct regression in transgenic mice. *Circulation research* 96:110-8

31. Chaudhry HW, Dashoush NH, Tang H, Zhang L, Wang X, et al. 2004. Cyclin A2 mediates cardiomyocyte mitosis in the postmitotic myocardium. *The Journal of biological chemistry* 279:35858-66

32. Rybkin, II, Markham DW, Yan Z, Bassel-Duby R, Williams RS, Olson EN. 2003. Conditional expression of SV40 T-antigen in mouse cardiomyocytes facilitates an inducible switch from proliferation to differentiation. *The Journal of biological chemistry* 278:15927-34

33. Bersell K, Arab S, Haring B, Kuhn B. 2009. Neuregulin1/ErbB4 signaling induces cardiomyocyte proliferation and repair of heart injury. *Cell* 138:257-70

34. Engel FB, Hsieh PC, Lee RT, Keating MT. 2006. FGF1/p38 MAP kinase inhibitor therapy induces cardiomyocyte mitosis, reduces scarring, and rescues function after myocardial infarction. *Proc Natl Acad Sci U S A* 103:15546-51

35. Li P, Cavallero S, Gu Y, Chen TH, Hughes J, et al. 2011. IGF signaling directs ventricular cardiomyocyte proliferation during embryonic heart development. *Development* 138:1795-805

36. Heallen T, Zhang M, Wang J, Bonilla-Claudio M, Klysik E, et al. 2011. Hippo pathway inhibits Wnt signaling to restrain cardiomyocyte proliferation and heart size. *Science* 332:458-61

37. Wang QT. 2012. Epigenetic regulation of cardiac development and function by polycomb group and trithorax group proteins. *Dev Dyn* 241:1021-33

38. Vallaster M, Vallaster CD, Wu SM. 2012. Epigenetic mechanisms in cardiac development and disease. *Acta biochimica et biophysica Sinica* 44:92-102

39. van Weerd JH, Koshiba-Takeuchi K, Kwon C, Takeuchi JK. 2011. Epigenetic factors and cardiac development. *Cardiovascular research* 91:203-11

40. Reckova M, Rosengarten C, deAlmeida A, Stanley CP, Wessels A, et al. 2003. Hemodynamics is a key epigenetic factor in development of the cardiac conduction system. *Circulation research* 93:77-85

41. Movassagh M, Choy MK, Goddard M, Bennett MR, Down TA, Foo RS. 2010. Differential DNA methylation correlates with differential expression of angiogenic factors in human heart failure. *PloS one* 5:e8564

42. Handy DE, Castro R, Loscalzo J. 2011. Epigenetic modifications: basic mechanisms and role in cardiovascular disease. *Circulation* 123:2145-56

43. Hang CT, Yang J, Han P, Cheng HL, Shang C, et al. 2010. Chromatin regulation by Brg1 underlies heart muscle development and disease. *Nature* 466:62-7

44. Kirmizis A, Bartley SM, Kuzmichev A, Margueron R, Reinberg D, et al. 2004. Silencing of human polycomb target genes is associated with methylation of histone H3 Lys 27. *Genes & development* 18:1592-605

45. Gilsbach R, Preissl S, Gruning BA, Schnick T, Burger L, et al. 2014. Dynamic DNA methylation orchestrates cardiomyocyte development, maturation and disease. *Nat Commun* 5:5288

46. Nothjunge S, Nuhrenberg TG, Gruning BA, Doppler SA, Preissl S, et al. 2017. DNA methylation signatures follow preformed chromatin compartments in cardiac myocytes. *Nat Commun* 8:1667

47. Pederson T. 1972. Chromatin structure and the cell cycle. *Proc Natl Acad Sci U S A* 69:2224-8

48. Hirano T, Mitchison TJ. 1991. Cell cycle control of higher-order chromatin assembly around naked DNA in vitro. *The Journal of cell biology* 115:1479-89

49. Hinde E, Cardarelli F, Digman MA, Gratton E. 2012. Changes in chromatin compaction during the cell cycle revealed by micrometer-scale measurement of molecular flow in the nucleus. *Biophysical journal* 102:691-7

50. Bracken AP, Helin K. 2009. Polycomb group proteins: navigators of lineage pathways led astray in cancer. *Nature reviews. Cancer* 9:773-84

51. Ben-Saadon R, Zaaroor D, Ziv T, Ciechanover A. 2006. The polycomb protein Ring1B generates self atypical mixed ubiquitin chains required for its in vitro histone H2A ligase activity. *Molecular cell* 24:701-11

52. Kalb R, Latwiel S, Baymaz HI, Jansen PW, Muller CW, et al. 2014. Histone H2A monoubiquitination promotes histone H3 methylation in Polycomb repression. *Nature structural & molecular biology* 21:569-71

53. Dobreva G, Braun T. 2012. When silence is broken: polycomb group proteins in heart development. *Circulation research* 110:372-4

54. He A, Ma Q, Cao J, von Gise A, Zhou P, et al. 2012. Polycomb repressive complex 2 regulates normal development of the mouse heart. *Circulation research* 110:406-15

55. Gil J, Bernard D, Martinez D, Beach D. 2004. Polycomb CBX7 has a unifying role in cellular lifespan. *Nature cell biology* 6:67-72

56. Morey L, Pascual G, Cozzuto L, Roma G, Wutz A, et al. 2012. Nonoverlapping functions of the Polycomb group Cbx family of proteins in embryonic stem cells. *Cell Stem Cell* 10:47-62

57. Klauke K, Radulovic V, Broekhuis M, Weersing E, Zwart E, et al. 2013. Polycomb Cbx family members mediate the balance between haematopoietic stem cell self-renewal and differentiation. *Nature cell biology* 15:353-62

58. Scott CL, Gil J, Hernando E, Teruya-Feldstein J, Narita M, et al. 2007. Role of the chromobox protein CBX7 in lymphomagenesis. *Proc Natl Acad Sci U S A* 104:5389-94

59. Pallante P, Federico A, Berlingieri MT, Bianco M, Ferraro A, et al. 2008. Loss of the CBX7 gene expression correlates with a highly malignant phenotype in thyroid cancer. *Cancer research* 68:6770-8

60. Karamitopoulou E, Pallante P, Zlobec I, Tornillo L, Carafa V, et al. 2010. Loss of the CBX7 protein expression correlates with a more aggressive phenotype in pancreatic cancer. *Eur J Cancer* 46:1438-44

61. Zhang XW, Zhang L, Qin W, Yao XH, Zheng LZ, et al. 2010. Oncogenic role of the chromobox protein CBX7 in gastric cancer. *Journal of experimental & clinical cancer research : CR* 29:114

62. Forzati F, Federico A, Pallante P, Fedele M, Fusco A. 2012. Tumor suppressor activity of CBX7 in lung carcinogenesis. *Cell Cycle* 11:1888-91

63. Kim HY, Park JH, Won HY, Lee JY, Kong G. 2014. CBX7 inhibits breast tumorigenicity through DKK-1-mediated suppression of the Wnt/beta-catenin pathway. *FASEB J*

64. Shinjo K, Yamashita Y, Yamamoto E, Akatsuka S, Uno N, et al. 2014. Expression of chromobox homolog 7 (CBX7) is associated with poor prognosis in ovarian clear cell adenocarcinoma via TRAIL-induced apoptotic pathway regulation. *International journal of cancer. Journal international du cancer* 135:308-18

65. Simhadri C, Daze KD, Douglas SF, Quon TT, Dev A, et al. 2014. Chromodomain antagonists that target the polycomb-group methyllysine reader protein chromobox homolog 7 (CBX7). *Journal of medicinal chemistry* 57:2874-83

66. Bernstein E, Duncan EM, Masui O, Gil J, Heard E, Allis CD. 2006. Mouse polycomb proteins bind differentially to methylated histone H3 and RNA and are enriched in facultative heterochromatin. *Molecular and cellular biology* 26:2560-9

67. Bao ZZ, Bruneau BG, Seidman JG, Seidman CE, Cepko CL. 1999. Regulation of chamber-specific gene expression in the developing heart by Irx4. *Science* 283:1161-4

68. Bruneau BG, Bao ZZ, Tanaka M, Schott JJ, Izumo S, et al. 2000. Cardiac expression of the ventricle-specific homeobox gene Irx4 is modulated by Nkx2-5 and dHand. *Dev Biol* 217:266-77

69. Wang GF, Nikovits W, Jr., Bao ZZ, Stockdale FE. 2001. Irx4 forms an inhibitory complex with the vitamin D and retinoic X receptors to regulate cardiac chamber-specific slow MyHC3 expression. *The Journal of biological chemistry* 276:28835-41

70. O'Brien TX, Lee KJ, Chien KR. 1993. Positional specification of ventricular myosin light chain 2 expression in the primitive murine heart tube. *Proc Natl Acad Sci U S A* 90:5157-61

71. Kubalak SW, Miller-Hance WC, O'Brien TX, Dyson E, Chien KR. 1994. Chamber specification of atrial myosin light chain-2 expression precedes septation during murine cardiogenesis. *The Journal of biological chemistry* 269:16961-70

72. Heyduk T, Heyduk E. 2002. Molecular beacons for detecting DNA binding proteins. *Nat Biotechnol* 20:171-6

73. Tsourkas A, Behlke MA, Bao G. 2002. Structure-function relationships of shared-stem and conventional molecular beacons. *Nucleic Acids Res* 30:4208-15

74. Rhee WJ, Bao G. 2009. Simultaneous detection of mRNA and protein stem cell markers in live cells. *BMC Biotechnol* 9:30

75. Rhee WJ, Santangelo PJ, Jo H, Bao G. 2008. Target accessibility and signal specificity in live-cell detection of BMP-4 mRNA using molecular beacons. *Nucleic Acids Res* 36:e30

76. Santangelo P, Nitin N, Bao G. 2006. Nanostructured probes for RNA detection in living cells. *Ann Biomed Eng* 34:39-50

77. Ban K, Wile B, Kim S, Park HJ, Byun J, et al. 2013. Purification of cardiomyocytes from differentiating pluripotent stem cells using molecular beacons that target cardiomyocyte-specific mRNA. *Circulation* 128:1897-909

78. Zuker M. 2003. Mfold web server for nucleic acid folding and hybridization prediction. *Nucleic Acids Res* 31:3406-15

79. Popenda M, Szachniuk M, Antczak M, Purzycka KJ, Lukasiak P, et al. 2012. Automated 3D structure composition for large RNAs. *Nucleic Acids Res* 40:e112

80. Brundel BJ, Henning RH, Ke L, van Gelder IC, Crijns HJ, Kampinga HH. 2006. Heat shock protein upregulation protects against pacing-induced myolysis in HL-1 atrial myocytes and in human atrial fibrillation. *Journal of molecular and cellular cardiology* 41:555-62

81. Claycomb WC, Lanson NA, Jr., Stallworth BS, Egeland DB, Delcarpio JB, et al. 1998. HL-1 cells: a cardiac muscle cell line that contracts and retains phenotypic characteristics of the adult cardiomyocyte. *Proc Natl Acad Sci U S A* 95:2979-84

82. Takahashi K, Yamanaka S. 2006. Induction of pluripotent stem cells from mouse embryonic and adult fibroblast cultures by defined factors. *Cell* 126:663-76

83. Xu C, Police S, Rao N, Carpenter MK. 2002. Characterization and enrichment of cardiomyocytes derived from human embryonic stem cells. *Circulation research* 91:501-8

84. Fujiwara M, Yan P, Otsuji TG, Narazaki G, Uosaki H, et al. 2011. Induction and enhancement of cardiac cell differentiation from mouse and human induced pluripotent stem cells with cyclosporin-A. *PloS one* 6:e16734

85. Chan LL, Wilkinson AR, Paradis BD, Lai N. 2012. Rapid image-based cytometry for comparison of fluorescent viability staining methods. *J Fluoresc* 22:1301-11

86. Sasaki DT, Dumas SE, Engleman EG. 1987. Discrimination of viable and non-viable cells using propidium iodide in two color immunofluorescence. *Cytometry* 8:413-20

87. Hume JR, Uehara A. 1985. Ionic basis of the different action potential configurations of single guinea-pig atrial and ventricular myocytes. *J Physiol* 368:525-44

88. Chen HW, Yu SL, Chen WJ, Yang PC, Chien CT, et al. 2004. Dynamic changes of gene expression profiles during postnatal development of the heart in mice. *Heart* 90:927-34

89. Halo TL, McMahon KM, Angeloni NL, Xu Y, Wang W, et al. 2014. NanoFlares for the detection, isolation, and culture of live tumor cells from human blood. *Proc Natl Acad Sci U S A* 111:17104-9

90. Lahm H, Doppler S, Dressen M, Werner A, Adamczyk K, et al. 2015. Live fluorescent RNA-based detection of pluripotency gene expression in embryonic and induced pluripotent stem cells of different species. *Stem Cells* 33:392-402

91. Prigodich AE, Randeria PS, Briley WE, Kim NJ, Daniel WL, et al. 2012. Multiplexed nanoflares: mRNA detection in live cells. *Anal Chem* 84:2062-6

92. Chen AK, Davydenko O, Behlke MA, Tsourkas A. 2010. Ratiometric bimolecular beacons for the sensitive detection of RNA in single living cells. *Nucleic Acids Res* 38:e148

93. Zhang X, Song Y, Shah AY, Lekova V, Raj A, et al. 2013. Quantitative assessment of ratiometric bimolecular beacons as a tool for imaging single engineered RNA transcripts and measuring gene expression in living cells. *Nucleic Acids Res* 41:e152

94. Chen AK, Behlke MA, Tsourkas A. 2008. Efficient cytosolic delivery of molecular beacon conjugates and flow cytometric analysis of target RNA. *Nucleic Acids Res* 36:e69

95. van Laake LW, Passier R, Doevendans PA, Mummery CL. 2008. Human embryonic stem cell-derived cardiomyocytes and cardiac repair in rodents. *Circulation research* 102:1008-10

96. Itzhaki I, Maizels L, Huber I, Zwi-Dantsis L, Caspi O, et al. 2011. Modelling the long QT syndrome with induced pluripotent stem cells. *Nature* 471:225-9

97. Moretti A, Bellin M, Welling A, Jung CB, Lam JT, et al. 2010. Patient-specific induced pluripotent stem-cell models for long-QT syndrome. *N Engl J Med* 363:1397-409

98. Liang P, Lan F, Lee AS, Gong T, Sanchez-Freire V, et al. 2013. Drug screening using a library of human induced pluripotent stem cell-derived cardiomyocytes reveals disease-specific patterns of cardiotoxicity. *Circulation* 127:1677-91

99. Li F, Wang X, Capasso JM, Gerdes AM. 1996. Rapid transition of cardiac myocytes from hyperplasia to hypertrophy during postnatal development. *Journal of molecular and cellular cardiology* 28:1737-46

100. Brooks G, Poolman RA, McGill CJ, Li JM. 1997. Expression and activities of cyclins and cyclin-dependent kinases in developing rat ventricular myocytes. *Journal of molecular and cellular cardiology* 29:2261-71

101. Kang MJ, Kim JS, Chae SW, Koh KN, Koh GY. 1997. Cyclins and cyclin dependent kinases during cardiac development. *Mol Cells* 7:360-6

102. Kang MJ, Koh GY. 1997. Differential and dramatic changes of cyclin-dependent kinase activities in cardiomyocytes during the neonatal period. *Journal of molecular and cellular cardiology* 29:1767-77

103. Liao HS, Kang PM, Nagashima H, Yamasaki N, Usheva A, et al. 2001. Cardiac-specific overexpression of cyclin-dependent kinase 2 increases smaller mononuclear cardiomyocytes. *Circulation research* 88:443-50

104. Soonpaa MH, Kim KK, Pajak L, Franklin M, Field LJ. 1996. Cardiomyocyte DNA synthesis and binucleation during murine development. *Am J Physiol* 271:H2183-9

105. Soonpaa MH, Koh GY, Pajak L, Jing S, Wang H, et al. 1997. Cyclin D1 overexpression promotes cardiomyocyte DNA synthesis and multinucleation in transgenic mice. *J Clin Invest* 99:2644-54

106. Yoshizumi M, Lee WS, Hsieh CM, Tsai JC, Li J, et al. 1995. Disappearance of cyclin A correlates with permanent withdrawal of cardiomyocytes from the cell cycle in human and rat hearts. *J Clin Invest* 95:2275-80

107. Kuhn B, del Monte F, Hajjar RJ, Chang YS, Lebeche D, et al. 2007. Periostin induces proliferation of differentiated cardiomyocytes and promotes cardiac repair. *Nature medicine* 13:962-9

108. Engel FB, Schebesta M, Duong MT, Lu G, Ren S, et al. 2005. p38 MAP kinase inhibition enables proliferation of adult mammalian cardiomyocytes. *Genes & development* 19:1175-87

109. Xin M, Olson EN, Bassel-Duby R. 2013. Mending broken hearts: cardiac development as a basis for adult heart regeneration and repair. *Nat Rev Mol Cell Biol* 14:529-41

110. Sauvageau M, Sauvageau G. 2010. Polycomb group proteins: multi-faceted regulators of somatic stem cells and cancer. *Cell Stem Cell* 7:299-313

111. del Mar Lorente M, Marcos-Gutierrez C, Perez C, Schoorlemmer J, Ramirez A, et al. 2000. Loss- and gain-of-function mutations show a polycomb group function for Ring1A in mice. *Development* 127:5093-100

112. Voncken JW, Roelen BA, Roefs M, de Vries S, Verhoeven E, et al. 2003. Rnf2 (Ring1b) deficiency causes gastrulation arrest and cell cycle inhibition. *Proc Natl Acad Sci U S A* 100:2468-73

113. Vincenz C, Kerppola TK. 2008. Different polycomb group CBX family proteins associate with distinct regions of chromatin using nonhomologous protein sequences. *Proc Natl Acad Sci U S A* 105:16572-7

114. O'Loghlen A, Munoz-Cabello AM, Gaspar-Maia A, Wu HA, Banito A, et al. 2012. MicroRNA regulation of Cbx7 mediates a switch of Polycomb orthologs during ESC differentiation. *Cell Stem Cell* 10:33-46

115. Poss KD, Wilson LG, Keating MT. 2002. Heart regeneration in zebrafish. *Science* 298:2188-90

116. Soonpaa MH, Field LJ. 1998. Survey of studies examining mammalian cardiomyocyte DNA synthesis. *Circulation research* 83:15-26

117. Soonpaa MH, Field LJ. 1997. Assessment of cardiomyocyte DNA synthesis in normal and injured adult mouse hearts. *Am J Physiol* 272:H220-6

118. Li Q, Wang X, Lu Z, Zhang B, Guan Z, et al. 2010. Polycomb CBX7 directly controls trimethylation of histone H3 at lysine 9 at the p16 locus. *PloS one* 5:e13732

119. Simon JA, Kingston RE. 2009. Mechanisms of polycomb gene silencing: knowns and unknowns. *Nat Rev Mol Cell Biol* 10:697-708

120. Bernard D, Martinez-Leal JF, Rizzo S, Martinez D, Hudson D, et al. 2005. CBX7 controls the growth of normal and tumor-derived prostate cells by repressing the Ink4a/Arf locus. *Oncogene* 24:5543-51

121. Ehler E, Moore-Morris T, Lange S. 2013. Isolation and Culture of Neonatal Mouse Cardiomyocytes. *Jove-J Vis Exp*

122. Bell RM, Mocanu MM, Yellon DM. 2011. Retrograde heart perfusion: the Langendorff technique of isolated heart perfusion. *Journal of molecular and cellular cardiology* 50:940-50

123. Thomas MA, Lichtenstein DL, Krajcsi P, Wold WS. 2007. A real-time PCR method to rapidly titer adenovirus stocks. *Methods Mol Med* 130:185-92

124. Chomczynski P, Sacchi N. 1987. Single-step method of RNA isolation by acid guanidinium thiocyanate-phenol-chloroform extraction. *Anal Biochem* 162:156-9

125. Pallante P, Terracciano L, Carafa V, Schneider S, Zlobec I, et al. 2010. The loss of the CBX7 gene expression represents an adverse prognostic marker for survival of colon carcinoma patients. *Eur J Cancer* 46:2304-13

126. Bullwinkel J, Baron-Luhr B, Ludemann A, Wohlenberg C, Gerdes J, Scholzen T. 2006. Ki-67 protein is associated with ribosomal RNA transcription in quiescent and proliferating cells. *J Cell Physiol* 206:624-35

127. Cuylen S, Blaukopf C, Politi AZ, Muller-Reichert T, Neumann B, et al. 2016. Ki-67 acts as a biological surfactant to disperse mitotic chromosomes. *Nature* 535:308-12

128. Bruno S, Darzynkiewicz Z. 1992. Cell cycle dependent expression and stability of the nuclear protein detected by Ki-67 antibody in HL-60 cells. *Cell Prolif* 25:31-40

129. Hendzel MJ, Wei Y, Mancini MA, Van Hooser A, Ranalli T, et al. 1997. Mitosis-specific phosphorylation of histone H3 initiates primarily within pericentromeric heterochromatin during G2 and spreads in an ordered fashion coincident with mitotic chromosome condensation. *Chromosoma* 106:348-60

130. Porrello ER, Mahmoud AI, Simpson E, Johnson BA, Grinsfelder D, et al. 2013. Regulation of neonatal and adult mammalian heart regeneration by the miR-15 family. *Proc Natl Acad Sci U S A* 110:187-92

131. Puente BN, Kimura W, Muralidhar SA, Moon J, Amatruda JF, et al. 2014. The oxygen-rich postnatal environment induces cardiomyocyte cell-cycle arrest through DNA damage response. *Cell* 157:565-79

132. Nakada Y, Canseco DC, Thet S, Abdisalaam S, Asaithamby A, et al. 2017. Hypoxia induces heart regeneration in adult mice. *Nature* 541:222-7

133. Mollova M, Bersell K, Walsh S, Savla J, Das LT, et al. 2013. Cardiomyocyte proliferation contributes to heart growth in young humans. *Proc Natl Acad Sci U S A* 110:1446-51

134. Stopp S, Grundl M, Fackler M, Malkmus J, Leone M, et al. 2017. Deletion of Gas2l3 in mice leads to specific defects in cardiomyocyte cytokinesis during development. *Proc Natl Acad Sci U S A* 114:8029-34

135. Jonker SS, Louey S, Giraud GD, Thornburg KL, Faber JJ. 2015. Timing of cardiomyocyte growth, maturation, and attrition in perinatal sheep. *FASEB J* 29:4346-57

136. Jin P, Hardy S, Morgan DO. 1998. Nuclear localization of cyclin B1 controls mitotic entry after DNA damage. *The Journal of cell biology* 141:875-85

137. Ahuja P, Perriard E, Perriard JC, Ehler E. 2004. Sequential myofibrillar breakdown accompanies mitotic division of mammalian cardiomyocytes. *J Cell Sci* 117:3295-306

138. Guerrero PA, Schuessler RB, Davis LM, Beyer EC, Johnson CM, et al. 1997. Slow ventricular conduction in mice heterozygous for a connexin43 null mutation. *J Clin Invest* 99:1991-8

139. Thomas SA, Schuessler RB, Berul CI, Beardslee MA, Beyer EC, et al. 1998. Disparate effects of deficient expression of connexin43 on atrial and ventricular conduction: evidence for chamber-specific molecular determinants of conduction. *Circulation* 97:686-91

140. Alkass K, Panula J, Westman M, Wu TD, Guerquin-Kern JL, Bergmann O. 2015. No Evidence for Cardiomyocyte Number Expansion in Preadolescent Mice. *Cell* 163:1026-36

141. Patterson M, Barske L, Van Handel B, Rau CD, Gan P, et al. 2017. Frequency of mononuclear diploid cardiomyocytes underlies natural variation in heart regeneration. *Nat Genet* 49:1346-53

142. Bergmann O, Zdunek S, Alkass K, Druid H, Bernard S, Frisen J. 2011. Identification of cardiomyocyte nuclei and assessment of ploidy for the analysis of cell turnover. *Exp Cell Res* 317:188-94

143. Olson EN. 1992. Interplay between proliferation and differentiation within the myogenic lineage. *Dev Biol* 154:261-72

144. Takahashi K, Tanabe K, Ohnuki M, Narita M, Ichisaka T, et al. 2007. Induction of pluripotent stem cells from adult human fibroblasts by defined factors. *Cell* 131:861-72

145. Laflamme MA, Chen KY, Naumova AV, Muskheli V, Fugate JA, et al. 2007. Cardiomyocytes derived from human embryonic stem cells in pro-survival factors enhance function of infarcted rat hearts. *Nat Biotechnol* 25:1015-24

146. Dubois NC, Craft AM, Sharma P, Elliott DA, Stanley EG, et al. 2011. SIRPA is a specific cell-surface marker for isolating cardiomyocytes derived from human pluripotent stem cells. *Nat Biotechnol* 29:1011-8

147. Hattori F, Chen H, Yamashita H, Tohyama S, Satoh YS, et al. 2010. Nongenetic method for purifying stem cell-derived cardiomyocytes. *Nat Methods* 7:61-6

148. Quaife-Ryan GA, Sim CB, Ziemann M, Kaspi A, Rafehi H, et al. 2017. Multicellular Transcriptional Analysis of Mammalian Heart Regeneration. *Circulation* 136:1123-39

149. Pasumarthi KB, Field LJ. 2002. Cardiomyocyte cell cycle regulation. *Circulation research* 90:1044-54

150. Stopfkuchen H. 1987. Changes of the cardiovascular system during the perinatal period. *Eur J Pediatr* 146:545-9

151. Luxan G, Casanova JC, Martinez-Poveda B, Prados B, D'Amato G, et al. 2013. Mutations in the NOTCH pathway regulator MIB1 cause left ventricular noncompaction cardiomyopathy. *Nature medicine* 19:193-201

152. Kim GH. 2013. Murine fetal echocardiography. *J Vis Exp*

153. Lundell BP, Wallgren CG. 1982. Assessment of left ventricular adaptation to extrauterine circulation. *Acta Paediatr Scand* 71:745-52

154. Berman W, Christensen D. 1983. Effects of acute preload and afterload stress on myocardial function in newborn and adult sheep. *Biol Neonate* 43:61-6

155. Faxelius G, Hagnevik K, Lagercrantz H, Lundell B, Irestedt L. 1983. Catecholamine surge and lung function after delivery. *Arch Dis Child* 58:262-6

156. Gitto E, Reiter RJ, Karbownik M, Tan DX, Gitto P, et al. 2002. Causes of oxidative stress in the pre- and perinatal period. *Biol Neonate* 81:146-57

157. Roberts PJ, Der CJ. 2007. Targeting the Raf-MEK-ERK mitogen-activated protein kinase cascade for the treatment of cancer. *Oncogene* 26:3291-310

158. Naqvi N, Li M, Calvert JW, Tejada T, Lambert JP, et al. 2014. A proliferative burst during preadolescence establishes the final cardiomyocyte number. *Cell* 157:795-807

159. Louch WE, Sheehan KA, Wolska BM. 2011. Methods in cardiomyocyte isolation, culture, and gene transfer. *Journal of molecular and cellular cardiology* 51:288-98

160. Ducat D, Zheng Y. 2004. Aurora kinases in spindle assembly and chromosome segregation. *Exp Cell Res* 301:60-7

161. Emanuele MJ, Lan W, Jwa M, Miller SA, Chan CS, Stukenberg PT. 2008. Aurora B kinase and protein phosphatase 1 have opposing roles in modulating kinetochore assembly. *The Journal of cell biology* 181:241-54

162. Lee Y, Song AJ, Baker R, Micales B, Conway SJ, Lyons GE. 2000. Jumonji, a nuclear protein that is necessary for normal heart development. *Circulation research* 86:932-8

163. Shirai M, Osugi T, Koga H, Kaji Y, Takimoto E, et al. 2002. The Polycomb-group gene Rae28 sustains Nkx2.5/Csx expression and is essential for cardiac morphogenesis. *J Clin Invest* 110:177-84

164. Erickson RP. 1979. Biology of penetrance and variable expressivity. *Birth Defects Orig Artic Ser* 15:3-12

165. Hamilton BA, Yu BD. 2012. Modifier genes and the plasticity of genetic networks in mice. *PLoS Genet* 8:e1002644

166. Uygur A, Lee RT. 2016. Mechanisms of Cardiac Regeneration. *Dev Cell* 36:362-74

167. Yuan X, Braun T. 2017. Multimodal Regulation of Cardiac Myocyte Proliferation. *Circulation research* 121:293-309

168. Xie D, Shang C, Zhang H, Guo Y, Tong X. 2015. Up-regulation of miR-9 target CBX7 to regulate invasion ability of bladder transitional cell carcinoma. *Medical science monitor : international medical journal of experimental and clinical research* 21:225-30

169. Chao TF, Zhang Y, Yan XQ, Yin B, Gong YH, et al. 2008. [MiR-9 regulates the expression of CBX7 in human glioma]. *Zhongguo yi xue ke xue yuan xue bao. Acta Academiae Medicinae Sinicae* 30:268-74

170. Wan G, Mathur R, Hu X, Zhang X, Lu X. 2011. miRNA response to DNA damage. *Trends Biochem Sci* 36:478-84

171. Gil J, O'Loghlen A. 2014. PRC1 complex diversity: where is it taking us? *Trends Cell Biol* 24:632-41

172. Kaustov L, Ouyang H, Amaya M, Lemak A, Nady N, et al. 2011. Recognition and specificity determinants of the human cbx chromodomains. *The Journal of biological chemistry* 286:521-9

173. Ren C, Smith SG, Yap K, Li S, Li J, et al. 2016. Structure-Guided Discovery of Selective Antagonists for the Chromodomain of Polycomb Repressive Protein CBX7. *ACS Med Chem Lett* 7:601-5

174. Ren C, Morohashi K, Plotnikov AN, Jakoncic J, Smith SG, et al. 2015. Small-molecule modulators of methyl-lysine binding for the CBX7 chromodomain. *Chem Biol* 22:161-8

175. Stuckey JI, Dickson BM, Cheng N, Liu Y, Norris JL, et al. 2016. A cellular chemical probe targeting the chromodomains of Polycomb repressive complex 1. *Nat Chem Biol* 12:180-7

176. Simhadri C, Gignac MC, Anderson CJ, Milosevich N, Dheri A, et al. 2016. Structure-Activity Relationships of Cbx7 Inhibitors, Including Selectivity Studies against Other Cbx Proteins. *Acs Omega* 1:541-51